“Structured Antibody Surfaces for Bio-Recognition and a Label-free Detection of Bacteria”

Dissertation
zur Erlangung des Grades
„Doktor
der Naturwissenschaften“

am Fachbereich Biologie
der Johannes Gutenberg-Universität
in Mainz

Cornel Wolf
geb. in Erfurt

Mainz, 2010

Die vorliegende Arbeit wurde in der Zeit von Januar 2008 bis November 2010 im Arbeitskreis Materialforschung des Max-Planck-Instituts für Polymerforschung in Mainz angefertigt.

Dekan:

1. Berichterstatter:

2. Berichterstatter:

Tag der mündlichen Prüfung: 20. Dezember 2010

Inmitten der Schwierigkeiten liegt die Möglichkeit.

Albert Einstein

Table of Contents

Summary

Antibody microarrays are of great research interest because of their potential application as biosensors for high-throughput protein and pathogen screening technologies. In this active area, there is still a need for novel structures and assemblies providing insight in binding interactions such as spherical and annulus-shaped protein structures, e.g. for the utilization of curved surfaces for the enhanced protein-protein interactions and detection of antigens. Therefore, the goal of the presented work was to establish a new technique for the label-free detection of bio-molecules and bacteria on topographically structured surfaces, suitable for antibody binding.

In the first part of the presented thesis, the fabrication of monolayers of inverse opals with 10 μm diameter and the immobilization of antibodies on their interior surface is described. For this purpose, several established methods for the linking of antibodies to glass, including Schiff bases, EDC/S-NHS chemistry and the biotin-streptavidin affinity system, were tested. The employed methods included immunofluorescence and image analysis by phase contrast microscopy. It could be shown that these methods were not successful in terms of antibody immobilization and adjacent bacteria binding. Hence, a method based on the application of an active-ester-silane was introduced. It showed promising results but also the need for further analysis. Especially the search for alternative antibodies addressing other antigens on the exterior of bacteria will be sought-after in the future.

As a consequence of the ability to control antibody-functionalized surfaces, a new technique employing colloidal templating to yield large scale (~cm^2) 2D arrays of antibodies against *E. coli* K12, eGFP and human integrin $\alpha_v\beta_3$ on a versatile useful glass surface is presented. The antibodies were swept to reside around the templating microspheres during solution drying, and physisorbed on the glass. After removing the microspheres, the formation of annuli-shaped antibody structures was observed. The preserved antibody structure and functionality is shown by binding the specific antigens and secondary antibodies. The improved detection of specific bacteria from a crude solution compared to conventional “flat” antibody surfaces and the setting up of an integrin-binding platform for targeted recognition and surface interactions of eukaryotic cells is demonstrated. The structures were investigated by atomic force, confocal and fluorescence microscopy. Operational parameters like drying time, temperature, humidity and surfactants were optimized to obtain a stable antibody structure.

Finally, three-dimensional structures of 1 μm inverse opals were used to generate filters with opening diameters of 200 nm and a flatness of only a few micrometer, for application in bacteria detection.

Abbreviations

2D	two-dimensional
3D	three-dimensional
AE-S	11-Pentafluorophenylundecanoatetrimethoxysilane
AFM	atomic force microscopy
APTES	3-Aminopropyltriethoxysilane
CC	colloidal crystals
CLSM	confocal laser scanning microscopy
DAPI	4',6-Diamidino-2-phenylindol Dihydrochlorid
DiD	1,1'-dioctadecyl-3,3,3',3'-tetramethylindodicarbocyanine perchlorate
DiD648	1,1'-dioctadecyl-3,3,3',3'-tetramethyl-indodicarbocyanine perchlorate
DOPC	1,2-dioleoyl-sn-glycero-3-phosphocholine
E. coli	*Escherichia coli*
EDC	1-Ethyl-3-(3-dimethylaminopropyl)carbodiimide
eGFP	enhanced green fluorescent protein
GA	glutaraldehyde
HD	horizontal deposition
iopals	inverse opals
K. pla.	*Klebsiella planticola*
LB-medium	Lysogeny broth medium
MTMS	Methoxytriethyleneoxypropyltrimethoxysilane
OH-PEG-S	[Hydroxy(polyethyleneoxy)propyl]triethoxysilane
P. myx.	*Proteus myxofaciens*
PCM	phase contrast microscopy
PFP	Pentafluorophenol
PS-MS	polystyrene microspheres
PTFE	Polytetrafluoroethylene
S-NHS	Sulfo-N-Hydroxysuccinimide
SC	spin casting
SCR	surface coverage
SEM	scanning electron microscopy
T20	Polysorbate 20 (Tween20®)
VLD	vertical lifting deposition

1 General Introduction and Motivation

The following sections give a brief overview of the issues of diseases and pathogens and present some of the most important established methods for their detection. Subsequently, the subject matter of biosensors and some examples thereof is highlighted. This introductory chapter is concluded with a description of the resulting aims and motivation of the presented work.

Detailed descriptions of the obtained results are presented in the corresponding chapters 4 – "Label-free Detection of Microorganisms in an Integrated Biosensor Array", 5 – "2D Array-Patterning of Antibody Annuli", 6 – "Structured Antibody Surfaces for Bio-recognition" and eventually 7 – "Size Exclusion Filters".

1.1 Bacteria and Microbial Diseases

Bacteria, viruses and other pathogens are ubiquitous in our environment and nature in general, like in soil, water and air. Furthermore, bacteria especially occupy the intestinal tract of animals as well as humans and can be found in elevated concentrations in water contaminated with fecal matter. For example, an average human being carries more than 150 bacteria strains.[1] About 10^{15} microorganisms (compared to 10^{13} – 10^{14} human cells) constitute a mass of 0.5 – 1 kg in- and outside the body.[2]

Although most bacteria strains live in close relation to plants and animals and can even be essential for living, certain species are potentially harmful. They may cause severe infectious diseases like, for example, tuberculosis, cholera, pneumonia and many more. Some may even be misused as warfare agents such as anthrax. As consequence of just requiring food, moisture and a favorable temperature, bacteria have the ability to adapt and grow under versatile conditions, and hence multiply and evolve rapidly. Therefore, some diseases caused by microorganisms can have disastrous effects on plants, animals and first and foremost humans. Worldwide, infectious diseases account for nearly 40% of the total 50 million annual estimated deaths and microbial diseases constitute the major cause of death in many developing countries.[3] Although they appear to represent a small proportion of all diseases in developed countries, communicable diseases are worldwide of particular concern and carry an elevated risk of pandemic nowadays. Reasons are many people still suffering from hygiene and nutrition problems, fast distribution channels in a

global network or extreme annual rainfalls and floods. Furthermore, there is a particular concern regarding antibiotic resistances which have been growing most markedly for years, like nosocomial infections with *Legionella* or *Methicillin Resistant Staphylococcus Aureus* (*MRSA*).[4] In Europe around 3 million people contract a nosocomial infection and 50,000 decease per year.[5]. As a consequence, already well characterized and vanquished diseases, like cholera, meningitis and tuberculosis recur, also linked to increasing human immunodeficiency virus (HIV) infections,[6] and new diseases emerge.

Among the wide variety of diseases caused by bacteria, a growing number of bacterial pathogens have been identified as food- and waterborne pathogens, which are in particular important.[7,8] According to the World Health Organization, just diarrhea is causing estimated 1.5 million deaths of under-five old children every year.[9] The Centers for Disease Control (CDC) accounts about 325,000 hospitalizations and 5000 deaths related to foodborne diseases in the U.S. each year.[10,11]

The bacterium *Escherichia coli* (*E. coli*) is naturally occurring in the flora of the intestine. However, some strains like, for example, O157:H7, *enterotoxic* and *enterohemorragic E. coli*, can if ingested, be enteropathogenetic and cause diarrhea.[12] Outside the intestine *E. coli* can cause urinary tract infections, inflammations and peritonitis in immunosuppressed patients like children and elderly people.[13] *E. coli* contaminations can be found in drinking water, caused by, for instance, feces but also in spoiled ground beef, raw milk and chicken. Therefore, the systematic and careful control of this pathogen is extremely important, especially in the field of food production. Another example of a dangerous foodborne bacterium, all of the strains of which are presumed to be pathogenic for human beings, is *Salmonella*. In order to prevent bacteria like *E. coli* and *Salmonella* making their way to food products and eventually to the consumer, there exist large scientific efforts to detect the presence of bacteria in perishable food products and water.[14]

Besides the detection of pathogens in food in advance to a disease transmission, the diagnosis after an infection and outbreak of disease is still very important and constitutes a severe problem. In order to treat all these diseases effectively, to prevent their spreading and antibiotic resistances, it is essential to be able to identify the pathogenic bacteria extremely fast, whilst it is still in its early stages and before mutations and complications can occur, and to identify the specific treatment necessary.

Effective testing methods for bacteria need to fulfill several ambitious objectives, like a fast detection, selectivity and sensitivity, robustness, and the distinction between living and and dead bacteria in antibiotic susceptibility. Time and sensitivity of analysis play key roles and are the most important limitations related to the usefulness of microbiological testing. Furthermore, the development of a method or sensor capable of rapid detection and quantification of bacteria in real world samples is urgently needed.[14] Since for some pathogens very small concentrations can be already an infectious dose,[15] higher sensitivity and specificity have become crucial factors for effective biosensors used in these applications.[16] Extremely selective detection methods are required since pathogenic bacteria are often present in a complex biological environment along with many other non-pathogenic organisms. Hence the possibility of false-positive results is relative high, which can lead to, for instance, wrong medication.

There exist several analytical methods for the detection and identification of microorganism in different environments. They can roughly be divided into primary physico-chemical techniques, requiring cultivation and mostly being based on whole cell detection, and molecular biology techniques which involve the detection and identification of naturally occurring molecular compounds of bacteria, such as genes or proteins. Some of the already established "golden standard" techniques are described in short in the next section. In addition to this, the concept of biosensors for the detection of pathogens and recent developments and advancements in this field are explained in section 1.3 – "Biosensors in Pathogen Detection".

1.2 Established Methods for Pathogen Detection

For a long time, a multiplicity of methods has been used for pathogen detection. They involve amongst others counting of bacteria, antigen–antibody interactions and DNA analysis. In spite of disadvantages, such as the time required for the analysis or the complexity of their application, they still represent the "golden standard" methods and are often combined together to yield more robust results. Therefore, culture and colony counting and immunology-based methods as well as the polymerase chain reaction (PCR) are the most common tools used for pathogen detection.[17]

In general, no single test provides a definitive identification of an unknown bacterium. Hence, the conventional bacteria detection methods comprise usually multiple analyses. These can be, for example, morphological evaluation of the microorganisms by a microscope and a test for the organisms ability to grow in various media under a variety of conditions.[3] Furthermore, before the

traditional biochemical screening and serological confirmation can take place, pre-enrichment and selective enrichment have to be accomplished.[18] Thereby a required signal amplification takes place. In this process single cells are grown into colonies, which is time-consuming. For instance, the development of a colony of a reasonable number of 10^6 coliform bacteria can take between 18 and 24 hours.[3] The adjacent classical enumeration methods can take up to additional 48 hours to obtain confirmed results. Hence, a complex series of protocols and tests is required and the results are often difficult to interpret and not available on the time scale sought-after in the clinical laboratory.

To solve these problems, considerable efforts have been directed in the last years towards the development of techniques that can rapidly detect low concentrations of pathogens in various environments like water, food and clinical samples. Some of the classical and advanced methods like culture and colony counting, polymerase chain reaction (PCR) and immunology-based methods are explained briefly in the following sections. In summary, new molecular biology-based methods have overcome several issues but are still lengthy and not comprehensive, since bacteria viability cannot be monitored based on the mere presence of DNA. They are extremely sensitive but require pure samples, hours of processing and advanced expertise in molecular biology.[19] Hence the development of improved detection methods is sought-after.

1.2.1 Classical and Modified Cultural Methods

In microbial analysis, culturing and plating methods are the classical bacterial detection techniques and the “golden standard” methods for microbial analysis are often International Organization for Standardization (ISO) methods.[20] However, they are excessively time-consuming. In some cases 4 to 9 days are needed to obtain a negative result and between 14 and 16 days for confirmation of a positive result.[21] This is an obvious bottle neck in many applications.

Conventional methods for the enumeration of bacteria are colony counting methods. Herein, the total number of bacteria is determined by inoculating dilutions of suspensions of the sample onto the surface of a solid growth medium (agar) by the spread-plate method or by mixing the test portion with the liquefied agar medium in Petri dishes. Enumeration is performed after incubation for fixed periods at temperatures varying from 7 to 55 °C in an aerobic, micro-aerobic or anaerobic atmosphere depending upon the target organisms. During incubation each individual cell multiplies into a colony that was visible to the naked eye. Classical culture methods have a quantification limit

of about 4 to 40 colony-forming units (cfu) per milliliter [20] and the sought-after culturing conditions have to be known, which is often not the case.

As an advancement automation in enumeration methods can be very useful to reduce the time needed for the preparation of media, serial dilutions, counting colonies, etc. Many improvements in this field have been made that permit laboratories to increase the efficiency and the number of samples processed such as agar preparation machines, automated dilutors, automated counting devices and spiral plates.[22] In addition, different selective media can be used to detect particular bacteria species. They can contain inhibitors (in order to stop or delay the growth of non-targeted strains), particular substrates that can only be degraded by the targeted bacteria or that confers a particular color to the growing colonies.[23] Detection is then carried out by using optical methods.[17]

1.2.2 Molecular based Methods

Two bio-chemical methods, i.e. polymerase chain reaction (PCR) and fluorescent hybridization (FISH) are in particular relevant for detection of bacteria. The selection of a specific DNA or RNA sequence, to serve as a probe or primer, along with the conditions for hybridization, is the determinant factor for the specificity of these molecular methods.

PCR was developed in the mid 1980s and is a nucleic acid amplification technology.[24] It is based on the isolation, amplification and quantification of DNA sequences including the targeted bacteria's genetic material. PCR is much less time-consuming than other techniques, like culturing and plating but still takes from 5 to 24 h to produce a reliable result, depending on the specific PCR variation used and does not include any previous enrichment steps.[17] However, it is prone to contamination and gives no information about the bacteria viability.

In FISH ribosomal RNA (rRNA) is targeted by labeled complementary oligo-nucleotide probes. The choice to target RNA instead of DNA results in a more precise and sensitive technique (higher copy numbers available) and the link to viability. In the elaboration of FISH, microbial cells are treated with appropriate chemical fixatives and then hybridized under stringent conditions on a glass slide or in solution with oligo-nucleotide probes. Like PCR, FISH is commercially exploited by detection kits for different pathogenic and non-pathogenic micro-organisms.[20] Nevertheless, it cannot be automated and is therefore cost-intensive.

1.2.3 Immunology-based Methods

All immunoassays are based on the highly specific binding reaction between antibodies and antigens. The selection of an appropriate monoclonal or polyclonal antibody is the determinant factor for the method's performance. Furthermore, usually any positive result for pathogens obtained with immunoassays is considered presumptive and requires further confirmation. The detection limit is approximately 10^4 to 10^5 cfu/ml, depending upon the type of antibody and its affinity for the corresponding epitope. Hence, for the enrichment step often a two-step procedure is needed. Several types of immunoassays are available in diagnostics. Enzyme linked immunosorbent assays (ELISAs)[25] and enzyme linked fluorescent assays (ELFAs)[26] are widely used. Furthermore, ELISA is the most established technique nowadays, and exploited in many biosensor applications. Mostly, a sandwich ELISA is used. It comprises different successive steps and combines the specificity of antibodies and the sensitivity of simple enzyme assays by using antibodies or antigens coupled to an easily assayed enzyme.[20] The detection itself takes 2 – 3 hours [27] and today many tests are available as robotized automated systems. In contrast, ELFA employs fluorescence for endpoint detection. Alternative immunoassays are the lateral flow devices (LFD) and immunomagnetic separation (IMS)[28], which is a sample preparation tool that has been developed for shortening the enrichment step prior to detection. Disadvantages of immunology-based methods are the need of labels and the hence resulting possibility of false positive results due to secondary antibodies or antigens binding to open well sites.[29]

1.2.4 Further Methods and Future Trends

Newer methods for the detection of pathogens are based on, for example, the utilization of bacteriophages [30] or the use of instrumental methods for the identification of bacteria. Physical parameters are measured by impedance or detecting cellular compounds such as ATP, protein and lipid derivates. Associated with that, the concept of so-called biosensors has arisen and is further highlighted in the next section.

1.3 Biosensors in Pathogen Detection

Biosensors are a generic term for several new technologies for the rapid detection of bacteria and other biological substances. The International Union of Pure and Applied Chemistry (IUPAC) defines a biosensor as "a device that uses specific biochemical reactions mediated by isolated

enzymes, immunosystems, tissues, organelles or whole cells to detect chemical compounds usually by electrical, thermal or optical signals".[31]

Biosensors detect, transmit and record information regarding physiological, chemical and biological compounds of a living environment with the help of a specific biological recognition element, the properties of which change upon binding of the compound. The three main classes of such elements, used in biosensor applications so far, are antibodies, nucleic acids and aptamers. Furthermore, in the detection of pathogenic bacteria, enzymes can be used to label, for instance, antibodies [32] or DNA probes [33] much in the same fashion as in an ELISA assay. For example technically, a biosensor is a probe that integrates a biological component with an electronic transducer thereby converting a biochemical signal into a quantifiable electrical or optical response.[34,35] Biosensors can be divided by several characteristics: For instance, depending on the method of signal transduction, into optical, mass, electrochemical and thermal sensors.[36] Furthermore, they can be classified into sensors with direct detection of the target analyte and sensors with indirect, i.e. labeled, detection. In the following sections a selection of these concepts is explained.

Biosensors combine high specificity and sensitivity, which allows the detection of a broad spectrum of analytes in complex samples matrices like, for instance, blood, serum, urine or food, aiming for a minimum of sample pretreatment.[37] Therefore, they are developed to detect the presence and amount of microorganisms in any given environment. This is important since another target in the development of new identification methods is the decentralization of the processes. Currently most microbiological tests take place in large stationary laboratories because complex instruments and qualified technical staff are needed, at the moment. In order to make detection of pathogens available for a multiplicity of humans and virtually anywhere including field conditions and far away from civilization, the development of portable biosensor technologies with "on-the-spot" interpretation of results is sought.[38]

1.3.1 Label and label-free detection of bacteria

Indirect detecting or labeled biosensors are those in which a preliminary biochemical reaction takes place and the products of that reaction are detected by a sensor. Examples for the employed techniques are fluorescence labeling, electrochemical immunodetection and sensors that transduce metabolic redox reactions into quantifiable electrical signals.

On the other hand, direct detecting or label-free biosensors are usually designed in such a way that a physical phenomena occurring during a biochemical reaction on a transducer surface is measured. Signal parameters such as changes in pH, oxygen consumption, ion concentrations, potential difference, current, resistance, or optical properties can be measured by electrochemical or optical transducers. Such advanced techniques operating without labeling the recognition element are, for instance, surface plasmon resonance, piezoelectric or impedimetric biosensors.[3]

Before a detection can occur, in many biosensors the biological sample has to be immobilized to the transducer surface. The use of antibodies for this immobilization in biosensors is currently more common than that of DNA probes. They are most frequently immobilized on a substrate, which can either be the detector surface or a carrier, by for example adsorption on gold, the avidin-biotin system or by self-assembled monolayers.[17] Nevertheless, an antibody area to be available in the first place, and the oriented immobilization of antibodies, are still challenging and sought.[170]

1.3.2 Optical Biosensors

Optical biosensors are probably the most popular types in bio-analysis due to their selectivity and sensitivity. They are particularly attractive for application in the direct (label-free) detection of bacteria and they have been developed for the rapid detection of contaminants [39], toxins or drugs [40] and pathogenic bacteria.[41] Optical biosensors are able to detect minute changes in the refractive index or thickness which occur when cells bind to receptors immobilized on the transducer surface.

Recently, fluorescence and surface plasmon resonance (SPR) based methods have gained momentum because of their sensitivity. Further optical techniques are bioluminescence, dielectric waveguides, ellipsometry, the resonant mirror, interferometer and ellipsometric techniques utilized for the development of a label-free instrument for detection of bacteria.

1.3.3 Electrochemical Biosensors

Electrochemical sensors have some advantages over optical-based systems. They can operate in turbid media, offer comparable instrumental sensitivity and are more amenable to miniaturization and simplification and hence reduction of costs. On the other hand, electrochemical methods show a slightly more limited selectivity than their optical counterparts. Modern electro-analytical techniques have very low detection limits (typically 10^{-9} M) that can be achieved using small

volumes (1 – 20 ml) of samples.[42] Furthermore, the continuous response of an electrode system allows on-line control.[3]

The electrochemical techniques are mainly based on the observation of electrical changes due to interactions occurring at the sensor-sample matrix interface. They are generally classified according to the observed parameter: current (amperometric), potential (potentiometric) or impedance (impedimetric).[17]

1.4 Applications of Biosensors

Biosensors may be applied wherever traditional and standard bacterial detection methods are limited in either viability-detection, time and/or selectivity and sensitivity. Hence, potential applications could be found in medical diagnostics, food quality control, environmental monitoring or defense industry. Thereby the exploitation of biosensors, especially for bacterial detection and disease treatment in clinical diagnostic, shows great opportunities in the fast and specific diagnosis of nosocomial infections and infectious diseases with regard to increasing antibiotic resistances. Unfortunately, in this field only few products have already been commercialized yet, like for instance the the blood glucose biosensor or the so-called piezo-electronic nose.

The most viable openings in food industry will arise where a biosensor can rapidly detect total microbial contamination in, for instance, diary products. The largest area of application for the environment lies in the development of biosensors for monitoring bacteria in drinking and waste water, rivers, reservoirs and supplies. The reasons for that are that water shortage and population increase will presumably be important issues in the upcoming century.

1.5 Desired Properties of Bacterial Biosensors

During the processes of specific binding and detection, even small causes may have large effects. For instance, the bacterial cell sensor sensitivity is often decreased due to fluid forces that have to be overcome before cells can reach the sensor surface for antibody capture.[43] Or, once cells are captured by a specific antibody, the antibody-cell-binding avidity must be able to withstand the effect of shear force created by the laminar flow.[44] Hence for the construction of a “good” biosensor several tasks, covering biological, chemical, physical and engineering issues, need to be fulfilled. The improvement on existing and the fabrication of new and advanced biosensors is a

multidisciplinary and challenging task. At this point some examples of sought-after properties are presented.

Compared to the standard techniques, a biosensors have to be reliable and effective when used in routine applications and the diagnosis of bacteria diseases in an early stage. The system must have the specificity to distinguish the targeted bacteria in a multi-organism matrix. Species and also strain selectivity are important because relative small morphological changes can already have profound consequence in the influence on human beings. The same accounts for the viability status of the pathogens. Hence a good biosensor should be able to distinguish between living and dead cells.[45] Thereby, the detection of a single bacterial cell in 1 to 100 ml of sample volume seems to be sought. Today, only antibodies seem to achieve this task,[16] but recent developments in aptamer syntheses are promising.[46] Furthermore, the readout process can be extremely simplified and accelerated if the target molecules, and therefore the bacteria, are physisorbed on a solid substrate.[47]

A biosensor must be adaptable to detect different bacteria and sensitive enough to detect them directly, on-line and without pre-enrichment. Furthermore, it should be designed in such a way that multiple analytes could be detected simultaneously and rapid enough to give real-time results.

Concerning assay time only a few minutes should be necessary to test a multiplicity of samples in a routine checkup. Hence, a highly automated format with no need of skilled operators is sought, especially if the potential biosensor should also be readily available in developing countries and independent from medical centers. Hence a compact and portable device is also needed. The principle should be as easy as possible, excluding labeling and reagent addition. Eventually, the biosensor must have relatively simple and inexpensive configurations, to make it affordable for as many people as possible. This can, for instance, be achieved if parts of the biosensor combine several functions, like being a filter and a transducer, at once.

Still there is no biosensor which can fulfill all those needs. For example, there is no biosensor system to date that has a bacterial specificity compared to the plate culture method, which is one of the crucial requirements of today's market. To distinguish between living and dead cells is also challenging.[3] Because of all those reasons, the development of new biosensors, which are able to overcome at least some of these issues and fulfill more of the tasks, is sought. The resulting motivation and aims of this thesis are presented in section 1.6.

1.6 Motivation and Aims

In the following sections brief motivations are given for the projects accomplished in the course of this work. The start is marked by "Label-free Detection of Microorganisms in an Integrated Biosensor Array", presented in chapter 4.

1.6.1 Label-free Detection

As explained in section 1.5 – "Desired Properties of Bacterial Biosensors", the fabrication of a biosensor is an intricate task and a multiplicity of issues, like a fast detection, selectivity and sensitivity, and robustness, have to be overcome.

In the multidisciplinary project, presented in chapter 4 – "Label-free Detection of Microorganisms in an Integrated Biosensor Array", surface chemistry, nanotechnology, micro-fabrication and biophysics should converge into an integrated portable detection system for bio-sensing applications. The project thereby focused on a fast and specific detection of bacteria without any labeling. As support a microporous inverse opal material (cf. section 2.3) was coated with a bioactive antibody layer to specifically bind bacteria. In the potential next step these bound bacteria are detected and identified by the place, and hence specific antibodies, they were bound to.

This platform technique should pave the way for a multiplexed bio-sensing array which comprises antibody-decorated, highly-ordered macroporous inverse opal (iopal) structures, able to detect several potential pathogens at the same time. Therefore, several compartments should be designed to address different bacteria strains by combining the corresponding antibodies on the inner walls of suitable 3D structures and the intrinsic size exclusion effect of the material.

Inverse opals were chosen because they feature a number of advantages for bio-sensing platform development. First, its porous nature and mono-sized cavities provide a superior specific surface area, homogeneity and eventually filtrating abilities. These are the ubiquitous sought-after properties for achieving the sensors' high sensitivity and reliability. Second, the sizes of the cavities and channels are tunable in a broad range (several tens of nanometers to several tens of micrometers), which offers an extreme flexibility in adapting to various sensing targets, a particular sought-after feature in microbial sensing due to their wide size spread. Third, the material being inverted has an extreme broad selection range. Material that enhances mechanical strength is particularly advantageous because of the following micro-fluidic integration. Silica is also often chosen due to its compatibility with the versatile process of silanization which results in, for

instance, amine or active ester terminated surface, providing the opportunity for bio-functionalizations. Together with a high specific surface area, it offers a high loading density for antibodies. Fourth, if the cavity and cavity opening sizes are selected according to the size of target species, the diffusion rate of the target species can be significantly decreased, and the residence time of the sample can be increased, which is another salient advantage compared to conventional planar platforms. And last, the fabrication of such a material is fast and inexpensive with a promising perspective to be scaled up into parallel processing, which may yield a parallel sensing platform.[48]

The specific biochemical recognition of bacteria to the surface was attempted by the employment of antibodies against the appropriate bacteria strain – in the presented work mainly *E. coli.*. Because the inverse opals consisted of glass, the establishment of a covalent antibody binding on a silica surface was sought.

In a potential follow-up project the sensing platform should be parallelized, i.e. several compartments of the inverse opal chip will be functionalized with specific antibodies against different pathogens. Hence, when a specific binding is detected, the presence of the according antigen in the applied solution will be detected, as depicted in Figure 1.1. The detection of the bound bacteria shall be accomplished with an appropriate method like, for instance, a Fabry-Perót resonator or another optical spectroscopy technique.

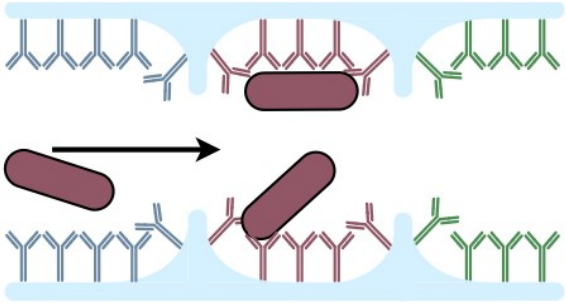

Figure 1.1 Schematic illustration of the detector principle. A bacteria strain is detected by the specific binding to its according antibody (red), which is covalently bound on the surface of an iopal (blue). Not to scale.

The presented identification system is a generic platform, which takes advantage of antibody technologies and which can be employed for virtually any infectious disease for which a microorganism has been annotated and for which a respective antibody is available. The development of such a detector device will lead to a label-free, quantitative and fast detection of microorganisms by antibody detection, therefore bypassing the time consuming and cost-intensive procedure of bacterial cultivation, DNA amplification and other conventional diagnostic methods, as delineated in section 1.2 – "Established Methods for Pathogen Detection". The important impact of porous silica materials for the label-free detection of bacteria in an optical biosensor was also described and underlined recently.[49]

1.6.2 Protein Microarrays

The two following sections should motivate the projects "2D Array-Patterning of Antibody Annuli" and "Structured Antibody Surfaces for Bio-recognition", later on described in chapters 5 and 6, respectively.

Specific adsorption of proteins from complex analytes such as serum, total cell extracts and urine at solid-liquid interfaces and protein microarrays constitute an essential element in the fields of genomics and proteomics.[50] In particular, microarray technologies enable the evaluation of tens of thousands of molecular interactions simultaneously in a high-throughput manner.[51] Hereby, the size as well as the density of the binding structure guarantee the high-throughput analysis and a large amount of information gathered per volume of sample.[52,53] Since proteins, in contrast to nucleic acids, can not yet be artificially synthesized, the development of protein micro- and nanoarrays for analyzing protein expression and functions of complex protein mixtures is of major significance.[54,55] Functional antibody arrays are often used for the detection of specific biomolecules and larger objects, such as viruses and bacteria.[56] Microarrays of antibodies as bio-recognition molecules have also been extensively used in sandwich assays.[57,58] Herewith high-density immunosensor arrays for investigating cellular based diseases and therapeutics can be developed. In addition, site-selective protein immobilization can be analyzed and controlled by modifying the topology of the surface [52,53,59], and the immobilization of antibodies on solid supports is an essential step in immunoanalysis and a prerequisite for a number of immunoassay formats.[60]

The in the literature described techniques for the patterning of protein microarrays can roughly be divided into lithographic techniques,[51,59,61] microspot printing [51,62,63,64,65] as well as methods

exploiting the chemical heterogeneity of surfaces.[51,66,67] Although these techniques have resolution limits down to the nanometer range, large scale crystalline patterning combined with a fewer-step and low-cost „bench -top“ process is still of further interest. For example, for large-scale microparticle templating, the already well-established technique of micro-contact printing, has gained large achievements [68,69,70] but also shows limitations. Typically a polydimethylsiloxane (PDMS) is used as the stamping substrate but allows only apolar inks due to its highly hydrophobic character,[71] limiting the use of biomolecules.[72] Furthermore almost all organic ink solvents cause a swelling of the PDMS stamp, hence changing its dimension.[73] Micro-contact printing can go down to 500 nm [72] but low aspect ratios can cause a “roof collapse“.[74] Consequently, if the quality of the stamp is decreased during printing the printed pattern as well as the reproducibility deteriorate. Micro-contact printing also has several limitations concerning biological application. In terms of length scale, block copolymer self-assembly has made recent advances in protein patterning with nano-size resolutions (30 nm) which is complimentary to the micrometer/sub-micrometer patterns.[75]

Furthermore, almost all protein array techniques lack the possibility to create annuli-shaped protein patterns. Mostly, only 2D flat samples are accessible, while 3D surfaces can be advantageous, since accessibility of antibody binding sites might be optimal. Certain analytes, especially spheroidal analytes, such as bacteria and whole cells, may be difficult to capture on the microarray slide’s flat surface but can be recognized by the curved surface structures.[76]

The complex phenomenon of protein adsorption onto a solid substrate is based on hydrophobic and electrostatic interactions of the proteins and the surface and can be tuned by many diverse intrinsic factors like surface chemistry, protein structure and concentration as well as surrounding factors like temperature, pH, ionic strength and fluidic conditions of the solution.[60,77,78,79,80,81] For example, it has been shown that the charge and polarity of the surface can alter the orientation of adsorbed proteins.[82] Also the way a possible washing solution is applied can have such a strong impact. Li et al. have recently shown that the stability of physisorbed IgG antibody nano-patterns strongly depend on the kind of substrate as well as on the flow rates and the time of fluid flow.[83] This strong physisorption dependance on different internal and external factors can be exploited to produce quality and durable patterns by optimizing the conditions during and after the adsorption process.

In this work, a novel, reliable and facile method for the production of large area hexagonal patterns of immobilized protein, i.e. for example, antibodies on the surface of a transducer, have

been realized. Hence, it bears the potential to serve as the bio-molecule recognition element of a future biosensor. A large-scale and annuli-shaped protein arrays without suffering from limited resolution or laborious and expensive operations should be produced. Consequently the protocol should be feasible for a broad variety of applications. The process is based on a drying lithography method and the evaporation of a solution of antibodies which afterwards form annuli ring structure around a two dimensional hexagonal structure of polystyrene latex particles (1 to 50 µm diameter).

1.6.3 2D Arrays of Structured Antibody Surfaces

The exploration of bioactive nanomaterials and -structures has gained much research interest, especially in the field of bio-diagnostics.[84] The underpinning biomolecular nanotechnology holds great promise for the development of new platforms with broad applications in the area of optics, electronics and catalysis.[85] In terms of device development, miniaturization and parallel fabrication processes are among the most sought-after features that contribute to efficiency enhancement and cost reduction.[86]

The novel patterning strategy for producing antibody annuli, presented in chapter 5 and by Wolf et. al.,[87] should be investigated more deeply and supported with further examples for bacteria and protein binding. Biological applications such as cell-based sensors and assays are based on the fundamental interactions between the biological systems and synthetic materials and surfaces.[88]

Considerable advancement in materials science is required to generate effective sensing platforms that organically integrate the functions of detector and transducer, such as bioelectronic devices [89] and sensing networks.[90] The development of a “universal” tool-set for constructing artificial biomolecular recognition surfaces [183] and for systematically attaching any kind of biomolecule to any kind of surface [91] has been identified as a promising approach. One possible tool for tailoring a surface with biomolecules or synthetic recognition molecules in the nanometer scale is dip-pen nanolithography (DPN) [59,92] which allows the positioning of molecules with 10 nm precision,[93] but has the intrinsic drawback of ink usage [94] and its inherent serial nature.[95] Therefore it is cost-intensive, time-consuming and incompatible with large-scale production. Nevertheless, DPN has led to the insight that a certain scaffold can mediate cell attachment processes [96] and that the physical shape and size of the surface features strongly affect the cellular attachment.[97] These findings have motivated further explorations for more effective and efficient methods to create

nanoscale features for bioactive patterning, such as co-polymer self-assembly [75,67,98] and silane functionalization.[99,100]

1.6.4 200 nm Size Exclusion Filters for Nano-Filtration

For many applications, including biosensors, the filtration of samples is important. Nano-filtration processes have a long history of providing a water quality superior to that obtained from conventional treatment technologies for organic and inorganic substances to be removed from sea- and ground-water.[101] The removal of natural organic matter is necessary for most production units, especially when surface water is treated, and can efficiently be done by nanofiltration. Furthermore, the removal of viruses and bacteria is extremely important during drinking water production, and is subject to many discussions. Traditional chlorination is still often applied as a disinfection method, but has some intrinsic drawbacks like the formation of disinfection by-products (DBPs) and the development of resistances to, for instance, chlorine.[102] Therefore nanofiltration might help to improve the disinfection process because it creates an extra barrier for viruses and bacteria.[103] It was also found that disinfection by removal of viruses is also possible but requires even smaller pore sizes.[104] Because bacteria have a typical size between 0.5 and 10 µm a complete removal by filtration through pores with less than 500 nm is theoretically possible.[102] Nowadays, it is generally assumed that bacteria are unable to pass through 200 nm filters, and filtration of liquids through such filters is a common and often-used method for the removal of microorganisms from heat-sensitive solutions. Such 200 nm filtrations are frequently referred to as “sterile filtration”.[105]

The main aim of this project was the development of a very flat porous material with the critical value of 200 nm pore size and a surface roughness of only a few micrometers. The reason for the low sought-after roughness was the combination of the transparent silica nano-filter with an optical read-out system for pathogens. It was developed by a collaboration partner of the Institut für Mikrotechnik Mainz (IMM) and necessitated a flat filter for its working principle. Colloidal particles can be utilized to construct three-dimensional periodic nanostructures by a self-assembly process (cf. section 2.3 – “Inverse Opals (iopals)). These self-assembled opaline lattices of colloidal particles provide a simple and fast approach to produce size-controlled nanostructures over a large area.[106] Therefore, porous filter structures should be constructed by inverse opals in conjunction with the IMM. Nevertheless, the emergence of cracks on inverse opals is well-known and constitutes a severe problem for filter materials, which needed to be overcome during this project.

A potential 200 nm size exclusion filter for bacteria, can be seen as an additional module of a final biosensor. By filtering special sizes and hence components, even very complex samples matrices like, for instance, blood, serum or urine, could be investigated with an integrated biosensor based on inverse opals, which would otherwise rapidly be blocked. Hence this project supports and perfects the outcomes of the other.

2 Materials

2.1 Chemicals and Compounds

In the following sections the chemicals used in the course of this work, compounds and solutions as well as used surface modification techniques are specified.

2.1.1 Preparation of Silane-Functionalized Glass Surfaces

In order to immobilize antibodies covalently to a glass substrate, it is necessary to bind anchor molecules with functional groups to the glass beforehand. For this purpose silane chemistry is widely used [175,107,108] and was also exploited in course of this thesis. Silanes are chemical compounds of silicon and hydrogen, which are analogues of alkane hydrocarbons.[109] They are capable of forming covalent bonds to silicon oxide groups on glass substrates and hence perfectly suited for the covalent functionalization of such substrates.

2.1.2 Silanization Reaction

The principle of a silanization is depicted in Figure 2.1, taken from [110]. The reaction mechanism for the chemical binding of silanes from a depleted solution to glass has been explained by several groups and is accepted for a long time.[111] Before the actual surface reaction takes place, a hydrolysis of the silanes occurs. The needed water is provided by the solvent which can, for instance, be water or toluene. Furthermore, most oxidic surfaces like silica carry a physisorbed water layer. The condensation of the silanol molecules formed through hydrolysis is introduced by the formation of hydrogen bonds among silanol molecules in several dimensions. In the next step hydrogen bonds are established towards silanol groups on the glass surface, hence leading to a first physisorption of the polymers to the substrate. By dehydration reaction a chemical siloxane bond (Si-O-Si) is created, therefore converting the physical into a chemical adsorption. To assure a complete formation of all possible siloxane bonds and associated with that a cross-linking of the single molecules, an elevated temperature of 80 ° – 120 °C is necessary. Eventually, the silanes is covalently bound to the substrate by a multiplicity of siloxane bonds. Short-chain silanes, which are easy to evaporate, can also be deposited from the gas phase. In this case the silane is together with

the substrate heated to the sought-after temperature in a closed vessel, and the reaction of the silanes with the surface takes place in one step.

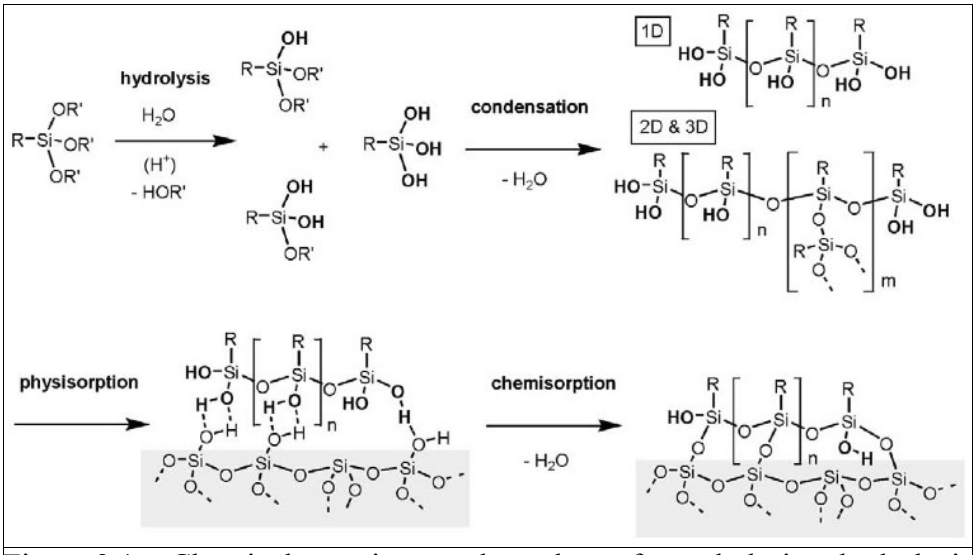

Figure 2.1 Chemical reactions and products formed during hydrolysis and adsorption of trialkoxysilanes. Scheme taken from [110].

In the presented work miscellaneous silanes were used for different purposes. They are summed up in Table 2.1. The used protocol was similar to the steps described above. The employed silane solution was, if not stated otherwise, about 1 mg/ml and the cleaned glass slides were immersed in it over night.

Abbreviation	*Name*	*Manufacturer*	*CAS Number*
APTES	3-Aminopropyltriethoxysilane	ABCR, Karlsruhe, Germany	919-30-2
OH-PEG-S	[Hydroxy(polyethyleneoxy)propyl]-triethoxysilane	ABCR, Karlsruhe Germany	–
Alk-S	n-Propyltrimethoxysilane	ABCR, Karlsruhe Germany	1067-25-0
MTMS	Methoxytriethyleneoxypropyltrimethoxysilane	ABCR, Karlsruhe Germany	132388-45-5
AE-S	11-Pentafluorophenylundecanoatetrimethoxysilane	Sikémia, Clapiers, France	944721-52-2

Table 2.1: Properties of employed silanes.

2.1.3 Chemicals and Solutions

Ultrapure water used in this work was prepared by a Millipore Milli-Q® element system to a resistance of 18.2 MΩ·cm. PBS (10 mM phosphate buffer, 2.7 mM KCl and 137 mM NaCl, pH 7.4 at 25 °C), Hellmanex® (alkaline cleaner concentrate, used concentration 2 % in H_2O) and Tween® 20 (non-ionic detergent, used concentration: 0.1 vol% in PBS, T20) were purchased from Sigma-Aldrich Chemie GmbH, Steinheim, Germany. Enhanced Green Fluorescent Protein (eGFP) was purchased from AMS Biotechnology (Europe), Frankfurt am Main, Germany. Human Integrin $\alpha_v\beta_3$ Purified Protein Octyl-β-D-Glucopyranoside Formulation, namely integrin, was purchased from Millipore Bioscience Division, Schwalbach, Germany. The membrane dye 1,1'-dioctadecyl-3,3,3',3'-tetramethyl-indodicarbocyanine perchlorate (DiD648) was purchased from Invitrogen, Darmstadt, Germany. The fluorescence DNA dye 4',6-Diamidino-2-phenylindol Dihydrochlorid (DAPI) was purchased from Carl Roth, Karlsruhe, Germany. 1,2-dioleoyl-sn-glycero-3-phosphocholine (DOPC) was purchased from Avanti Polar Lipids Inc., Alabaster, USA. BSA (Bovine Serum Albumin Fraction V, average molecular weights of 67 kDa) was purchased from SERVA Electrophoresis GmbH, Heidelberg, Germany. Chemicals not mentioned above were of reagent grade.

2.1.4 Other Materials

Standard glass slides by Menzel Glaser were purchased from VWR, Darmstadt, Germany and cut into sizes of approximately 26 × 26 mm^2. Piranha solution made of 75 % concentrated sulfuric acid and 25 % concentrated hydrogen peroxide. Polystyrene microparticles with a diameter of (0.967 ± 0.025), (10.45 ± 0.08), (19.71 ± 0.19), (50 ± 0,5) and (98.7 ± 1) µm were purchased from microparticles GmbH, Berlin, Germany and used in the provided concentration of 10 % (w/v) in water. Ludox® SM-30 colloidal silica nano-particles with an average diameter of 7 nm were purchased from Sigma-Aldrich Chemie GmbH, Steinheim, Germany. The PTFE trough used for the spin-coating was self-made in the institute's workshop.

2.2 Colloidal Crystals

So-called colloidal crystals were assembled with different techniques and for different purposes in the course of this work. In the following sections an overview of these types of crystals and their properties is given. The three utilized fabrication routes are explained in detail in sections

2.2.1 – “Spin Casting (SC)”, 2.2.2 – “Horizontal Deposition (HD)” and 2.2.3 – “Vertical Lifting Deposition (VLD)”. In between the correlations to the following sections, especially 2.3 – “Inverse Opals (iopals)” are pinpointed.

Colloidal particles are objects in the size range between 1 nm and 1 µm.[112] They constitute such versatile substances like cosmetics (e.g. hair spray), food (e.g. milk), dyes and inks (pigments), gels (e.g. gelatin), industrial products (e.g. aerogel) and are almost ubiquitous in the environment (e.g. air particulates). Due to the fact that spherical objects are much easier to synthesize than non-spherical particles, they and their fabrication play a pivotal role in colloidal science.

The close-packed arrays of spherical colloidal particles with a very small polydispersity (< 5 %) are called colloidal crystals. They are almost exclusively obtained by the self-assembly of adequate particles.[113] These crystals can be two- or three-dimensional. In 1909 Perrin described for the first time the formation of two-dimensional (2D) arrays of colloidal particles.[114] Because of their spherical shape the 2D arrays are typically in hexagonal order and the three-dimensional (3D) crystals face centered cubic (fcc). Due to their analogy in fabrication and characteristics, in the presented work the term colloidal crystal is also used for periodic lattices consisting of larger spherical particles up to 100 µm. A typical example for a 2D colloidal crystal of 10 µm polystyrene spheres is depicted in Figure 2.2.

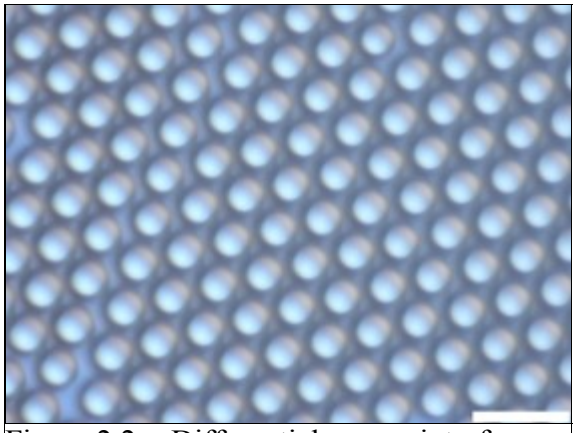

Figure 2.2: Differential interference contrast (DIC) image of a hexagonal structure of 10 µm polystyrene microspheres (PS-MS). (Scale bar: 20 µm)

Due to the periodic alternation in the dielectric constant and the occurring bandgap, phononic crystals have outstanding optical properties.[115,116,117,118] Furthermore, their ordered structure in the nano- and micrometer size makes them perfect templates and precursors for other structures with complex architectures and novel properties.[119,120] Such patterned structures are constituent parts in the construction of devices used in electronics, optics and sensors.[121,122] For example, the deposition of very small (nanometer size) colloids in the free voids of larger (micrometer size) host colloidal crystals and the adjacent displacement of the latter sacrificial template allows the fabrication of so called inverse opals.

In the present work mainly 2D arrays of polystyrene microspheres (PS-MS) colloidal crystals were produced. The several existing methods for their fabrication all have in common that the particles of the so-called internal phase are dispersed in the continuous phase. This is for polymeric colloids in the majority of cases water. Hence, the challenge is to get the spheres out of this unordered “milky” mixture into an ordered structure.

In the simplest technique the particles’ self-assembly into a hexagonal pattern is driven by gravity and called sedimentation.[123] During centrifugation an additional force is applied in the centrifuge and the sedimentation highly accelerated.[124] Alternatively the supplemental force can be generated by a stream of the continuous phase as it occurs during filtration. In this case the dispersion is extruded and the colloidal particles deposit on a membrane the pores of which are smaller than the diameter of the sedimented spheres.[125] Another possibility to induce self-assembly is the exploitation of the fact that the colloids are stabilized by Coulomb forces. A constant or alternated electric field is applied perpendicularly to the substrate on which the particles should be assembled. The direction of the field either enhances or counteracts the effect of gravity and therefore modifies the assembly velocity. On the other hand, an alternating field can create an ordered monolayer by continuously creating and destructing the particle layers.[126]

At the end of all methods mentioned until this point the remaining water has to be removed. This can take place by active or passive drying (vaporescence) or suction. In contrast to this, there exist techniques in which the colloidal particles arrange while the continuous phase is evaporating. One possibility is that during the application of centrifugal forces the solvent evaporates, which is called spin casting (SC). Another popular method is based on the convective flow of the particles to the exterior fringe of the wetted area. Depending on the size of the colloidal spheres, an exclusive aggregation in a ring-like structure can occur, which is called coffee-ring phenomenon.[127]

In the presented work this behavior was observed for particles smaller than 1 µm. To overcome this issue of sedimentation, the particle solution can be placed on a tilted or vertically mounted substrate. Thereby the particles flow due to an enhanced evaporation rate to a so-called crystallization edge. It moves during evaporation down the substrate hence creating line by line a homogenous film of ordered particles.[128] This technique can be further extended by actively pulling the substrate out of the colloidal solution, which is called vertical lifting deposition. The lifting speed constitutes another tunable parameter in addition to particle concentration, temperature and humidity, allowing control over the number of particle layers, quality and domain size.[129] In fact, although a multiplicity of self-assembling methods has been established, the existence of cracks, domain boundaries, colloid vacancies, and other defects is still an open question and a main problem for further applications of colloidal crystals, also in the present work. The difficulties in producing and processing large areas of defect- and crack-free particle layers limit the dimensions of ordered domains and the performance thereof in many applications.[130] Therefore, different methods for the manufacturing were conducted during this thesis, each showing its own benefits but also disadvantages. This leads to the employment of different techniques for different purposes, like the creation of templates for antibody patterning, inverse opals or nanometer-size filters, described in detail later on.

Due to the simplicity of their application and the nonetheless convincing results, horizontal and vertical lifting deposition together with spin casting, were used in the course of this work. Colloidal crystals consisting of particles between 1 and 100 µm were fabricated. The corresponding methods are explained in more detail in the following sections.

2.2.1 Spin Casting (SC)

In order to create templates for the later antibody patterning a monolayer of polystyrene microspheres (PS-MS) with crystalline subareas, as shown in Figure 2.3,[131] was generated on a glass slide substrate. With this procedure it was possible to produce a circular two dimensional almost defect-free colloidal crystal of 10 µm PS-MS with an area in the order of 10 to 50 mm^2. The spin casting method is similar to the proceeding described by Ogi et al.[132] and Hulteen et al.[133], respectively. In contrast much larger polystyrene spheres (1 – 100 µm compared to 500 nm SiO_2 and 265 nm polystyrene particles, respectively) and, as substrates, simple and cheaper glass slides instead of sapphire were used.

Most investigations in the presented work were accomplished with 10 µm PS-MS. The selection of this size was based on the typical dimensions of potential applications in this work like vesicle and bacteria binding as well as the fabrication of inverse opals with a size multiple bacteria fit in.

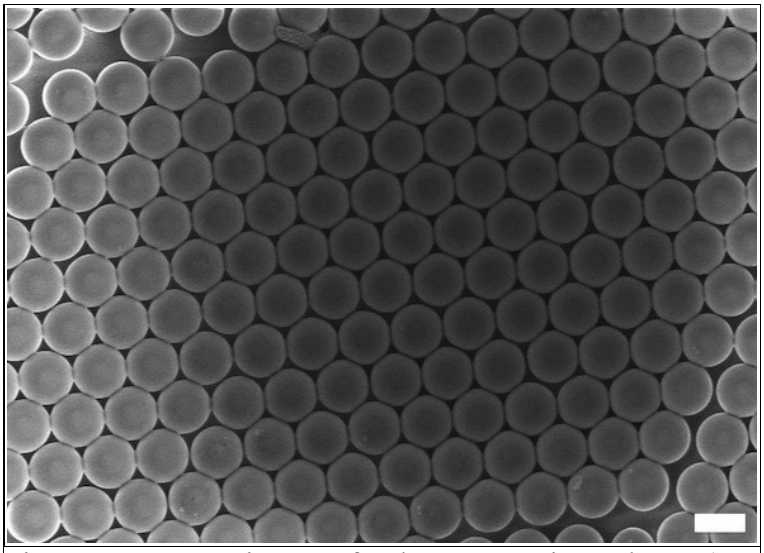

Figure 2.3 SEM image of polystyrene microspheres (PS-MS). The structure was annealed for 30 min at 100 °C for connecting the particles. (Scale bar: 10 µm)[131]

For the spin casting a custom-built polytetrafluoroethylene (PTFE) trough, similar to the one depicted in Figure 2.6, with an inner diameter of 16 mm was mounted on the spin caster (Delta 80 BM, Suess MicroTec) in order to provide a barrier for the relatively heavy particles. With the aid of that it was possible to press a 16 mm O-ring on a cleaned glass slide (Menzel Glaser, VWR). It was thereby crucial to tightly seal the space between the rubber and the glass by applying an extra force from above the ring through a plunger. Otherwise the liquid together with the particles would have flowed through and no ordered deposition of the particles would have taken place. Subsequently to the mounting procedure, cleaned glass slides were fixed firmly in the trough. Due to the rubber sealing between the glass slides and the trough walls, the former could work as the water-tight bottom of the trough. The PS-MS were received from the manufacturer (microparticles GmbH, Berlin) as a 10 % suspension in water and not further diluted. Between 10 and 20 µl of the solution were pipetted into the trough, which was immediately transferred to the spin caster and rotated at 500 revolutions per minute (rpm) for 15 min. Since for most further proceedings only a PS-MS

monolayer was sought, the applied volume of the suspension, i.e. the applied amount of spheres to the glass surface, had to be adjusted very exactly. A scheme of the spin casting process is depicted in Figure 2.4.

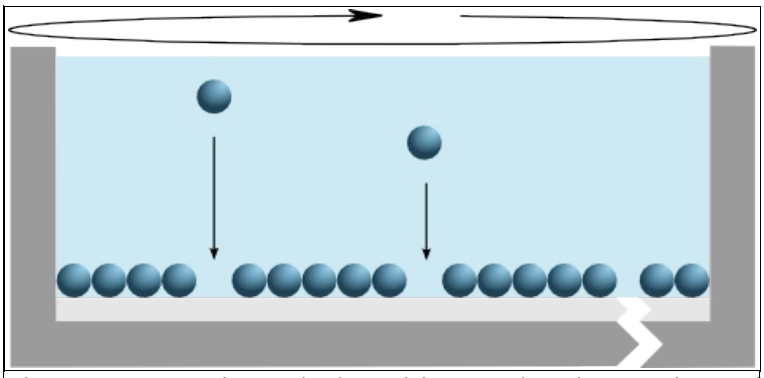

Figure 2.4 Horizontal deposition and spin coating of polystyrene microparticles on a glass substrate (light grey) in a teflon trough (dark grey).

In the following step, the monolayer of hexagonal close-packed PS-MS was dried at ambient conditions and annealed for 30 minutes at 100 °C, as reported by Denkov et al.[134]. The selected annealing temperature is moderately below the glass transition temperature T_G of polystyrene (110 °C), but possibly due to the small size of the microspheres, a certain gluing effect between the sphere and the glass substrate as well as among the particles was observed. Without annealing, the 2D colloidal crystals tend to dissolve when they encounter water afterwards, as for instance during antibody treatment in the potential next step.

Although spin casting is a simple and, for a single substrate, very fast method, samples need to be prepared one after another, which is very time-consuming for large amounts of substrates. Furthermore the strong centrifugal force and its radial gradient prevented the constitution of crystalline domains larger than approximately 50 mm². In addition, since the mass of the single PS-MS crucially affects the centrifugal force and hence the particle assembly, the rotational speed and time had to be adjusted exactly and separately for different particle diameters. Therefore other methods for the concurrent assembly on multiple substrates in conjunction with the constitution of larger domains and easy scalable parameters were sought, and are found in the next two preparation methods.

2.2.2 Horizontal Deposition (HD)

As an alternative to the aforementioned method, sedimentation was used to create many large colloidal particle monolayers in parallel, as depicted in Figure 2.5. Because in this case the substrate is assembled horizontally this technique is in this work also called horizontal deposition (HD), in particular to distinguish it from the next delineated method – the vertical lifting deposition.

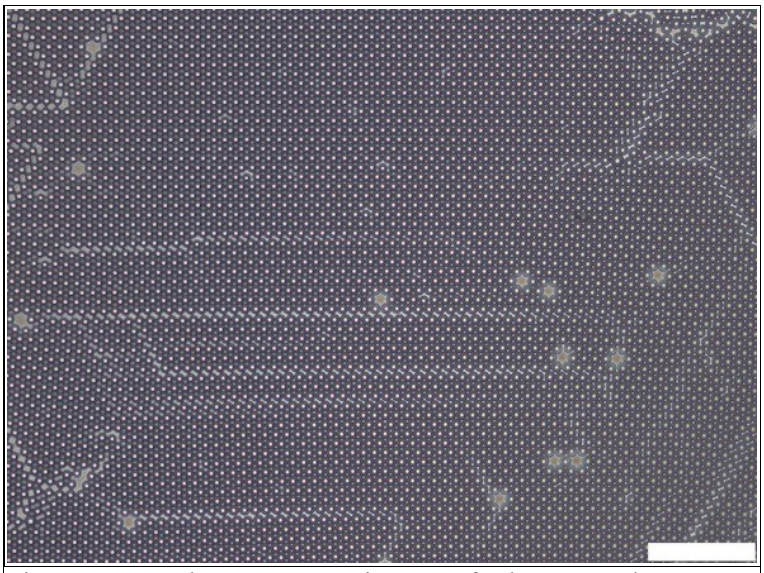

Figure 2.5 Phase contrast image of a hexagonal structure of 10 µm polystyrene microspheres (PS-MS). (Scale bar: 100 µm)

In the first step, a cleaned glass slide as the bottom was mounted in a PTFE trough similar to the one described in section 2.2.1 – "Spin Casting (SC)" and depicted in Figure 2.6. Subsequently, the top part of the construction was put on and tightly fixed to the bottom by four screws. In the next step, the sought-after volume of the particle suspension (18 µl for 10 µm PS-MS) was pipetted in a tube with ultrapure water, the volume of which was adjusted beforehand, so that the total volume was 370 µl. The depleted suspension was thoroughly mixed, instantly pipetted in the PTFE trough and let sediment and dry without any movement. According to the theoretical explanation, the self-assembly process that presumably finally creates a pattern structure of PS-MS consists of two steps. First, the water evaporates until the thickness of the water layer containing spheres approaches the diameter of the particles. Then the therewith created liquid menisci around the protruding tops of the spheres induce inter-particle attraction due to the water evaporating from them. The capillary forces cause a convective flow of the liquid and with it the particles toward the ordered regions.

This leads to the hexagonal close packed array of PS-MS.[134] Depending on the temperature and humidity this process lasted between one and two days. Afterwards, the PTFE trough was disassembled and the glass slides with the colloidal crystal monolayer annealed for 30 minutes at 100 °C as described before.

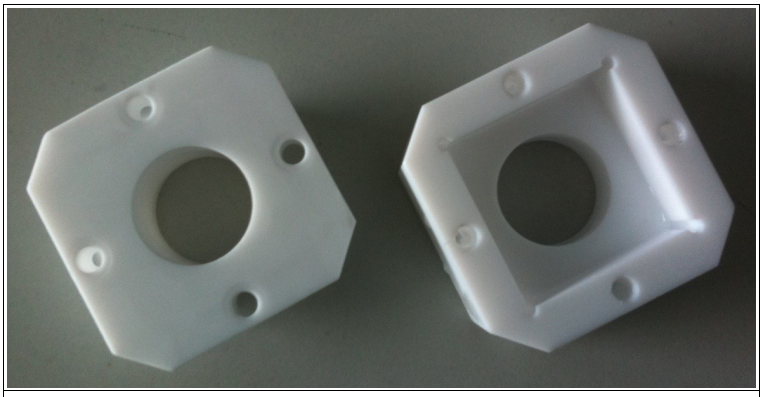

Figure 2.6 Image of two parts of a PTFE trough for the horizontal deposition of colloidal particles. A cleaned glass slide is placed in the bottom part (right) and the top part (left) is put on top and fixed with four screws.

The appropriate volume of particle solution had to be identified experimentally and was higher than theoretically calculated by geometrical considerations, because a certain amount of particles always remains in the pipette tip as well as in the tube. For instance, for a 10 % (w/v) suspension of 10 µm particles and the PTFE trough depicted in Figure 2.6, 18 µl PS-MS solution suspended in 352 µl ultrapure water were necessary to form a monolayer with as much as possible ordered domains. The volume of PS-MS, experimentally determined for one microsphere size suspension, could easily be conferred to other diameters by multiplying it with the ratio of the two particle batches. For example, at the same weight concentration a five fold higher volume of 50 µm particles is needed compared to 10 µm particles.

There existed mainly two advantages of sedimentation. On the one hand larger colloidal monolayers compared to the afore described spin casting technique could be created. The reason is that the whole glass slide inside the trough was covered, instead of only creating single ordered domains. On the other hand it was possible to fabricate many alike samples in parallel and with relatively low effort. Both characteristics made this technique a perfect tool when many similar samples were needed, for instance during the optimization of parameters in one of the following

steps like inverse opal constitution or antibody patterning. Contrariwise the spin casting led to smaller, but more ordered colloidal crystals. Therefore both techniques were used in parallel depending on the sought-after purpose.

The sedimentation of particles on a single substrate is a very facile but, due to evaporation, long lasting process (1 – 2 days). And because it is based on gravity, the effectiveness of the technique strongly depends on the density of the applied microspheres. The density of, for instance, polystyrene particles (1.05 g·cm^{-3}) is only a little bit higher than that of water (1.00 g·cm^{-3}, the continuous phase). Therefore the sedimentation process takes some time and must not be disturbed. In addition, the surface-to-volume ratio and hence the diameter of the particles are relevant since inter-particle and electrostatic surface forces affect the sedimentation process as well. For instance, with sedimentation no colloidal crystals of 1 µm PS-MS could be constituted. This led to the consequence of conducting at least for this size regime and potential applications in nanometer-size filters a third assembly method, the vertical lifting deposition. It could solve some of these problems and is described in the next section.

2.2.3 Vertical Lifting Deposition (VLD)

The direct, highly ordered constitution of small spheres of up to 1 µm on substrates can be achieved by drying the colloidal suspension on a vertical substrate or by the utilized vertical lifting deposition.[129,135] Therefore this third method was used in the frame of this work for the assembly of especially very small particles like 1 µm PS-MS.

The principle behind the conventional vertical deposition method can be explained as follows. when the substrate is immersed into water, a concave meniscus is formed due to the hydrophilicity of the substrate (glass, silicon, ceramic). The water evaporates faster near the meniscus and consequently a convective particle flow towards the substrate-suspension-air contact line occurs.[129] At some point while the water is evaporating, the liquid thickness gets lower than the diameter of the spheres, hence causing a concave meniscus between adjacent particles. It induces a surface tension which pulls the spheres together, therefore forming closed ordered structures, when the sample is pulled out of the suspension.

As the first step, the aforementioned cut and cleaned substrates were mounted vertically in a mechanical stepper (OWIS high precision z-stage Limes 60 in combination with a home-built control unit), which was capable of moving them upward by a speed down to 200 nm s^{-1}. The

apparatus was placed in a climate chamber for easily adjusting temperature and humidity. Following this, the mounted samples were by the instrument lowered completely in beakers containing 10 ml of the particle suspension (0.75 – 3 wt%). Finally the system was programmed in a way that the samples were lifted vertically with a speed of 200 – 800 nm s^{-1} until a height of 2 cm was reached, which took approximately 7 – 28 hours. The temperature was 20 °C and the relative humidity 50 %. A scheme of the vertical lifting deposition method is presented in Figure 2.7.

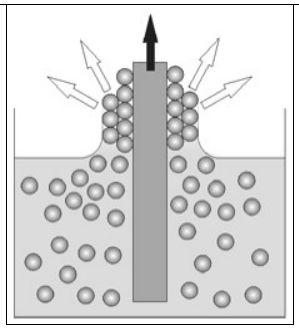

Figure 2.7 Schematic representation of the formation of colloidal crystals on a substrate by vertical lifting deposition. Image taken from [136].

Depending on the sought-after purpose, in the subsequent steps the colloidal suspension either consisted of 1 µm PS-MS in ultrapure water or a mixture of PS-MS and 7 nm silica colloids as the matrix for inverse opals. The so-called vertical lifting co-deposition, i.e. the simultaneous assembly of two different types of colloidal particles in one crystal, presents a very convenient preparation route to hierarchical structures, which only requires two fabrication steps, namely template particle and matrix co-deposition, and template removal.[136] Therefore, this technique was extensively exploited for the fabrication of inverse opals with cavity sizes of 1 µm and is presented together with a more detailed description of the method in section 2.3.2 – "Co-deposition" and its application in chapter 7 – "Size Exclusion Filters".

In order to adjust the number of particle layers and hence thickness of the colloidal crystal, the deposition can be controlled by the suspension concentration and lifting speed. The lower the concentration and the higher the speed are, the less number of particle layers are deposited. Furthermore the process is also affected by temperature and humidity but not that explicitly. In the presented work the concentration of PS-MS in ultrapure water was between 0.25 and 3 wt % and created together with the aforementioned speeds one to approximately ten layers of 1 µm particles.

When applied the concentration of silica nano-colloids in the PS-MS suspension was 0.3 wt %. Although this method led to relatively large domains of highly ordered crystals with only few defects, the formation of stripes on the substrate could not be prevented entirely. The reason was that the pinning of the meniscus limits the VLD for large area samples.[137]

The vertical lifting deposition combines both disadvantages of the aforementioned methods spin casting and horizontal deposition. Due to the complexity of nano stepper and climate chamber only a few samples could be created at the same time and the task, being with up to 28 hours, very time-consuming. Furthermore, the demand of 10 ml suspension, which could only be reused a few times, resulted in a high usage of particles. Also eventually, VLD became unsuitable for colloidal particles that were larger than a few micrometer. Beyond this size gravity starts to overcome the hydrodynamic effect caused by the meniscus motion. For such dimensions sedimentation is an alternative for forming colloidal crystals.

Nevertheless vertical lifting deposition generated the best colloidal crystals with regard to correctness and size of ordered domains. Furthermore only by vertical lifting deposition the fabrication of inverse opals with cavities of 1 µm could be realized. Therefore the technique was almost exclusively used in the last mentioned case.

2.3 Inverse Opals (iopals)

As stated in the last section 2.2 – “Colloidal Crystals”, the constituted patterns of microspheres were as one implementation exploited as templates for the assembly of so-called inverse opals (iopals). Generally, iopals are mostly fabricated by using colloidal crystal as template.[125,138,140]

In the following section a brief overview of this material class, and how it was created and utilized in the present work is given. Especially the two used fabrication techniques are delineated in sections 2.3.1 – “Sequential Deposition” and 2.2.3 – “Vertical Lifting Deposition (VLD)”. The first method was mainly used for the assembly of many similar samples for parameter optimization of larger inverse opals with cavities of 10 µm. The latter was employed for smaller structures with 1 µm diameter, which could exclusively be created by this approach.

Inverse opals are the three-dimensional inverted or negative structure of colloidal crystals. Consequently an exoskeleton-like structure of a certain material, which was in the case of this work glass, encloses cavities of a gas or liquid medium, in this case air and water. The structures are often referred to as highly-ordered three-dimensional (3D) porous structures, as shown in Figure 2.8A.

The concept is in the course of this work also used as a reference to two-dimensional (2D) highly ordered porous films, as depicted in Figure 2.8B. Such inverted structures can show a high degree of interconnected porosity (approximately 75 %) with extremely uniform and periodic distributions of pores due to the colloidal monodispersity. The average size lies normally in the range of 0.1 – 10 µm.

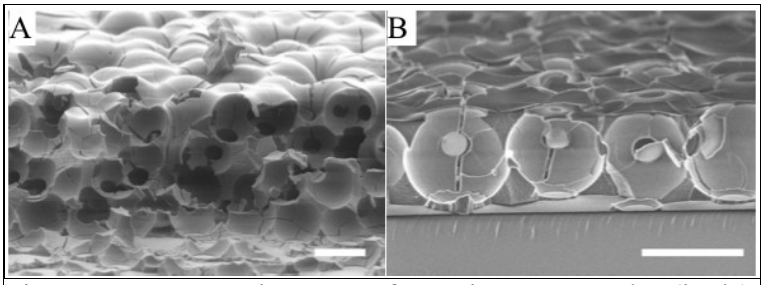

Figure 2.8 SEM images of an inverse opals (ipals), multilayer (A) and monolayer (B), assembled from 10 µm PS-MS. (Scale bars: 10 µm)

For the generation of inverse opals many materials and methods have been investigated in the past.[136] The conventional self-assembly of inverse opals from colloidal crystals occurs in three phases. In the first step, the sacrificial template for the final inverted structure is formed by a colloidal crystal as described in section 2.2 – "Colloidal Crystals". It is commonly made of polymer latex spheres. In the second step, this template is infiltrated by the matrix which is deposited and surrounds the template like a padding. Step one and two can take place simultaneously. This is called co-deposition. Eventually, in the third phase the colloidal crystal is removed selectively, leaving behind the aforementioned replica structure.

The easiest techniques for the second phase are co- and sequential deposition. They were exploited in the present work and are presented in more detail in the following two sections. The techniques have in common that large colloidal particles are encased, either simultaneously or consecutively, with very small colloidal particles in the nanometer size as filler and finally shell material. Alternative possibilities for the syntheses of porous materials, consisting of SiO_2, TiO_2 or Al_2O_3, can be sol-gel solutions as matrix precursors.[139,140,141] The inverted structure can also be established by infiltration of polymer [142], salt [143] and vapor phase precursors[144]. At the end of this step a solidification of the structure takes place.

The third and final stage, the removal of the colloidal template, can be accomplished by either dissolution with an adequate solvent, pyrolysis or chemical etching. For colloidal precursors made of polymer spheres like polystyrene, the first two methods are in principle feasible. Toluene or tetrahydrofuran can be used, for example, for the dissolving. The advantage of this method lies in the relatively gentle conditions which facilitate the preservation of the inverse structure. Both the template and the matrix can be composed of polymers if a solvent is available that specifically dissolves only the colloidal crystal. The technique's drawback is the fact that polymers swell before they are dissolved. Hence the matrix is exposed to an additional stress and cracks as well as other defects can evolve in compact structures. For this reason, the method is restricted to "soft" matrices. Due to the used material combination and its conveniences the second removal possibility, namely combustion, was exclusively used during this thesis. The arrangement of template and padding was heated to temperatures between 400 and 500 °C and the polystyrene colloidal spheres were burned away. In principle, the pyrolysis temperature has to be adjusted with respect to the material properties. Inorganic, like in this case silica, nano-particles constituting the matrix are sintered together at such conditions as an additional benefit of this technique, therefore leading to a stronger physical strength of the porous structure. The third method of chemical etching can, for instance, be used for colloidal templates composed of silica which is removed by hydrofluoric acid.

Inverse opals have been shown to be potentially useful in different fields, like photonics,[145] tissue engineering,[146] sensing,[147] and catalysis.[148] Although much progress was made to obtain ordered inverse opal structures over modest length scales, still many processes are plagued by the uncontrolled formation of defects over larger distances, hence limiting potential applications.[149,150] This severe problem also occurred during the presented work and could not be solved completely. Some approaches are presented in section 7.2 – "Anti-Crack Approaches". The reasons for this are capillary forces which are generated during the drying process after self-assembly of the template or after infiltration by the matrix material. They lead to additional cracks since the templates are mechanically very fragile. Several efforts have been made to strengthen the self-assembled structures by partial sintering or growth of necks between spheres.[151,152] Furthermore, if the colloidal crystal is, in the second step, infiltrated with too much of the matrix material the formation of an overlay can occur. On the other side, incomplete deposition can result in a structural collapse during template removal in the third step. Therefore, it was crucial during all steps of inverse opal fabrication to fine-tune the appropriate experimental conditions. They are highlighted in the according sections.

Among others, there are two main advantages of the material class of inverse opals, exploited intensively in different projects during this thesis. On the one hand inverse opals offer a large internal surface compared to the area of support. On the other hand the single cavities are uniformly interconnected with pores smaller than the cavities. Their sizes can easily be tuned by the diameter of the colloidal crystal forming microspheres and the conditions during the adjacent fabrication steps. As an estimation, the diameter of the cavities is one fifth of the precursor colloids.

In this thesis inverse opals were mainly created for two purposes: on the one hand the selected macroporous arrangement should, instead of conventional planar one, serve as the bacteria-binding substrate in a potential detector. Therefore, 10 µm PS-MS were utilized so that multiple bacteria with dimensions of 1 to 3 µm would fit nicely in the cavities. This concept is described in chapter 4 – "Label-free Detection of Microorganisms in an Integrated Biosensor Array". On the other hand, inverse opals with smaller cavity and conjunction sizes were intended as an alternative material for very flat nano-sized filters. In this case 1 µm PS-MS were used. The approach is illustrated in chapter 7 – "Size Exclusion Filters".

2.3.1 Sequential Deposition

Sequential deposition was one of the two methods used during this thesis for the fabrication of inverse opals, described in the previous section. In contrast to the other technique, co-deposition, delineated in the next section, the formation of the colloidal crystal template and their encasement with very small (nanometer size) silica colloids took place one after the other. The three principal steps of the manufacturing process are depicted in Figure 2.9.

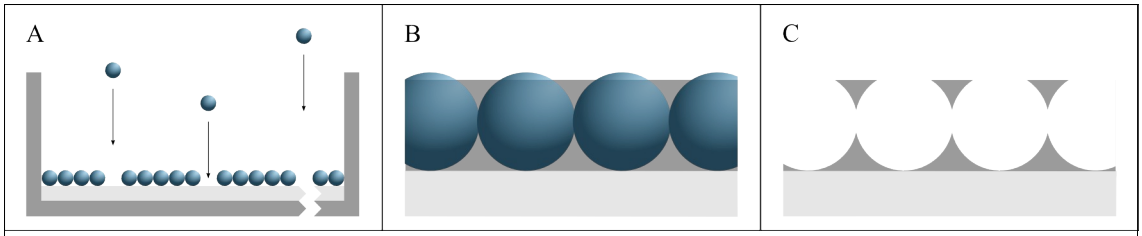

Figure 2.9 Schematic representation of the three sequential deposition steps: A) Template formation by colloidal crystal. B) Annealing and encasement by silica nano-particles. C) Template removal by pyrolysis.

After the polystyrene colloidal crystal was formed in the first step by one of the methods described in section 2.2 – "Colloidal Crystals", the template was tempered for 30 min at 110 °C,

which is slightly above the glass transition temperature (T_G) of that polymer (95 – 100 °C). Below that point it is hard and brittle but above it starts to become significantly softer because the polymer chains have enough thermal energy to slide past each other. Nevertheless, T_G is lower than the melting temperature T_m. Hence, the colloids still keep their physical shape but the connection points increase. Subsequently, the monolayer was cooled down again, and a suspension of 7 nm colloidal silica nano-particles (Ludox® SM-30, Sigma-Aldrich, 30 wt%) in 1 ml ultrapure water pipetted on it. For that purpose, the glass slide with the monolayer on top of it was mounted in a PTFE trough as already described in section 2.2.2 – "Horizontal Deposition (HD)". The amount of nano-particles in the suspension depended on the sought-after height of the final inverse opal structure and was usually in the order of 2 – 16 µl of a 30 wt % suspension. The solution was dried at 80 – 100 °C for about 2 – 6 hours. During this time the water evaporated and the silica nano-particles arranged around the polystyrene colloids, as depicted in Figure 2.9B and Figure 2.10. In Figure 2.10 larger colloids were incubated with too much nano-particles so that they were coated completely. This could lead to problems, as described in section 4.5 – "Inverse Opals Dimensioning".

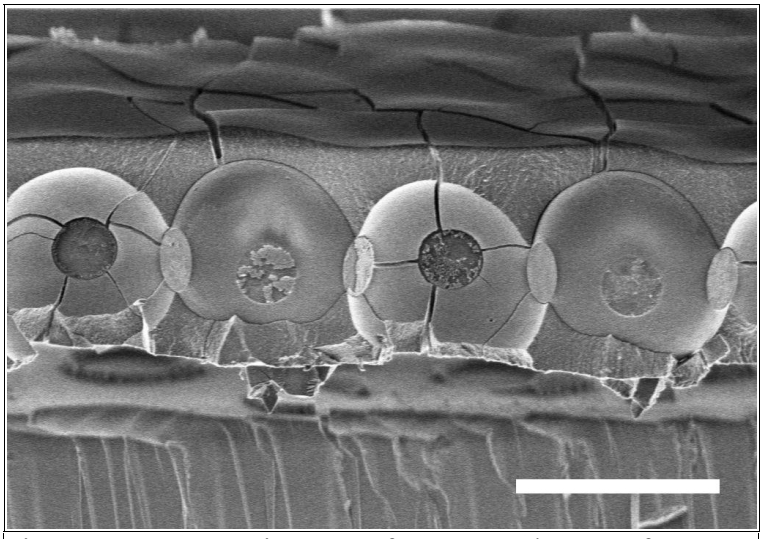

Figure 2.10: SEM image of a monolayer of 10 µm polystyrene colloids encased and overcoated with 7 nm silica nano-particles. (Scale bar: 10 µm)

After the encasement with nano-particles the colloidal crystals were removed and the silica sintered by annealing the structure at 400 – 500 °C for about 12 h. At this temperature regime the

polystyrene was combusted and the mere inverse opal structures were left over, as depicted in Figure 2.8, Figure 2.9C and Figure 2.11.

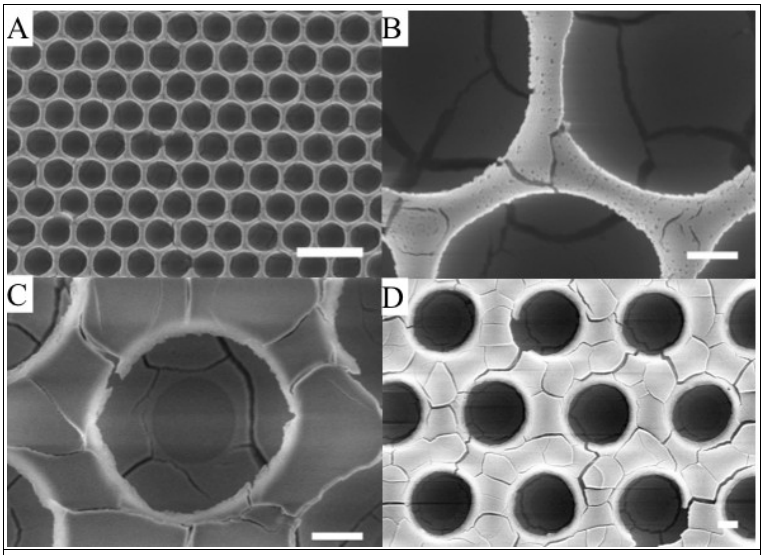

Figure 2.11: SEM images of inverse opals fabricated by sequential deposition from 10 µm PS-MS. In (A) and (B) less nano-particles were used than in (C) and (D). (Scale bars: 20 µm (A) and 2 µm (B – D)

The advantages of this technique compared to co-deposition was that the size of the pores connecting two cavities and the size of the openings on top of the structures could be tuned. Furthermore, these tunings could be conducted independent from each other. The first adjustment was accomplished by the tempering time and the second by the amount of employed nano-particles. Thereby less particles resulted in enlarged openings, as depicted in Figure 2.11A and B, and more particles in reduced openings, as depicted in Figure 2.11C and D.

The method of sequential deposition was almost exclusively utilized for the assembly of many similar larger samples with cavities of 10 µm. Associated with it the fabrication of inverse opals for use as the bacteria-capturing element in a potential biosensor was accomplished. This implementation is described in chapter 4 – "Label-free Detection of Microorganisms in an Integrated Biosensor Array".

2.3.2 Co-deposition

Co-deposition was the second method used for the fabrication of inverse opal structures in the course of this work. In contrast to the first technique, described in the previous section, the formation of the colloidal crystal and its encasement with silica nano-particles took place simultaneously and the different sized particles were jointly deposited on the substrate. The two principal steps of the fabrication process are depicted in Figure 2.12.

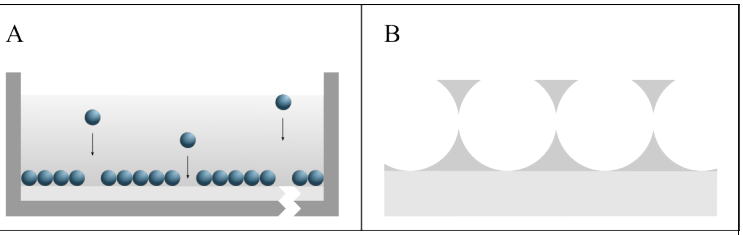

Figure 2.12 Schematic representation of the two co-deposition steps: A) Simultaneous template formation by colloidal crystals and encasement by silica nano-particles. B) Structure after template removal by pyrolysis.

The simultaneous template formation could either take place in a PTFE trough, similar to the technique described in the previous section, as depicted in Figure 2.12A, or by a method similar to the vertical lifting deposition. In both cases the colloidal suspension consisted of a mixture of PS-MS and 7 nm silica nano-particles (Ludox® SM-30, Sigma-Aldrich) as the matrix for inverse opals. The first possibility led for 1 µm PS-MS and 7 nm silica particles eventually only to very unordered structures. Highly ordered 1 µm inverse opals, as described in chapter 7 – "Size Exclusion Filters", could exclusively be created by a modified vertical lifting deposition technique (cf. section 2.2.3 – "Vertical Lifting Deposition (VLD)"). The substrate was, depending on the sought-after number of layers, pulled out of a suspension consisting of 0.25 – 3 wt % 1 µm PS-MS and additional 0.3 wt % silica nano-particles in ultrapure water. The lifting speed was 400 nm s^{-1}, the temperature to 20 °C and the relative humidity to 50 %. An example of results achieved by this technique is depicted in Figure 2.13A. Following both possibilities for template formation, the polystyrene got combusted and the mere inverse opal structures were left over, as depicted in Figure 2.12B and Figure 2.13B.

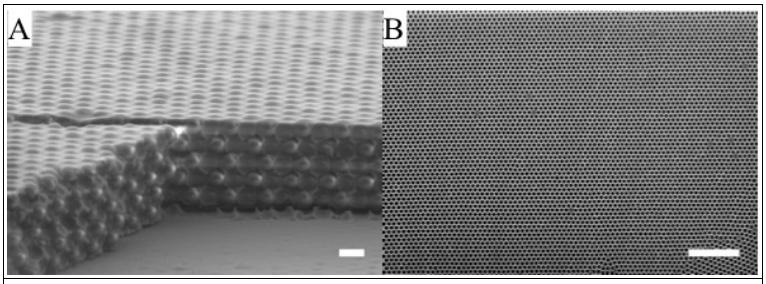

Figure 2.13 SEM images of 1 µm PS-MS encased with 7 nm silica particles (A) and top view of finished inverse opal after pyrolysis (B). (Scale bars: 1 µm (A) and 10 µm (B))

Co-deposition was also tested for the fabrication of inverse opals with cavity sizes of 10 µm. The process worked, but in comparison to sequential deposition, the dimensions of the openings could not be tuned. Furthermore, the technique resulted in very small openings with a diameter of about (3.2±0.7) µm on top of the resulting inverse opals, as depicted in Figure 2.15. Presumably, this distance was inappropriate for capturing bacteria in a potential biosensor application. Therefore co-deposition was exclusively exploited for the fabrication of individual inverse opals with cavities of 1 µm, as designated in chapter 7 – "Size Exclusion Filters", but not for the fabrication of 10 µm inverse opals.

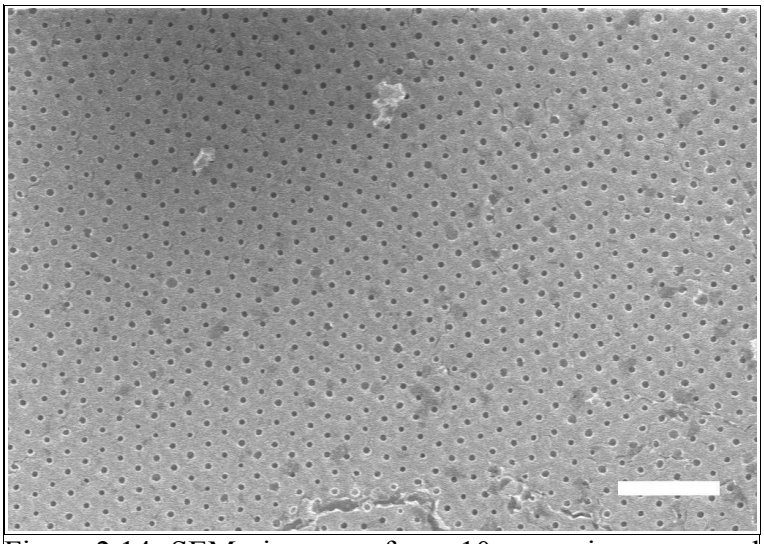

Figure 2.14 SEM image of a 10 µm inverse opal fabricated by co-deposition. The top openings have an average size of (3.2±0.7) µm. (Scale bar: 50 µm)

Alternatively, a sol-gel process was used in the course of this thesis for the production of inverse opals by co-deposition. The corresponding experiments are described in section 7.2.2 – "Co-assembly with Sol-Gel Precursor". A sol-gel process is also known as a chemical solution deposition. A chemical solution acts as a precursor, which is a metal alkoxide or metal chloride and can undergo hydrolysis and polycondensation. It solidifies as metal oxides in the sought-after porous shape. Therewith materials such as silica, titania, zirconia or alumina can be obtained.

The sol-gel precursor tetraethyl orthosilicate (TEOS) was used in the course of this thesis. 1 ml was mixed with 1 ml HCl (0.1 M) and 1.5 ml ethanol, stirred and added to 10 ml of a 0.1% solution of 1 µm PS-MS in ultrapure water. The solution was filled in a beaker and a cleaned glass slide pulled out of it and pyrolyzed as described beforehand.

2.4 Bacteria

2.4.1 Escherichia coli

The bacterium *Escherichia coli* (*E. coli*) was discovered by the German pediatrician and bacteriologist Theodor Escherich in 1885 and named after him in 1919, whereas c*oli* means "large intestine-based".[153] The bacteria are the most prominent representative of the *Enterobacteriaceae.* They are gram-negative, rod-shaped, facultative anaerobic and non-sporulating. *E. coli.* are about 2 µm long, have a diameter of approximately 0.5 µm and can prosper on a wide variety of substrates and under flexible environmental conditions.[154]

E. coli form a large and diverse group of bacteria and are classified as part of the *Enterobacteriaceae* family of *gammaproteobacteria*. A strain of *E. coli*, like the utilized K12, is a sub-group within the species having unique characteristics that distinguish it from other strains. These differences are often detectable only on the molecular level but may result in changes to the physiology or lifecycle of the bacterium. For example, a strain may gain pathogenic capacity, the ability to use a unique carbon source, the ability to inhabit a particular ecological niche or to resist particular anti-microbial agents. The bacteria cells have pili and many strains propel themselves with flagella arranged peritrichous as bundles rotating counter-clockwise and thus generating a torque to rotate the bacterium clockwise.[155]

The harmless strains of *E. coli* are part of the normal intestinal flora, and can benefit their hosts by producing vitamin K2, or by preventing the establishment of pathogenic bacteria within the intestine.[156,157,158]

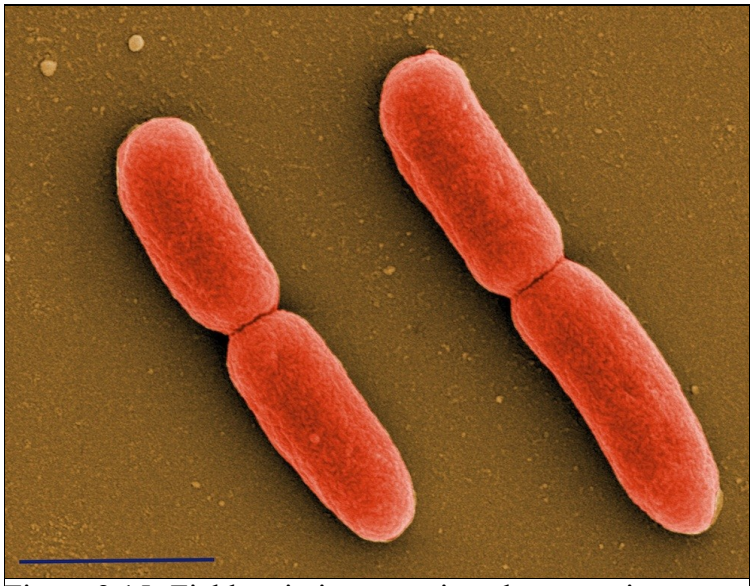

Figure 2.15: Field emission scanning electron microscopy (FESEM) exhibiting the rod-like morphology of *E. coli* K12. After fixation with formaldehyde and glutar-aldehyde samples were dehydrated with acetone, critical-point dried and sputter- coated with gold. Colorized. (Scale bar: 1 µm). Image taken from [162].

Although most strains of *E. coli* are harmless, among all bacterial pathogens it is a significant pathogenic bacterium and some strains such as the serotype O157:H7 can cause serious food poisoning in humans, and are occasionally responsible for costly product recalls. If ingested some kinds of *E. coli* can cause diarrhea, while others cause urinary tract infections, respiratory illness, pneumonia, peritonitis and other illnesses in immunosuppressed patients like children and elderly people.[13,159,160] In one of the most virulent outbreaks of *E. coli* in decades, fresh spinach was contaminated in multiple places in California in 2006. The outbreak presented a particularly virulent pathology in which 51 of the patients were hospitalized and 16 % developed hemolytic-uraemic syndrome (HUS) with kidney failure complications.[161] As mentioned before, *E. coli* naturally occurs in the intestinal tract of humans and warm-blooded organisms (*endotherms*), but due to its ability to

survive for brief periods outside the intestine, it is often used as a biomarker to detect fecal pollution of drinking water and food products.[14]

In the present work *E. coli* was chosen as the model bacteria because of several reason. It has a high biological and health care impact, is not very demanding and can easily be grown in *Lysogeny broth* medium (LB-medium, cf. section 2.5.1 – "Lysogeny Broth Growth Medium"). Eventually, a nonpathogenic strain (K12) is readily available for safe treatment in all kinds of performed experimental methods. The strain K12 is not a wild type, which is the denomination for an as normal classified peculiarity. Rather K12 is a so-called laboratory or security strain and genetically modified in a way that the bacteria do not possess pathogenic features any more. The strain is therefore prevalently applied in fundamental research and classified in risk group I. The morphology of *E. coli* K12 is presented in Figure 2.16, taken from [162].

2.4.2 Proteus Myxofaciens

The bacteria *Proteus myxofaciens* (*P. myx.*) was for the first time described by Consenza and Podgwaite in 1966.[163] In comparison with other members of the genus *Proteus,* the new species showed the unique feature of slime production. Therefore, the name *Proteus myxofaciens*, Proteus (Greek, very convertible), myxo (Greek, slime), faciens (Latin, producing), was proposed by the authors.

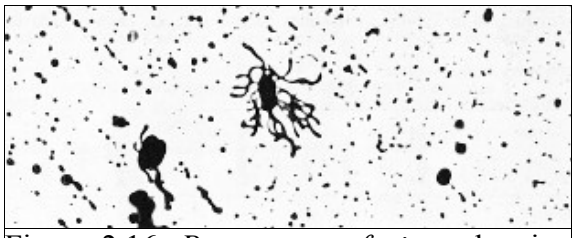

Figure 2.16: *Proteus myxofaciens* showing peritrichous flagellation. Leifson stain. 2000 x. Image taken from [163].

The bacteria was at that time isolated from living and dead gypsy moth larvae. It is motile, rod-shaped, gram-negative and averages about 0.8 µm in width by 2.0 µm in length. The bacteria show some analogies to the strongly exploited bacteria *E. coli* (e.g. being gram-negative, motile and rod-

shaped, and the growth medium). Hence in the present work *P. myx.* was chosen as the blank sample for *E. coli*. A typical flagellated cell is presented in Figure 5.8, taken from [163].

2.4.3 Klebsiella Planticola

As a second blank sample for *E. coli* and consequently an alternative forco-assembly*Proteus myxofaciens,* the bacterium *Klebsiella planticola* (*K. pla.)* was chosen. It is named after the bacteriologist Edwin Klebs and belongs to the genus *Klebsiella* and is like the two other used bacteria strains gram-negative, rod-shaped and like *P. myx.* surrounded by a mucilage capsule. But in contrast to it, *K. pla.* is non-motile.[164,165]. Hence with this blank sample it could be proved whether the interaction of the living bacteria with a surface depends on their motility. A typical sign of *Klebsiella* is a lubricous film which is formed on top of the colonies and presented in Figure 2.17, taken from [167].

Bacteria belonging to the genus *Klebsiella* frequently cause human nosocomial infections. It is seconded only by *E. coli* as a cause of nosocomial gram-negative bacteremia, *K. pla.* can furthermore cause a wide range of other diseases like, for instance, pneumonia, urinary tract infections or septicemia.[166,167]

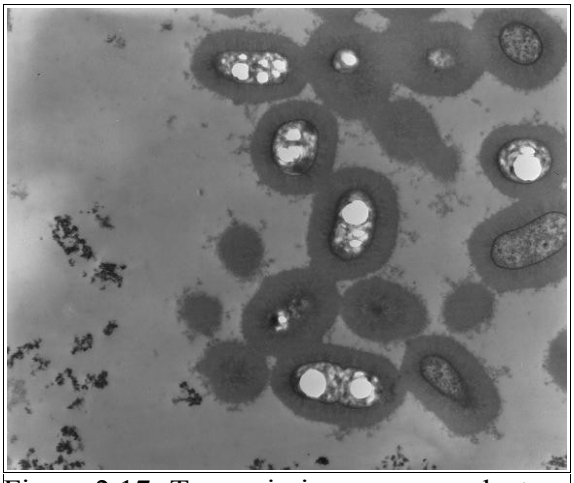

Figure 2.17: Transmission electron micrograph of *K. pneumoniae* cells surrounded by thick layers of fibrillous capsular material. Image taken from [167].

2.5 Bacteria Cultivation

2.5.1 Lysogeny Broth Growth Medium

All three bacteria strains were grown in lysogeny broth (LB) medium, which is eutrophic, commonly used for the growth of bacteria and an industry standard for the cultivation of *E. coli* as far back as the 1950s. It was created by Giuseppe Bertani and published for the first time in 1951 in his first paper about lysogeny.[168] There exist several formulations in use and in the presented work the following was applied: 2 g yeast extract, 4 g tryptone and 4 g NaCl were dissolved in 400 ml of ultrapure water. Subsequently, the solution was stirred until it was lucent, autoclaved at 121 °C to kill existing bacteria and finally stored at 4 °C. The medium was usable without any sign of decomposition or contamination for several weeks.

2.5.2 Long Term Storage

To have bacteria cells available for a long time at reproducible conditions, it was necessary to store the bacteria, once cultivated, for a long time in the frozen state. Therefore, previously published protocols were adopted.[169] In the first step, the obtained or purchased cells were cultivated at a concentration of about 1:1000 in 5 ml LB-medium in a rotary shaker incubator at 37 °C and 225 rpm for 16 h and stored at 4 °C afterwards. Subsequently, 1 ml of the bacteria suspension was mixed with 0,33 ml glycerol (heated up to 37 °C beforehand) in a cryotube, vigorously mixed by a vortex machine and rapidly frozen to -196 °C with liquid nitrogen. Finally all the cryotubes were stored at -80 °C in a freezer for subsequent usage. The 25 % glycerol in LB-medium worked well for storage purposes because it aids in avoiding protein denaturation. It prevents the formation of water crystal needles, hence minimizing the repeated freezing-thawing effect and thus extending the shelf life of the bacteria.

2.5.3 Cultivation for Experimental Use

E. coli K12, *P. myx.* and *K. pla.* were separately thawed from low long term storage (biomass optical density (OD_{600}) about 2.0, 25 % glycerol, -80 C,) and incubated at a concentration of 1:1000 in 5 ml LB-medium. For this purpose a rotary shaker incubator (37 °C, 225 rpm, 16 h) and the vials stored at 4 °C afterwards. With these conditions the bacterial biomass reached again an OD_{600} value of about 2.0. In the next step, the bacteria solution was diluted by a factor of 20 in PBS, Hence a

final OD_{600} of 0.1 and a bacterial concentration of approximately 2×10^7 cells ml^{-1} was achieved. If not stated otherwise, the bacteria were killed by heating them up to 90 °C for 30 min before applying the different solutions to the modified substrates. The samples were incubated for 1.5 – 3 h at 22 °C with the bacteria solutions, rinsed three times with PBS and investigated by the different mentioned methods.

2.6 Antibodies

Purified antibodies are used for multiple applications in research. These are, for instance, the identification and localization of intra- and extracellular proteins, the differentiation of cell types in flow cytometry and the separation of proteins in immunoprecipitation and electrophoresis. Furthermore, purified antibodies are employed in Western blot analyses or immunofluorescence. In the presented work antibodies were utilized for several tasks like the binding of eGFP, integrin vesicles (cf. section 2.8 – "Integrin Vesicle Formation") and bacteria, but also for the labeling and identification of the latter and the formation of annuli structures. Hence, they can be considered as parts of the central theme of this thesis. In the following sections some basic information about this remarkable class of proteins are given. Furthermore their structure is described, the principles of antibody-antigen-interaction elucidated and some possibilities for their immobilization to a solid substrate explained. Finally, the antibodies used in this work are summarized in a tabular form in which basic informations and properties are presented as well.

2.6.1 General Information and Structure

Antibodies, or immunoglobulins (Igs), are proteins that interact specifically with antigenic determinants (epitopes). They are found in the serum and other body fluids such as gastric secretions and milk. Serum containing antigen-specific antibodies is called *antiserum*. Immunoglobulins (Igs) can be separated into five major classes on the basis of their physical, chemical, and immunological properties: IgG, IgA, IgM, IgD and IgE. In most individuals, about 80 % of the serum immunoglobulins are the IgG proteins.[1] Therefore, and because they were exclusively used during the course of this thesis, the following description will focus on this class of antibodies. Nevertheless, some of the delineated properties hold also for the other classes. The structure of an IgG molecule is depicted in Figure 2.18.

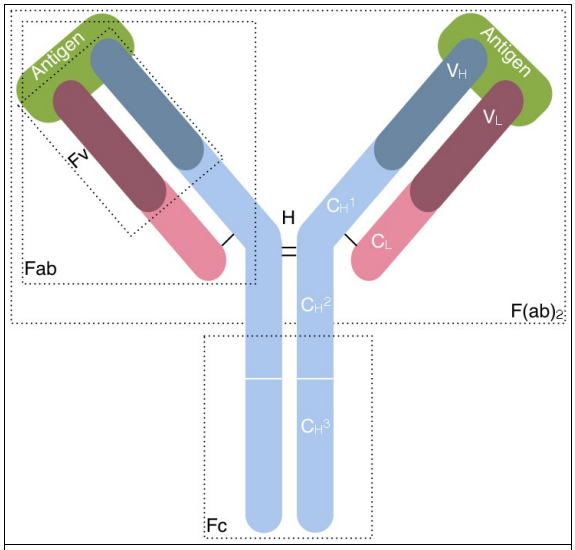

Figure 2.18 Schematic representation of an antibody molecule and its fragments. For detailed description, see text.

It has a molecular weight of about 150 kDa, contains two couples of polypeptide chains and is Y-shaped.[170] From top to bottom, the molecule measures about 10 nm [171] and the two arms are about 15 nm apart.[172] Each couple contains a heavy and light chain. The two heavy chains (blue) are linked by disulfide bonds and have a molecular weight of 50 kDa, the light chains (red) of 25 kDa.[173] The structure of IgG molecule comprises two fragments. The F(ab)$_2$ (fragment antigen binding) is used for binding specific antigens and contains two identical Fab fragments, which are held together by disulfide linkages in the hinge (H) region. A Fab fragment consists of the heavy (H) and light (L) variable (V) chains (V_H and V_L) and the constant (C_H^1 and C_L) chains. Other segments are the Fv (variable fragment) consisting of the V_H and V_L chains. The Fc (fragment, crystallizable) contains antibody-effector functions.[174,175] These are, for instance, complement activation, cell membrane receptor interaction and transplacental transfer.[176] Each light chain has about 220 and each heavy chain about 440 amino acids. Each heavy chain interacts with a light chain to form a functional antigen-binding site. Because it contains two binding sites and can bind two identical determinants, an IgG antibody is *bivalent*.[1] The other classes of antibodies differ from IgG by the structure of the heavy chain constant domains (Fc fragment). The process of antigen-binding and its causes are described in the next section.

2.6.2 Antibody-Antigen-Interaction

In immunology an antigen is defined as a substance to which a specific antibody binds with a dedicated affinity. Antigens are in the majority of cases proteins or polysaccharides.[177] Originally the term came from ANTIbody GENerator.[178]

The antigen-binding sites of all antibodies are formed by cooperative interaction between the variable domains of both, heavy and light chains.[1] The variable regions of the V subunits (V_L and V_H) form connecting segments, which occur in spatial proximity in the three dimensional structure. The specificity and affinity of antigen-binding-sites are determined by the sequence of these variable regions.[173] The interacting variable domains form a receptor that binds the antigen strongly but non-covalently. An antibody reacts only with subdomains of this antigen – the epitopes. Natural occurring antigens are mostly *multivalent*, i.e. they have multiple epitopes. An antigen-antibody-reaction is similar to a ligand-receptor- or enzyme-substrate-bond. The effective forces are steric complementarity, hydrogen bonds, van der Waals forces and hydrophobic interactions. The measurable strength of antibody-antigen-bindings is called *binding affinity*. A high-affinity antibody binds tightly to its antigen.

The production of antibodies by organism is a complex process and the main function of the humoral immune system. For research purposes, like in the presented work, specific antibodies are produced by injecting an antigen into a mammal, such as a mouse, rabbit or donkey. Blood isolated from these animals contains polyclonal antibodies – multiple antibodies that bind to the same antigen. To obtain antibodies that are specific for a single epitope of an antigen, antibody-secreting lymphocytes are isolated from the animal and immortalized by fusing them with a cancer cell line. The fused cells are called hybridomas, and will continually grow and secrete antibodies in culture. Single hybridoma cells are isolated by dilution cloning to generate cell clones that all produce the same antibodies, which are called monoclonal antibodies. Polyclonal and monoclonal antibodies are often purified using Protein A/G or antigen-affinity chromatography.[179,180,181]

Many biosensors, bioprocessing technologies and other immunoassays require for the antibody-antigen-interaction that one of the antibodies is immobilized onto a surface. This was also the case in the course of this work and is described in the following section.

2.6.3 Immobilization

The immobilization of antibodies is important for many applications like, for instance, two-dimensional polyacrylamide gel electrophoresis (2-D PAGE)[182] or multi-well enzyme-linked immunosorbent assays (ELISA).[25] Furthermore, the major type of immunosensors relies on the ability of an immobilized antibody to bind to its antigen.[170] In the presented thesis, the immobilization on a glass surface was a major step during development of bacteria-binding surfaces.

A variety of methods for antibody immobilization has been described in literature. Physical or non-covalent adsorption onto plastic, poly-lysine-coated glass or other surfaces seems to be the easiest method, and was also used partially in this work, but often suffers from random orientation and denaturation of immobilized antibodies, yielding poor reproducibility.[183] A more stable immobilization is obtained by covalent binding to chemically activated surfaces, which also yields better reproducibility. The coupling can occur through the reaction of lysine side chains. Proteins can be directly coupled to amine-reactive surfaces or they can be biotinylated using NHS-activated biotin and then immobilized onto streptavidin-coated surfaces.[184] Both techniques were exploited during this thesis. However, covalent immobilization can cause a direct chemical modification of the antigen-binding site, steric hindrance by the surface itself and adjacently immobilized antibodies. Furthermore, a disordered antibody orientation, resulting in the loss of binding capability and activity is possible.[185] It is known, that the main reason for reduction of binding capability is based on random orientation of antibody molecules and steric-hindrance induced by improper orientation.[186] In biosensors, the loss of sensor selectivity is mainly caused by random orientation of biological recognition elements.[187] It is expected that less than 10% of antibodies remain active when immobilized in a random orientation.[188] The possibilities of random orientation are depicted in Figure 2.19. Therefore, the development of a proper antibody immobilization method is strongly required to orient antibodies, to minimize steric hindrances and for the successful creation of immunosensors.[189]

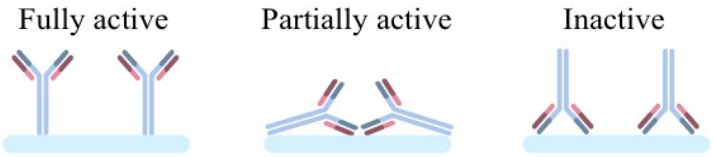

Figure 2.19 Ideal representation of IgG antibodies immobilized by random coupling procedure.

In the presented work, the proper immobilization of antibodies to different glass surfaces was a challenging problem to be addressed as well. Especially the search for an immobilization method, that kept the antibodies' conformation and the related ability to bind antigens and be labeled with secondary antibodies, and at the same time facilitates new ways of antigen-binding due to topological surface modifications, was challenging. To summarize, the employed methods comprised both physical adsorption (cf. chapter 5 – "2D Array-Patterning of Antibody Annuli") and immobilization by covalent coupling (cf. chapter 4 – "Label-free Detection of Microorganisms in an Integrated Biosensor Array"). They are described in detail in the corresponding sections.

2.6.4 Employed Antibodies

The miscellaneous antibodies used in the presented work are summed up in Table 2.2.

Abbreviation	*Antigen*	*Host*	*Clone*	*Conjugated*	*Manufacturer*	*Catalog-No.*
AbE1	*E. coli*	Rb	Pc	–	D	PA1-7213
AbE2	*E. coli**	Rb	Pc	–	B	E3500-06C
Ab-Cy2	Rb	Do	Pc	Cy2	D	711-225-152
Ab-Cy3	Rb	Do	Pc	Cy3	D	711-165-152
AbX-FITC	Mo	Do	Pc	FITC	M	AP192F
AbE-B	*E. coli**	Rb	Pc	Biotin	B	E3500-06D
AbK99	K99 Pili	Mo	Mc	–	T	MA1-10796
AbI-AF	HuI	Mo	Mc	Alexa Fluor 488	M	MAB1976X
AbGFP-DL	GFP	Go	Pc	DyLight™ 549	B	600-142-215

Table 2.2: Properties of employed IgG antibodies. Rb – Rabbit, Do – Donkey, Mo – Mouse, Go– – Goat, HuI – Human Integrin $\alpha_V\beta_3$, GFP – Green Fluorescence Protein, Pc – Polyclonal, Mc – Monoclonal, D – Dianova, B – Biomol, M – Millipore, T – Thermo Fisher Scientific, * O and K serotypes.

Two polyclonal antibodies with the general antigen *E. coli* and the host *Rabbit* were exploited, namely AbE1 and AbE2, whereas the latter was explicit suitable for the O and K serotypes of this bacteria strain. Since the strain used during this thesis was K12, both antibodies should bind to this strain and have adequate antigens. It needed to be tested whether these were located on the exterior of the bacteria, which was demanded. The corresponding experiments are presented in section 4.1 – "Antibody Specificity against E. coli".

Because both primary antibodies, AbE1 and AbE2, were not conjugated, secondary antibodies were needed to make them detectable. For this purpose Ab-Cy2 and Ab-Cy3, respectively were used. They are obtained from *Donkey* and should specifically bind to *Rabbit* antibodies, like AbE1 and AbE2. Ab-Cy2 is conjugated with the cyanine dye Cy2, having a maximum adsorption around 492 nm and fluorescence at 510 nm, therefore appearing green. Ab-Cy3 is conjugated with another cyanine dye, Cy3. It is maximally excited at 550 nm and shows a peak emission at 570 nm, hence appearing red. During the course of this work the excitation and detection of all fluorophores were conducted by fluorescence microscopy. The technique is described in short in section 3.2. The few exceptions, in which antibody detection was carried out by confocal microscopy are described in the accordant section 3.3.

To prove that the aforementioned secondary antibodies specifically bind to the primary antibodies, a non-specific antibody, namely AbX-FITC, was used as blank sample. It is likewise derived from *Donkey* but specific for *Mouse* antibodies. The antibody is conjugated with the fluorescein dye FITC, having a maximal adsorption at 492 nm and fluorescence at 520 nm.

For experiments with the biotin/streptavidin affinity system AbE-B was used. It is conjugated with biotin, originated from *Rabbit* and specific for *E. coli* O and K serotypes. Furthermore the monoclonal antibody AbK99 which is derived from *Mouse* and specific for the K99 pili of *E. coli* was used in some bacterial tests described in chapter 4.

Another monoclonal antibody, namely AbI-AF, was utilized during integrin binding assays. Its antigen is the *Human Integrin* $\alpha_1\beta_3$ and it originates from *Mouse*. Furthermore it is conjugated with the dye Alexa 488, being maximally excited at 495 nm and showing a peak emission at 519 nm, therefore appearing green. Due to its conjugation no further staining with a secondary antibody was needed in this case.

Finally, in experiments with the *Green Fluorescence Protein* (*GFP*) the antibody AbGFP-DL was utilized. It is derived from *Goat*, binds specifically to the aforementioned protein and is

conjugated with the fluorophore DyLight™ 549. Its maximal adsorption is at 562 nm and emission at 576 nm, hence appearing yellow.

All of the aforementioned antibodies were purchased from either dianova, company for biochemical, immunological and microbiological diagnostics, Hamburg, Germany, Biomol GmbH, Hamburg, Germany, Millipore Bioscience Division, Schwalbach, Germany, or Thermo Fisher Scientific, Bonn, Germany.

2.7 Antibody Structures

2.7.1 Antibody Annuli

The annealed PS-MS samples were incubated with AbE1 in concentrations ranging from 6.7 to 500 µg/ml and in varying volumes of either PBS or T20®. The treated samples were dried for the time periods, temperatures and humidities indicated in the text. Subsequently the microparticles were peeled off with the aid of adhesive tape.

2.7.2 Antibody Circle Structures

The microparticle template slide was cleaned by a 10 s bath in hot piranha solution, following fast rinsing in ultrapure water and ethanol. Afterwards the sample was incubated in a 1% solution of MTMS at ambient conditions and shook gently overnight. After 24 h the passivated slides were rinsed with ultrapure water and ethanol, annealed at 110 °C for one hour and subsequently cleaned by an ultrasonic bath in acetone for 15 min. The samples were incubated in a 25 µg/ml solution of AbE1 in PBS at ambient conditions overnight. On the next day they were washed once with a 16.7 mg/ml solution of BSA in PBS, incubated with 2.5 µg/ml solution of Ab-Cy3 overnight, rinsed once with PBS, T20® and ultrapure water, dried and visualized with the CLSM.

2.8 Integrin Vesicle Formation

In section 6.2 – "Cellular Mimics by Integrin Functionalized Lipid Vesicles", vesicles with membrane incorporated integrin molecules were required and their constitution is described at this point.

The general technique has been known for a long time [190] and the actual parameters used to obtain 100 nm vesicles are adapted from [191]. In principle, the vesicles were made by the extrusion of

lipid suspensions through the pores of polycarbonate membranes. A schematic illustration of the employed lipid 1,2-dioleoyl-sn-glycero-3-phosphocholine (DOPC) is presented in Figure 2.20, taken from [192].

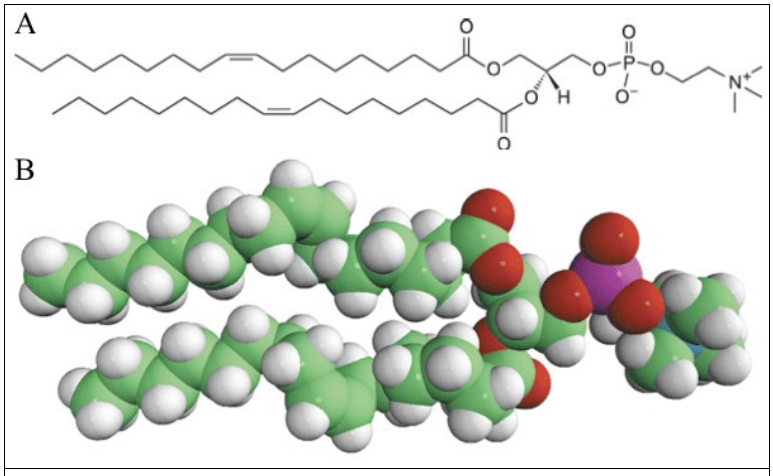

Figure 2.20 Chemical structure (A) and 3D illustration (B) of the lipid DOPC. Images taken from [192].

For the incorporation of integrin molecules in DOPC vesicles a 0.2 mg ml^{-1} solution of DOPC and, if needed, the fluorescent dye DiD648, in chloroform was vibrated in a 10 ml flask under a constant stream of nitrogen for 1 h. Thus the entire solvent was evaporated and the lipid covered the inner side of the glass flask. Adjacent after drying it was stored at 4 °C. The next day 300 µl PBS and, if needed, 10 µl of a 0.215 mg ml^{-1} human integrin $\alpha_v\beta_3$ solution were pipetted into the flask and vibrated several times over a period of 5 h at a temperature of 20 °C. In the next step the solution with the created integrin micelles was extruded 21 times through a 100 nm polycarbonate membrane, thus producing the required size of vesicles with and without incorporated integrin, respectively. 20 µl of the solution were pipetted on the modified substrates, covered with 1 ml of PBS and investigated by light and atomic force microscopy.

3 Methods

3.1 Phase Contrast Microscopy (PCM)

Phase contrast microscopy (PCM) is an optical microscopy illumination technique that converts phase shifts of the light passing through a transparent object into contrast variations. It was for the first time realized by Frits Zernike, resulting in his award of the Nobel prize in physics in 1953, and does not need any (fluorescence) staining, which is intricate and sometimes not applicable.[193]

Human eyes, as well as cameras are unable to detect differences in the phase of visible light. They are only sensitive to variations in the frequency, i.e. color, or amplitude, i.e. intensity, of the light wave. Unstained objects that are transparent and do not or only slightly absorb light are called phase objects because they slightly alter the phase of the light. Due to their index of refraction and/or thickness they usually retard the diffracted light by approximately ¼ wavelength. PCM converts these phase shifts in amplitude and respectively contrast changes. In positive or dark phase contrast, the undeviated direct light, passing through or around the specimen unaffected, arrives at a phase plate with a ring-shaped phase shifter attached to it at the rear focal plane of the objective. The narrow area of the phase plate is optically thinner than the rest of the plate. As a result, undeviated light passing through the phase ring travels a shorter distance in traversing the glass of the objective than the diffracted light does. Therefore it is speeded up by additional ¼ wavelength. When the direct undeviated light and the diffracted light proceed to the image plane, they are ½ wavelength out of phase with each other. In dark phase contrast the diffracted and direct light interfere destructively. The details of the specimen appear dark against a lighter background, just as they would for an absorbing or amplitude specimen.[194] Furthermore light and dark features can be found across the sample and fringes appear around regions with a change in optical density, for example, the boundary between water and cells, bacteria or inverse opals. This normally manifests as a light halo around a dark object.[195]

PCM is a mode available on most advanced light microscopes and is most commonly used to provide contrast of transparent specimens such as unstained and/or living objects. In the course of this work the inverted microscope IX70, Olympus Deutschland GmbH, Hamburg, Germany, was employed for imaging inverse opals, antibody structures and bacteria on these surfaces as well as on flat glass.

3.2 Fluorescence Microscopy

Fluorescence microscopy is an optical microscopy technique that exploits the phenomena of fluorescence (and more seldom phosphorescence) instead of or in addition to reflection and adsorption in standard transmitted-light microscopy.[196] It was for the first time described in 1852 by Georg G. Stokes when he observed that the mineral fluorspar emitted red light when it was illuminated by ultraviolet excitation. By now the technique has become an essential tool in cellular biology, material and life science due to properties that are not available in other contrast modes of traditional optical microscopy. It is possible to reveal the presence of a single molecule and to provide spatial resolution below the limit of diffraction.[197]

Fluorescence is based on the phenomena that certain materials, inorganic and organic compounds and organisms emit light at a specific (visible) wave length when they are irradiated with light of a shorter wave length. Therefore, in this technique the object to be studies is, after being excited, itself the light source. The samples can either be naturally fluorescent (primary or autofluorescence) like chlorophyll or some minerals, or being treated with fluorescing chemicals (secondary fluorescence).[198] Furthermore, it is possible to, for instance, multiply-stain different parts/organelles in a cell with different dyes and hence obtain a multi-colored image.[199]

In photoluminescence a susceptible molecule, which emits light from electronically excited states, was excited by ultraviolet or visible light beforehand. This phenomenon can formally be divided in phosphorescence and fluorescence. For the latter the emission of photons is nearly simultaneous (usually less than a microsecond) with the absorption of the excitation light. The brief interval is termed fluorescence lifetime. The process of phosphorescence occurs in a similar manner but with a much longer excited state lifetime. The fluorescence process occurs in three steps: First of all, the susceptible molecule is excited by an incoming photon. Then the excited electrons vibrationally relax to the lowest excited energy level. And finally, by emitting a longer wavelength photon, the molecule returns to the ground state.[200]

The basic function of a fluorescence microscope is to irradiate the specimen with the sought-after wavelength and to separate the much weaker emitted fluorescence from this specific excitation light. In a properly configured microscope only the emission light should reach the eye or detector so that the resulting fluorescent structures are superimposed with high contrast against a very dark (or black) background. The excitation light is typically several hundred thousand to a million times brighter than the emitted fluorescence.[201] The fundamental design behind and the optical path in a

fluorescence microscope are depicted in Figure 3.1. In inverted epifluorescence microscopes, widely used in life science, the excitatory light is passed from the side through an emission filter, deflected by a dichroic mirror, passed through the objective lens and finally onto the specimen. The light emitted by fluorescence is focused on the detector by the same objective. Since most of the excitatory light is transmitted through the specimen, only reflected excitatory light reaches the objective together with the emitted light, therefore giving an improved signal to noise ratio. An additional excitation filter between the objective and the detector filters out the remaining excitation from fluorescent light. The filters and the dichroic mirror are mostly mounted together in a cube and chosen to match the spectral excitation and emission characteristics of the fluorophore used to label the specimen.[196]

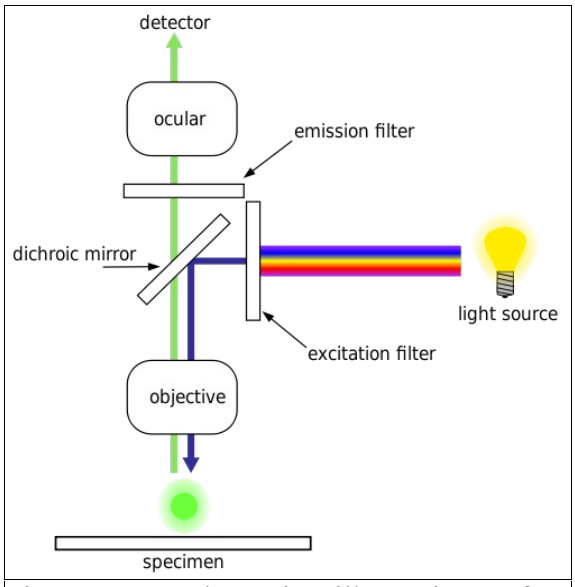

Figure 3.1 Schematic illustration of a fluorescence microscope. For detailed description, see text. Image taken from [196].

In the presented work the already in the last section mentioned microscope IX70 was used in inverted epifluorescence mode with several adequate filter sets. Both, antibody-stained bacteria as described in section 4.1 – "Antibody Specificity against E. coli", and different antibody structures, as delineated in chapter 5 – "2D Array-Patterning of Antibody Annuli", were thus investigated.

3.3 Confocal Laser Scanning Microscopy (CLSM)

Confocal Laser Scanning Microscopy (CLSM) represents one of the most significant advances in optical microscopy, described in the last sections, and offers several advantages over it. They caused a tremendous increase in the popularity of confocal microscopy in recent years.[202] It is widely-used in numerous biological and life science disciplines, from cell biology and genetics to micro- and developmental biology.[203,204]

The key to the confocal approach is a spatial illumination technique to eliminate out-of-focus light or flare in specimens that are thicker than the plane of focus. Therefore the recording of high-resolution optical images with depth selectivity is facilitated.[205] The principle of confocal microscopy is diagrammatically depicted in Figure 3.2, taken from [206].

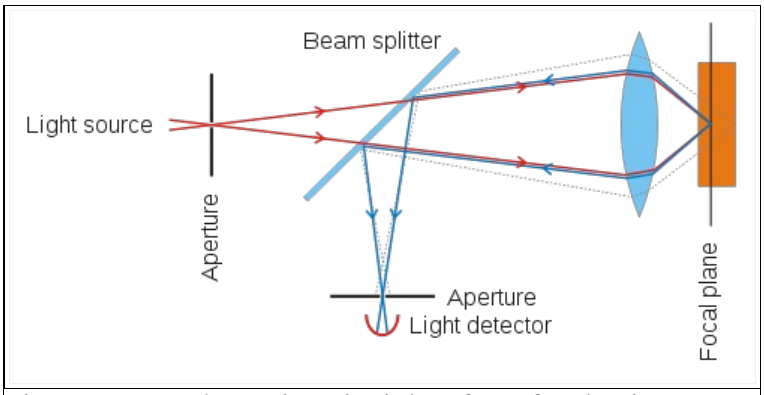

Figure 3.2 Schematic principle of confocal microscopy. For detailed description, see text. Image taken from [206].

Coherent light emitted by the light source (typical a laser system) passes through a pinhole aperture that is situated in the confocal plane with a scanning point on the specimen and a second pinhole aperture positioned in front of the light detector. Especially in biological applications, the specimen may be fluorescent. As the light beam is scanned across the specimen in a defined focal plane, light emitted from points on the specimen (in the same focal plane) passes back, is reflected by a beam splitter (dichromatic mirror) and focused as a confocal point at the detector pinhole aperture. The significant amount of reflected and scattered light that occurs at points above and below the objective focal plane is not confocal with the pinhole. Because only a small fraction of the out-of-focus fluorescence emission is delivered through the pinhole aperture, most of this

extraneous light is not detected by the light detector and does not contribute to the resulting image. As in a wide-field epifluorescence microscope, excitation and emission filter exist in fluorescence confocal microscopy and perform similar functions. In contrast to the direct concept of traditional wide-field epifluorescence microscopy, confocal requires amongst others multiple laser excitation sources, electronic detectors and a computer for image acquisition, processing and analysis.

In this thesis fluorescence confocal images of antibody structures, as described in chapter 5 – "2D Array-Patterning of Antibody Annuli", were investigated. Therefore another IX70 microscope in inverted confocal laser scanning configuration together with an FV300 laser scanning unit (Olympus Deutschland GmbH, Hamburg, Germany) was employed.

3.4 Atomic Force Microscopy (AFM)

Scanning probe microscopy (SPM) constitutes a family of microscopy forms of advanced techniques for surface analysis. A sharp probe is scanned across a surface and the probe-sample-interactions are monitored. The method is practically non-invasive. In comparison with other high-resolution microscopy methods like, for instance, scanning or tunneling electron microscopy (SEM and TEM, respectively) it provides additional capabilities. SPM offers the opportunity to measure in water and at ambient (physiological) conditions, still providing reliable measurements in the nanometer scale. Compared to conventional light microscopy it facilitates thousand times higher magnifications and resolutions.[207]

There exist more than ten SPM subtypes. The most common ones are scanning tunneling (STM) and atomic force microscopy (AFM). STM was developed by Binning, Rohrer, Gerber and Weibel at IBM in Zurich, Switzerland, in 1982. Four years later, in 1986, Binning, Quate and Gerber educed as a cooperation between IBM and the Stanford University the AFM. In the same year Binning and Rohrer got the Noble Prize in Physics for their invention.[208] Although scanning tunneling microscopy was invented first, the current progress in scanning probe microscopy of polymers is largely in the development of atomic force microscopy.[209] Since in the presented work the employed technique was also AFM, the focus is on its depiction.

By Atomic Force Microscopy the intermolecular forces between tip and sample can be measured with atomic-resolution and therefore allow the characterization of diverse materials, ranging from electronics and semi-conductors to polymers and bio-materials. As depicted in Figure 3.3, taken from [209], the AFM system basically consist of three parts: A micro-machined

cantileveprobe and a sharp tip mounted to a piezoelectric actuator, a laser and a position sensitive photo detector. The detection of the end-point of the laser beam provides a feedback of the cantilever deflection. The surface contour is scanned line by line and the microscope can be run in different modes which can be sorted by three systematics: 1) Either an image or a spectrum of the surface is created. An example for the last-mentioned are so-called force-distance curves. In this work only images were created. 2) If an adjustment setting by a closed-loop principle and a software control is existing the tip can either be maintained at a constant force or constant height above the sample surface. In the first case the height deviation and in the latter the deflection force can be monitored and illustrated in real time. 3) The kind of interaction used for the measurement. In this case one distinguishes between contact, non-contact and intermittent or tapping® mode. The three modes are depicted in Figure 3.4, taken from [207].

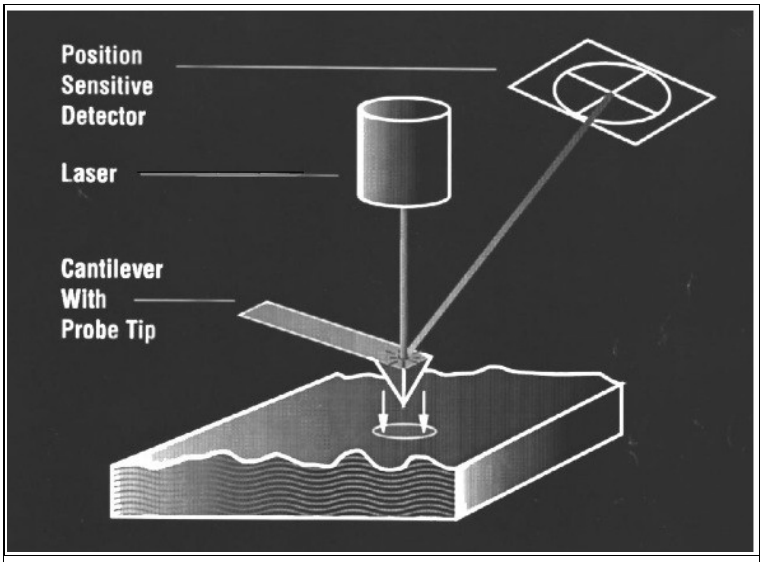

Figure 3.3 Schematic illustration of AFM operating principle. For detailed description, see text. Image taken from [209].

If the AFM operates in contact mode, the tip gets in contact with the surface through an adsorbed fluid layer on the sample's surface and the change in cantilever deflection is monitored. To maintain a constant deflection between the cantilever and the sample, and hence constant force between the tip and the sample, the scanner is moved vertically at each data point. A topographic image of the surface is created by plotting the distance which the scanner moves. This mode is

relatively unsusceptible to disturbances but can alter the sample by scratches. Therefore it is mostly used on hard and dry surfaces.

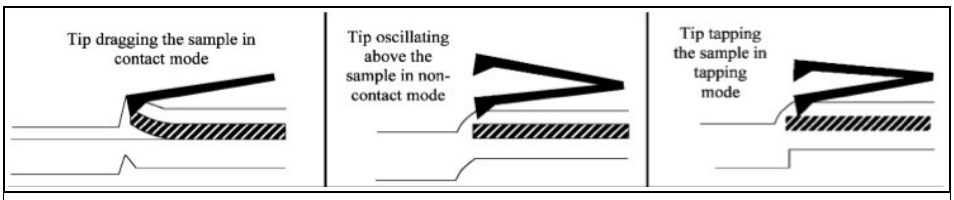

Figure 3.4 AFM closed-loop modes: Contact Mode (left), Non-contact Mode (middle) and Intermittent Mode (right). Image taken from [207].

In contrast to this in non-contact mode the cantilever oscillates slightly above its resonance frequency and with an amplitude below 10 nm. The tip does not contact the sample surface but the resonance frequency and hence the amplitude of oscillation is decreased by van der Waals and other long range forces extending from the surface. The feedback loop maintains the frequency and amplitude constant by vertically moving the scanner. Its position is also exploited to create a topographic image. This mode is not altering the surface and facilitates high-resolution images at low oscillation amplitudes but only on flat surfaces. Therefore it is mainly used for very soft samples like, for instance, biological cells. A disadvantage is that it is relatively susceptible to disturbances by the environment. Furthermore, a thin water film exists often between tip and surface because of humidity. Hence, the scanner does possibly not map the topography of the surface.

Finally in intermittent or tapping® mode the cantilever oscillates across the sample surface at or near its resonance frequency with an amplitude between 20 and 100 nm. Therefore the tip only slightly taps on the sample surface and contacts it only at the bottom of its swing. The feedback loop maintains in this case not a constant deflection but a constant oscillation amplitude and hence tip-sample interaction. Again the vertical position of the scanner is stored at each data point to create the topographic image of the sample surface. This mode constitutes a good compromise between the first two because the tip is only for a very short moment in contact with the surfaces. It is less sensitive to perturbations but also does not heavily alter the surface by scratches and so forth.

In non-contact and intermittent mode the cantilever can furthermore be excited with a fixed frequency, generating a phase shift between excitation and resonance. This shift depends on the mechanical properties of the surface and can be used to distinguish harder and softer materials independent from their topography.

In the presented work all images were taken in intermittent mode because it brings the aforementioned advantages when biological samples are examined without being very sensitive to external perturbations. Whether a certain image was taken in air or liquid environment is stated in the according part. 300 kHz silicon cantilevers (OMCL-AC 160 TS-W2, Olympus) were utilized in conjunction with a Dimension 3100 (Veeco, USA) and a NanoWizard (JPK, Germany) atomic force microscope. The taken images were processed with the software NanoScope (Veeco, USA) and Gwyddion (Open Source). In particular the images were flattened in first order, point and horizontal line errors were removed, and cross sections extracted from the indicated straight lines.

3.5 Scanning Electron Microscopy (SEM)

Scanning electron microscopy (SEM) is a microscopy technique in which micro- and nano-structured materials are scanned with a high-energy electron beam in raster pattern. The electrons emitted from the source interact with the sample atoms and are collected by a detector. Hence the measurement of the sample's surface topography, morphology, constitution and material properties, like for instance, electrical conductivity or crystallographic information is facilitated. Because electrons having a smaller wave length compared to photons, are utilized for the imaging process, smaller structures, down to several tens of nanometers, can be resolved and high resolution images obtained. The magnification in SEM can vary between 10 and 500,000 times. Furthermore, SEM has a large depth of field, which allows a considerable amount of the sample to be in focus at one time. The combination of high magnification and resolution, and ease of sample preparation and observation make SEM one of the instruments used most heavily in material and polymer research areas today.

A schematic illustration of SEM working principle is depicted in Figure 3.5, taken from [210]. A source, so-called electron gun, thermally emits an electron beam. Its energy typically ranges from 0.5 to 50 keV and it is accelerated toward the specimen using a positive electrical potential. The electrons are confined and focused, using metal apertures and magnetic lenses, into a thin, monochromatic beam. Furthermore the first condenser lens limits the amount of current. By passing

electro-magnetic lenses (pairs of scanning coils and deflector plates) in the electron column, the beam is deflected in the x-y-plane, hence scanning the aforementioned raster of the sample surface. When the primary beam strikes the sample, the electrons lose energy by repeated random scattering and absorption. Furthermore various reactions can occur in the bulk specimen, like the backscatter of electrons or the creation of so-called secondary and Auger electrons as well as X-rays. All these events can be detected and visualized by several different instruments inside SEM. Secondary electron detectors are common in all SEMs, but it is rare that a single machine would have detectors for all possible signals. After displaying a pixel the intensity of which is determined by the number of occurred events, the beam moves forward to its next dwell. The process is repeated until the raster scan is finished.[210,211]

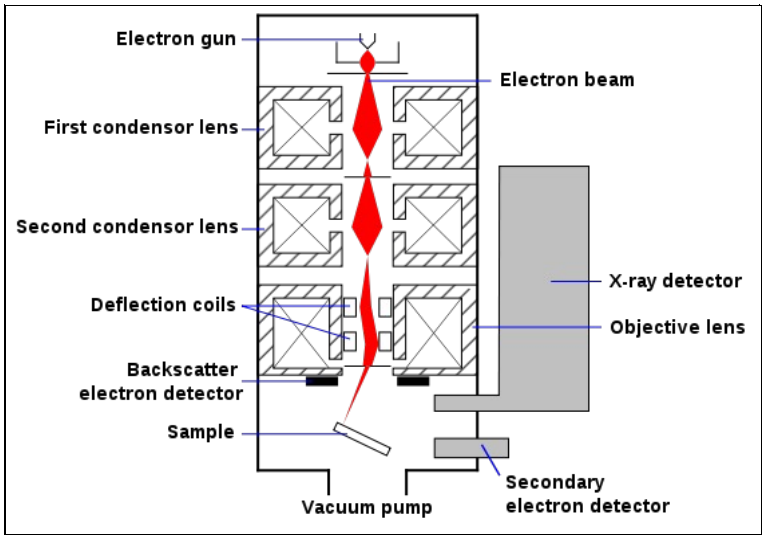

Figure 3.5 Schematic diagram of SEM working principle including scanning process and image formation. For detailed description, see text. Image taken from [210].

Depending on the applied voltage a distinction between conventional (10 – 35 keV) and low voltage (0.5 – 5 keV) scanning electron microscopy can be made. The advantages of the latter over the first are the reduced charging artifacts and a significantly improved topographic contrast.[212] The ability to produce quality images at low accelerating beam voltages furthermore minimizes beam damages to the sample and facilitates an operating window in which the sample does not build up negative charges. This obviates the normal requirement to coat samples with a conductive layer.[213]

In the presented work a Zeiss 1530 Gemini low voltage high resolution electron microscope with an In-lens/SE detection system was employed to gain mainly information about the structure and dimensions of inverse opals in the size of 1 to 10 µm. Furthermore, in one experiment bacteria, put on top of them, were investigated. In these cases accelerating voltages between 1 and 3 kV were applied and non-sputtered samples used. The instrument has a resolution limit down to 4 nm. Hence,it facilitates the investigation of the 7 nm glass spheres, which build up the inverse opal structure (cf. section 2.3 – "Inverse Opals (iopals)"). The taken images were processed with the software ImageJ (National Institutes of Health, Open Source) and the needed sizes and dimensions extracted.

3.6 Contact Angle Measurements

The evaluation of a surface's wettability by a contact angle can be a very sensitive measure for the surface's structure and constitution. For instance, the wetting with water provides information about the hydrophilic and hydrophobic properties of a surface.[214] The contact angle principle can furthermore be expanded to liquid/liquid, vapor/vapor and liquid/vapor interfaces.

If a flat and homogenous surface is wetted completely, a liquid film or, if the wetting is incomplete, a drop is generated. The shape of this drop of liquid is determined by the free energy of the surface, the liquid and the gaseous phase above. The tangential contact angle between the edge of the drop and the surface can be determined by, for example, a contact angle goniometer or a horizontal camera and image analysis. It is specific for any given system and described by the so-called Young's relation.

The contact angle can be used to investigate the interactions between the liquid and the surface. If there are no attractive forces, the angle will be ideally 180° and the drop a perfect sphere. As for water on a very hydrophobic surface like PTFE, the angle can achieve values close to 120°. In contrast to this, a liquid film is created for maximal interactions. Angles below 10° are hardly measurable. Hence, the value of the contact angle can provide a first indication for the kind of surface structure and, for instance, whether a surface functionalization with a hydrophilic of -phobic compound was successful.

In the presented work the measurement of the contact angle was used to obtain a first evaluation of the glass surfaces modified by silane chemistry. The drop shape analysis system DSA10-Mk2, Krüss GmbH, Hamburg, Germany, was employed.

3.7 Wester Blot

Western blot analysis represents an analytical technique typically used for the detection of specific proteins in a given sample or extract. Gel electrophoresis is utilized to separate denatured or native proteins by the length or by the three-dimensional structure of the polypeptide. The proteins are then transferred to a membrane (typically nitrocellulose or polyvinylidene fluoride), where they are detected using antibodies specific to the target protein.[215]

4 Label-free Detection of Microorganisms in an Integrated Biosensor Array

In the following sections the consecutive steps for accomplishing the task of binding bacteria specifically to an inverse opal glass surface are elucidated. As described in section 1.6.1, the aim was to fabricate an identification system as a generic platform, which takes advantage of antibody technologies and which can be employed for virtually any infectious disease for which a microorganism has been annotated and for which a respective antibody is available.

For this purpose, the retrieval of an appropriate antibody and a method for its covalent attachment to a glass surface are described in sections 4.1 – 4.4. Furthermore, the fabrication and modifications of the inverse opals are demonstrated in section 4.5, and proof of principle experiments with *E. coli* and antibody-modified inverse opals in section Fehler: Referenz nicht gefunden.

4.1 Antibody Specificity against E. coli

In order to bind bacteria by immobilized antibodies to a glass surface, the first step was to test whether the available antibodies are suitable for the sought-after task. The purchased antibodies were designated as specific against *E. coli* but without any further detailed information regarding the epitope. An essential prerequisite for binding bacteria to solid substrates is the antibody binding to the exterior of the bacterial cell wall.

The antibody specificity was tested by Western blot and is described in section 4.1.1. In addition, the existence of an antigen on the exterior of the bacteria cell wall was determined by immunofluorescence analysis, as stated in section 4.1.2.

4.1.1 Western Blot Analysis

In the presented work the Polyacrylamide gel-electrophoresis was charged with whole *E. coli* and probed with different combinations of antibodies, as depicted in Figure 4.1.

Lane A and E were charged with protein molecular weight markers SeeBlue® and MagicMark™, respectively. The corresponding scale is displayed on the left side of the picture. Lane B – D were charged with denatured *E. coli*. Subsequently, lane A was probed with AbE1 and Ab-Cy2, lane C

with only Ab-Cy2 and lane D with only AbE1. No signal was detectable for the control lanes C and D. In the case of C because Ab-Cy2 is not specific against *E. coli* and therefore washed off in the rinsing step during preparation. No signal was detectable for lane D because AbE1 is not fluorescent and hence not detectable by this method. Only if the applied bacteria were treated with both antibodies, AbE1 and Ab-Cy2, strong bands at about 5 and 40 kDa and weaker bands around, for example, 60 and 80 kDa were observable.

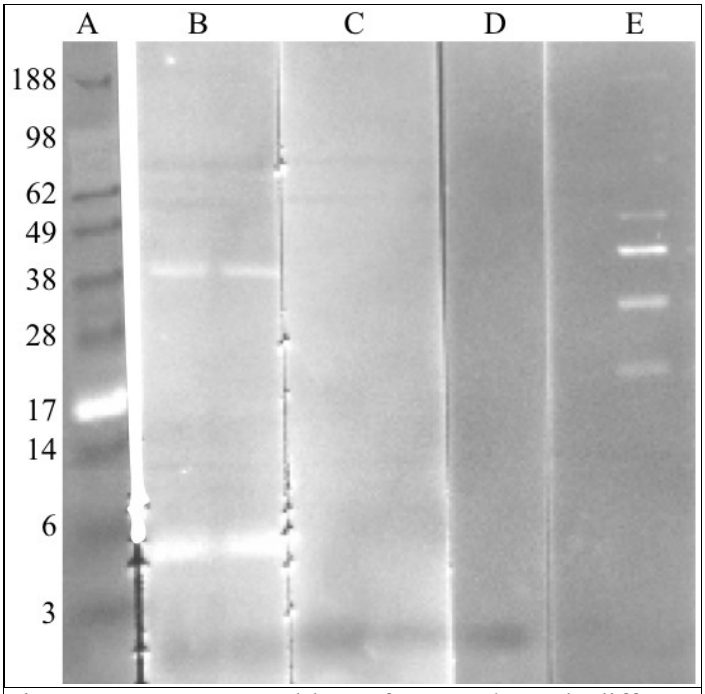

Figure 4.1 Western blot of *E. coli* and different antibodies. Scale: molecular mass in kDa. The following substances were added to the individual lanes: A) SeeBlue® marker. B) *E. coli* + AbE1 + Ab-Cy2. C) *E. coli* + Ab-Cy2, D) *E. coli* AbE1. E) MagicMark™ marker.

The Western Blot analysis showed two things. Firstly, AbE1 specifically binds to parts of *E. coli* and secondly Ab-Cy2 showed no cross-reactions with this bacteria strain, which was important for following blank samples. With this knowledge it was possible to locate the epitope of AbE1 on the bacteria cell, as described in the next section.

4.1.2 Immunofluorescence Analysis

In order to analyze the location of the *E. coli* epitope, the bacteria were treated with AbE1 and adjacently visualized with the fluorescent secondary antibody Ab-Cy3. Between the two steps and after the staining, the bacteria were centrifuged and rinsed. This was necessary to remove excessive antibodies. The resulting phase contrast as well as fluorescence images are depicted in Figure 4.2.

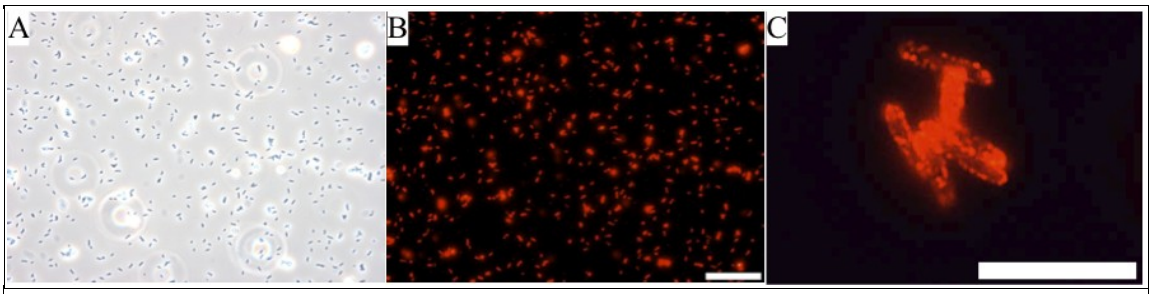

Figure 4.2 Microscopy images of labeled *E. coli.* A) phase contrast, B) fluorescence (570 nm), C) enlarged section. (Scale bars: 50 µm (A + B) and 10 µm (C))

In the phase contrast image, Figure 4.2A, the single intact bacteria were visible as small black ellipses, which are the fluorescence image clearly red, as depicted in Figure 4.2B. By the magnified image, Figure 4.2C, it is obvious that the antibodies AbE1, stained by Ab-Cy3, were at least localized on the extracellular parts of the bacteria cells. Hence it was reasoned that its potential epitope was also accessible from the outside.

With this test it could be shown that for intact *E. coli*, their AbE1 epitope is located on the extracellular side of the bacteria and externally accessible, which is a prerequisite for antibody immobilization on glass surfaces. In the next steps, the functionalization of the glass substrate was performed.

4.2 Antibody Binding by 3-Aminopropyltriethoxysilane (APTES)

The first attempts of antibody immobilization to a glass surface aimed on the direct covalent attachment of them. It was already shown that this possibility may provide stable surfaces with specifically oriented antibodies, provided there are unique moieties available for modification on the surface. But it was also found in some cases to result in lower activities of the immobilized biomolecules.[216]

Several different approaches started from glass surfaces functionalized with amine groups. For this purpose the aminosilane 3-Aminopropyltriethoxysilane (APTES), depicted in Figure 4.3A, was bound covalently by silane chemistry (cf. section 2.1.2 – "Silanization Reaction").

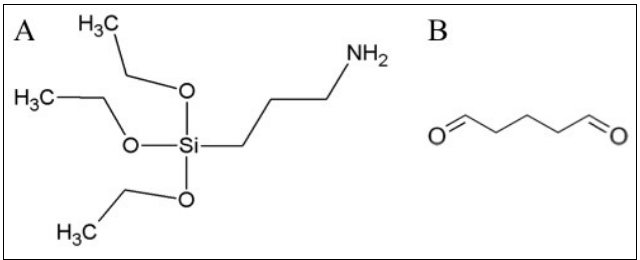

Figure 4.3 Chemical structure of APTES and GA

Starting from these amine groups on the substrate surface, different continuative functionalization steps were taken and are described in the following sections.

4.2.1 APTES and Glutaraldehyde

The idea of coupling two amine groups by a dialdehyde is known for a long time and has already been intensively exploited.[217] Thereby two Schiff bases are formed, which can be reduced in addition. Furthermore, the coupling of antibodies' lysine residues to surface amine groups by the dialdehyde glutaraldehyde (GA), depicted in Figure 4.3B, was described beforehand.[175] In the presented work this method should be used to immobilize AbE1 on cleaned and with APTES pretreated glass slides. Before the slides could be used, it was necessary to clean them thoroughly from residual organic contaminations which would otherwise circumvent the silanization procedure. In order to test which cleaning procedure was the most promising, the contact angles of the glass slides were determined afterwards and are reported in Table 4.1.

Cleaning step	*Contact angle*
uncleaned slides	(23.9±4.6) °
ethanol	(24.8±4.8) °
Hellmanex®	(14.6±3.9) °
Piranha	(15.2±3.8) °

Table 4.1: The different possibilities to clean a glass slide and the corresponding contact angles.

It is obvious that for a simple cleaning with ethanol, the contact angle only slightly changed. A clear change and accompanied with that the supposed cleaning of the surface could only be realized for a treatment with a 0.1 % solution of Hellmanex® or Piranha. The first is an alkaline cleaning concentrate and the latter a solution made of 75 % concentrated sulfuric acid and 25 % concentrated hydrogen peroxide. With Piranha, the surface was made hydrophilic and activated, i.e. the number of hydroxyl groups was maximized. The liquid, for instance, spreads more uniform as already described in literature.[132] Therefore, the glass substrates were either cleaned with Hellmanex® or cleaned and activated by immersing them in Piranha if a further activation was sought. This proceeding was carried out in all further experiments employing glass substrates.

To verify whether the surface functionalization was successful or not, the contact angle of differently modified substrates was measured. The results are reported in Table 4.2. It is evident that the values changed considerable compared to cleaned but untreated glass slides which showed angles below 20 °, as reported in Table 4.1. Also between APTES only and the additional step of glutaraldehyde modification a significant change in the contact angle of the surface from about 62 ° to 72 ° was visible. Therefore, it could be concluded that the GA was covalently bound to APTES.

Functionalization step	*Contact angle*
APTES	(62.4±5.2) °
Glutaraldehyde	(72.3±5.3) °

Table 4.2: The different steps of APTES-GA surface modification and the corresponding contact angles.

After the adjacent adding of antibodies (2 µg/ml in PBS) no additional reduction of the Schiff bases was performed in order to alter the structure of the proteins as little as possible. Subsequently, AbE1 was stained with Ab-Cy2 (7,5 mg/ml in PBS) and the modified glass slides examined by a fluorescence imaging system. The resulting image is depicted in Figure 4.4.

The glass slides treated with only AbE1 showed no fluorescence, which is reasonable because this antibody carried no dye. Furthermore, all three samples with stained AbE1 showed a fluorescence, and this was actually slightly stronger for APTES than for the other two. Hence, it could be concluded that the direct covalent immobilization by APTES and GA was not significantly higher than the simple physical adsorption of antibodies. This unspecific adsorption could not be prevented that easily and was presumably responsible for the fluorescence signal of

simple cleaned glass slides and those functionalized with APTES only. As a consequence, another possibility for the covalent immobilization of AbE1 was tested and is described in the following section.

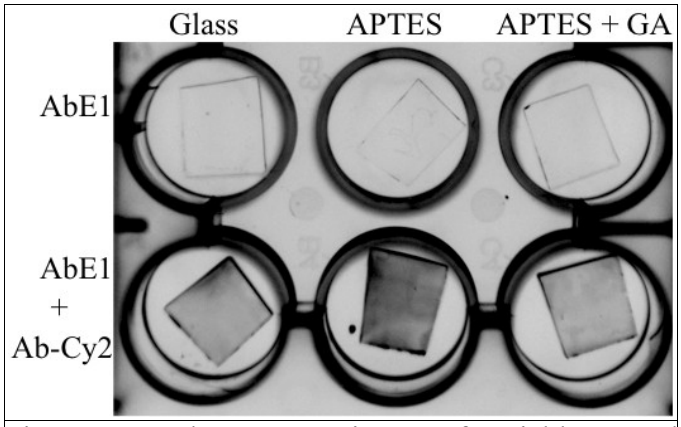

Figure 4.4 Fluorescence image of variably coated glass slides, incubated with AbE1 or AbE1 and Ab-Cy2 in PBS. Images taken with a Fuji LAS-3000 CCD-Imaging System.

4.2.2 APTES, EDC, S-NHS and PFP

As an alternative for coupling antibodies by their (amine) residues and glutaraldehyde to amine groups on the surface, the activation of antibodies' carboxyl groups by active ester chemistry was performed. Because it was also based on an amine-modified surface, APTES was also employed for the prior surface functionalization. The aim was to achieve a coating procedure better than the non-covalent physical adsorption, observed for glass and APTES only.

It is known that carbodiimides catalyze the formation of amide bonds between carboxylic acids and amines by activating the carboxylate to form an *O*-acylurea.[218] This is exploited for application in a variety of bio-conjugation and cross-linking methods. When this reaction is carried out in an aqueous solution with a water-soluble carbodiimide like EDC, the activated species are subject to hydrolysis, and this hydrolysis can severely limit the overall yields obtained.[219] But the activated species can be stabilized with compounds like Sulfo-N-Hydroxysuccinimide (S-NHS) and Pentafluorophenol (PFP), converting carboxyl groups to amine-reactive active esters.[220]

In the presented work two ester activation methods were compared. The carboxyl groups of AbE1 were activated by a mixture of EDC (~2 mM) and S-NHS (~5 mM), or EDC (~2 mM) and PFP (~5 mM). The two possibilities were compared to find out which one resulted in a better immobilization of antibodies to an amine-functionalized glass surface. AbE1 was stained with Ab-Cy2, to make the immobilization visible, and the modified glass slides again examined by a fluorescence imaging system. The corresponding images are depicted in Figure 4.5.

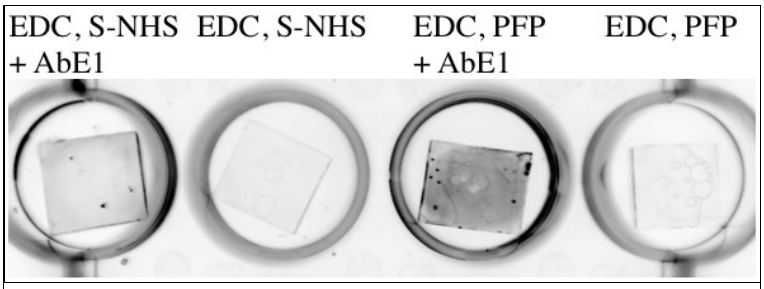

Figure 4.5 Fluorescence images of variably coated glass slides. Images taken with a Fuji LAS-3000 CCD-Imaging System.

Only when AbE1 as antibody material was applied to the surface a fluorescence signal was visible for both S-NHS and PFP. That means rinsing and therefore hydrolysis of active esters prevent a covalent or non-specific binding of Ab-Cy2 to the surface. Furthermore, it is obvious that the EDC-activation with PFP led to a significantly more intense fluorescence signal compared to S-NHS.

In order to examine whether the observed signal was the consequence of the aforementioned functionalization steps from APTES to the final application of AbE1, several controls were carried out. In each one a certain step was missing. The resulting fluorescence images for EDC/S-NHS and EDC/PFP are depicted in Figure 4.6 and Figure 4.7, respectively.

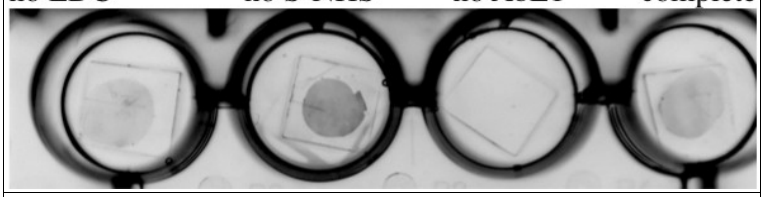

Figure 4.6 Fluorescence images of glass slides missing different single steps of the coating procedure (APTES, EDC, S-NHS, AbE1). Images taken with a Fuji LAS-3000 CCD-Imaging System.

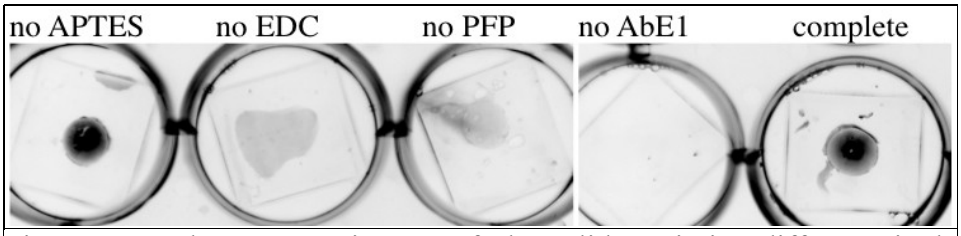

Figure 4.7 Fluorescence images of glass slides missing different single steps of the coating procedure (APTES-EDC-PFP-AbE1). Taken with a Fuji LAS-3000 CCD-Imaging System.

Fluorescence signals with differing intensities were visible for both strategies of active ester chemistry. This accounted also for missing steps in the coupling procedure. For example, in Figure 4.6, even if no S-NHS was applied, AbE1 was bound. Also in Figure 4.7 for a missing aminosilane on the glass substrate a fluorescence signal caused by AbE1 was visible. Because in both cases no signal was visible when AbE1 was missing, an unspecific binding of Ab-Cy2 to hydrolyzed active ester surfaces could be precluded.

Therefore, it was concluded that both functionalization protocols did not work as expected. Either the primary antibody got bound by an unknown surface chemistry reaction or simply again by unspecific physical adsorption. It is hypothesized that as soon as no complete active ester surface is present, non-specific binding occurs. Due to their hydrophilic and hydrophobic domains, proteins are well-known to bind non-specifically to a multiplicity of surfaces – obviously including the employed amine-functionalized ones. It can also be hypothesized that the activated antibodies' carboxyl groups bind to other antibodies' amine groups, hence leading to a kind of polymerization reaction. These polymerized antibodies could potentially adsorb to different surfaces even better that the single molecules.

For whatever reason, the method was not able to fulfill the sought-after task of specific covalent binding of antibodies. To overcome these issues, a protocol proposed by [229] was examined and is presented in the next section.

4.2.3 Bacteria Binding by APTES and BMPS

It has been shown that antibodies can be covalently linked to amino-terminated silicon substrates through the short succinimide cross-linker 3-(Maleimido)propionic acid N-succinimide ester (BMPS). However, at the same time the results suggested that an antibody for bacterial immuno-immobilization should target a surface antigen which extends out from the bacterial surface and is tightly attached to the bacterial cell wall.[229] In the cited work an antibody against CFA/I fimbriae was utilized.

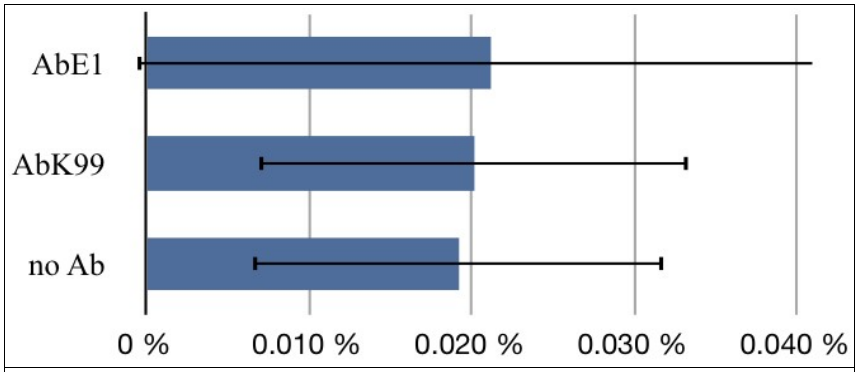

Figure 4.8 Correlation between the type of antibody, immobilized by BMPS, and the difference in SCR of 2 – 3 µm² particles after and before incubation.

Due to these promising results, the same procedure was tested in the course of this work. A glass surface was amino-functionalized with APTES, activated with BMPS and incubated with different types of antibodies. Eventually *E. coli* were applied. Before and after the incubation with bacteria several phase contrast images of the surfaces were taken and the surface coverage (SCR) of particles in the (typical of bacteria) size between 1 – 3 µm² determined. Particles and bacteria appearing before the incubation with *E. coli* presumably arose from impurities during the several surface preparation steps. The correlation between the difference in the (SCR) after and before incubation, and the type of applied antibody is depicted in Figure 4.8. Firstly, it is obvious that this methods comprised a large uncertainty, demonstrated by the wide error bars. Furthermore, no

difference between AbE1 and AbK99 was visible. However, the difference in SCR of particles and hence bacteria was the same when no specific antibodies were applied. Hence, it was concluded that the specific binding of bacteria was as high as the non-specific, for the applied types of antibodies. The reason may be a very high physical adsorption of bacteria to the aminosilane treated substrates.

To test the reproducibility of the obtained results and the impact of the bacteria's vitality, three different antibodies were bound by BMPS to an APTES-modified glass substrate and incubated with living and dead *E. coli*. Blank samples with no antibodies were incubated as well. The results are depicted in Figure 4.9.

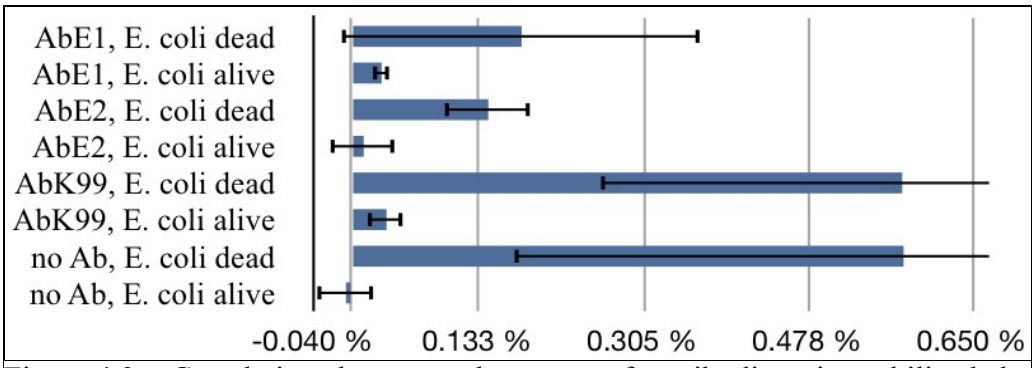

Figure 4.9 Correlation between the type of antibodies, immobilized by BMPS, the vitality of *E. coli* and the difference in SCR of 2 – 3 μm^2 particles after and before incubation.

In all cases it is evident that more dead than living bacteria were bound to the surface. This is reasonable since *E. coli* have flagella and can actively move themselves, which should interfere with both, a specific binding by antibodies and a non-specific physical adsorption. Although AbK99 showed a much higher ability to bind bacteria compared to AbE1 and AbE2, the unspecific binding of bacteria to surfaces with no antibodies was still just as high. The high difference between AbK99 and AbE1 or AbE2, respectively, also contrasts the results presented in Figure 4.8, in which their binding capability was comparable. Furthermore, the very large error bars attract attention again. This phenomenon was apparent throughout almost all experiments with bacteria, and was ascribed to the imperfect method of surface exploration by optical microscopy and a limited amount of taken pictures. Nevertheless this was an important issue and will have to be addressed in future explorations.

The differences between the obtained results and the cited reference may be due to several reasons but the most likely one is the applied type of antibody. This is also indicated by the very low, even for AbK99, SCR and hence amount of bound bacteria compared to the cited results and the therein underlined significance of the focused epitope.

Even the most promising of the three applied antibodies showed only a relatively weak specific binding. But since no exchange of antibody type and bacteria strain was promising, it was important for the following immobilization tests to find an immobilization method with a relatively weak unspecific binding. Therefore, the application of the biotin-streptavidin affinity system as an alternative to simple APTES-modified glass surface was investigated and is presented in the following section.

4.3 Bacteria Binding by Biotin, Streptavidin and NeutrAvidin

To decrease non-specific binding and to take advantage of the biotin-avidin affinity systems the application of biotin, streptavidin and two related compounds was investigated for the purpose of bacteria binding. In these experiments a biotin-labeled antibody against *E. coli*, namely AbE-B, was employed. Furthermore, the preparation of avidin-derivatized surfaces and the attachment of recognition species by avidin-biotin interactions has been proven to be convenient for preparing highly stable "generic" sensor substrates that can be patterned with biotinylated "capture" molecules.[221]

4.3.1 Biotin-Streptavidin Affinity System

The small biotin (or vitamin H) molecule with a molecular mass of around 0.24 kDa shows a very high affinity constant ($K_a = 10^{-14} – 10^{-15}$) to the tetrameric molecule avidin (around 66 kDa, produced in the oviducts of birds, reptiles and amphibians) and the related streptavidin (purified from the bacterium *Streptomyces avidinii*) and neutravidin (deglycosylated version of avidin). This makes it to one of the strongest non-covalent interactions known in nature.[222] Furthermore, biotin-streptavidin-binding is resistant to many external stresses like, for instance, pH, temperature or detergents. Hence, biotin-labeling and streptavidin are widely used to attach various biomolecules to one another or onto a solid support. Furthermore, streptavidin is widely used in Western blotting and immunoassays conjugated to some reporter molecules. A schematic representation of biotin is depicted in Figure 4.10.

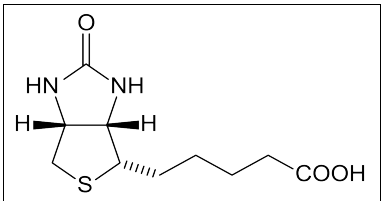

Figure 4.10 Biotin

In the presented work streptavidin and neutravidin were either bound to a surface by physical adsorption, APTES and the active esters Biotinamidohexanoic acid N-hydroxysuccinimide ester (biotin-X) or Biotinamidohexanoyl-6-aminohexanoic acid N-hydroxysuccinimide ester (biotin-XX-), respectively. The corresponding experiments are explained in the following sections.

4.3.2 Bacteria Binding by Physisorbed Streptavidin

In the first experiments with the biotin-streptavidin affinity system the large streptavidin molecule, or its related compound neutravidin, were immobilized to glass substrates by physical adsorption, as described by others.[223] Subsequently, the biotinylated antibodies AbE-B were applied and the substrates again incubated with *E. coli*. A schematic representation of this layer-by-layer construction is depicted in Figure 4.11. Before and after the incubation with *E. coli* several phase contrast images of the surfaces were taken and the difference in the surface coverage (SCR) of particles in the typical bacteria size between 1 – 3 μm^2 determined.

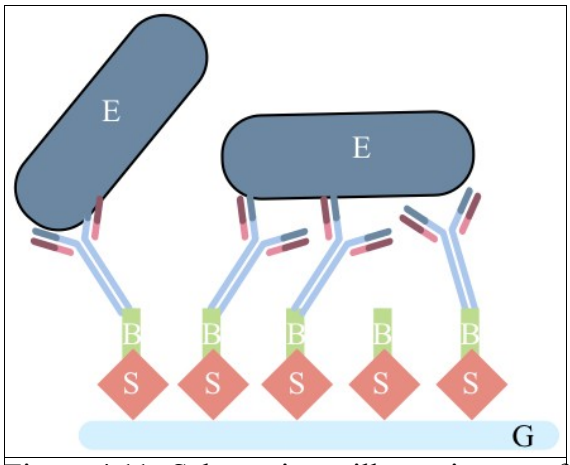

Figure 4.11 Schematic illustration of Streptavidin (S) physisorbed to a glass surface (G). *E. coli* (E) are bound to it by antibodies and biotin (B). (Not to scale)

The results of the comparison between streptavidin, neutravidin and a blank sample with only AbE-B physisorbed to the substrate is depicted in Figure 4.12. Therein X-Avidin stands for both avidin-related compounds.

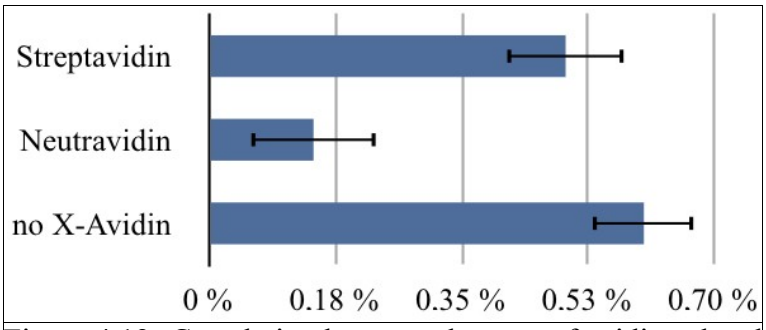

Figure 4.12 Correlation between the type of avidin-related compound and the difference in SCR of 2 – 3 μm^2 particles after and before incubation.

Although the streptavidin-based surface showed a much better specific binding, compared to the neutravidin-based surface, the unspecific physical adsorption of AbE-B was comparable high again. Hence, it could be concluded that the physical adsorption of streptavidin and the adjacent binding of biotinylated antibodies did not outmatch the physical adsorption of antibodies to glass.

To pursue this approach, streptavidin was in the next step chemically bound to glass instead of physisorbed. The corresponding experiments and their outcomes are described in the next section.

4.3.3 Bacteria Binding by Biotin-Silanes and Streptavidin

In order to bind streptavidin or neutravidin, chemically to a glass surface, the substrate was in the first step again coated with APTES. Subsequently, biotin was covalently linked to the aminosilane by active-ester chemistry. For this purpose, linkers of different length scales, namely biotin-X and biotin-XX, were employed. Then streptavidin was applied because it had bound more antibodies than neutravidin. Subsequently, AbE-B was immobilized on the bivalent linker. The completed surface was incubated with *E. coli* and analyzed by phase contrast imaging. A schematic representation of the full multilayer construction is depicted in Figure 4.13 and the evaluated data of the difference in SCR of 2 – 3 µm^2 particles after and before incubation are depicted in Figure 4.14.

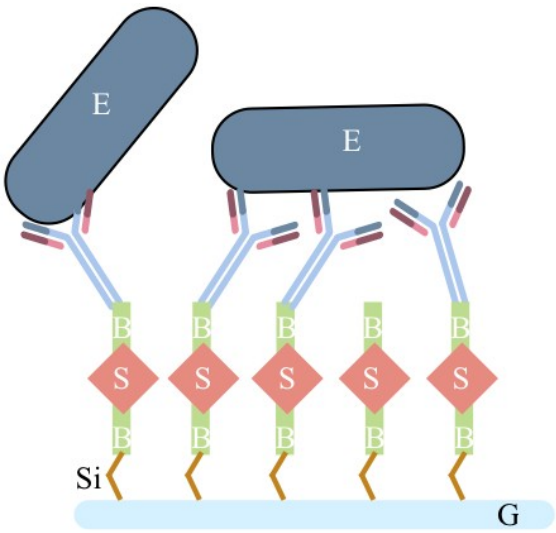

Figure 4.13 Schematic illustration of *E. coli* (E) immobilized to a glass substrate (G) by a silane (Si)-biotin (B)-streptavidin-biotin-antibody-system. (Not to scale)

It is apparent that compared to biotin-X-silane, the surface with the longer linker molecule (biotin-XX-silane) showed an improved specific binding of bacteria. This is reasonable because a longer linker molecule should make the bound antibody more flexible and hence capable of binding

to its antigen on the exterior of the bacteria. Nevertheless compared to pure, just cleaned glass slides, even the better-binding surface showed a significantly lower amount of bound bacteria.

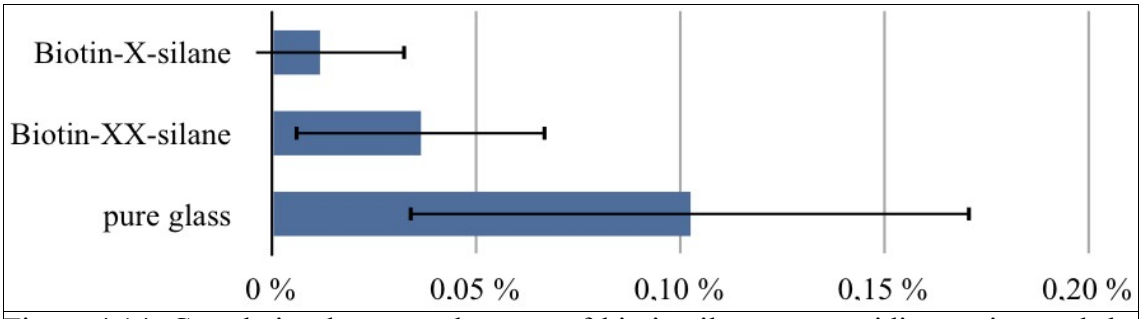

Figure 4.14 Correlation between the type of biotin-silane-streptavidin coating and the difference in SCR of 2 – 3 µm² particles after and before incubation.For detailed description, see text.

Hence, it could be concluded that although some bacteria were immobilized to the bound antibodies, the binding capability of the surface was relatively weak. The majority of bacteria seemed to be affected by a kind of antifouling property of the multilayer assembly. It could be hypothesized that the antibodies were not flexible enough to excel this antifouling influence of the surface. Therefore, this attempt for a specific binding of bacteria to a glass surface with immobilized antibodies turned also out to be not applicable for the sought-after task.

4.4 Bacteria Binding by Active Active-Ester-Silanes AE-S

In this binding procedure an innovative active ester silane, 11-Pentafluorophenylundecanoa-tetrimethoxysilane (AE-S), depicted in Figure 4.15, was employed to immobilize antibodies directly by amine residues and hence amine groups to a glass surface. It combined the direct covalent attachment of antibodies to a glass surface by active-ester chemistry, as for glutaraldehyde and BMPS, but without the need of using APTES which presumably assisted unspecific bacteria adhesion. In addition potential anti-fouling spacer molecules were employed to prevent unintentional physical adsorption of bacteria. This method needed only one surface modification step and therefore minimized the possibilities of degrading and/or incomplete intermediate reactions.

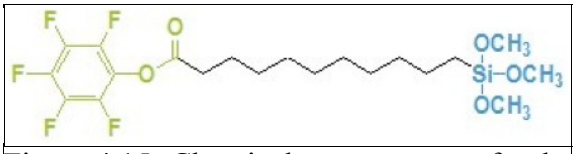

Figure 4.15 Chemical structure of the employed active ester silane (AE-S)

4.4.1 Preparation of AE-S Surfaces and Impact of Spacer Molecules

The surface was cleaned as described in section 2.1.1 – "Preparation of Silane-Functionalized Glass Surfaces", and subsequently immersed in a solution of AE-S and, if applicable, spacers molecules of differing concentrations in toluene at 80 °C over night. These spacers were also silane moieties with either a polyethylene glycol or alkyl head group. The next day the silane glass slides were rinsed and the antibodies applied in aqueous solution for one day. Hence the total preparation procedure could be minimized and associated with it some of the aforementioned drawbacks of more complex preparation protocols. Furthermore, the surface was eventually only covered with the functional silane for antibody immobilization and spacer molecules for antifouling. Their final ratio on the surface could easily be tuned by the ratio in solution beforehand, assuming a comparable silanization reaction rate. Therefore, no free amine or other groups, accounting for non-specific binding of antibodies and bacteria, were existing on the surface.

Two silanes were applied as spacer molecules, namely n-Propyltrimethoxysilane (Alk-S) and [Hydroxy(polyethyleneoxy)propyl]triethoxysilane (OH-PEG-S), having an alkyl and polyethylene glycol head group, respectively. In the first tests, the impact of Alk-S to the bacteria binding was investigated. Thereby the emphasis was on the difference between surfaces coated with antibodies and those without and whether the unspecific binding could be influenced by the spacer. The results of the corresponding experiments are depicted in Figure 4.16.

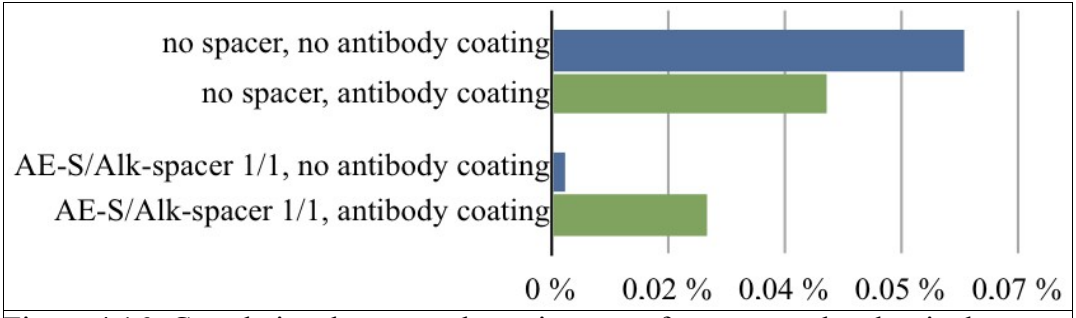

Figure 4.16 Correlation between the existence of spacer molecules in between active ester silane molecules, immobilized antibodies and the difference in SCR of 2 – 3 µm^2 particles after and before incubation. These data are only examples. Further have to be generated for an error estimation in the future.

It was evident that for the cases of only AE-S and no antifouling spacers in between, more bacteria were bound non-specifically to a surface without antibodies than specifically to an analogous surface with antibodies (two top bars). Hence, it could be concluded that the pure AE-S-functionalized surface showed the same behavior as APTES or glutaraldehyde. Compared to surfaces with immobilized antibodies, even more bacteria were physisorbed.

A different situation could be found when Alk-S-spacer were used in between the AE-S-molecules with a 1:1 ratio (two bottom bars). In these experiments the bacteria binding was decreased compared to the aforementioned ones. This could be interpreted in a way as the Alk-S-spacers reduced the non-specific binding of bacteria with and without antibodies. Furthermore, bacteria binding was clearly more decreased on surfaces with only AE-S and Alk-S-spacers than on surfaces with additional antibodies. Hence, it could be reasoned that the spacer molecules intensively blocked unspecific binding while at the same time still facilitated specific binding by antibodies.

In the next experiments, the difference between two spacer molecules was investigated. To this end, in each case two surfaces were coated with a 1:1 ratio of AE-S and Alk-S and OH-PEG-S, respectively. They were partially incubated with antibodies as before and subsequently *E. coli*. The resulting data are depicted in Figure 4.17.

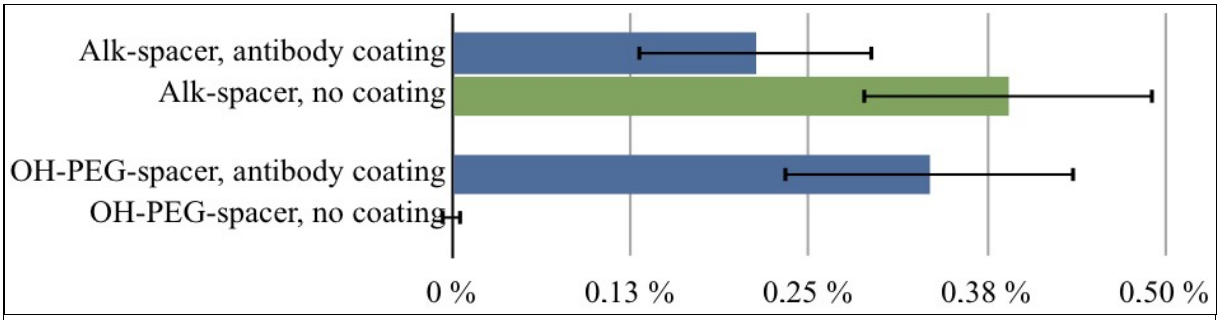

Figure 4.17 Correlation between the type of spacer, the existence of an antibody coating and the difference in SCR of 2 – 3 µm² particles after and before incubation.

In contrast to the last experiments, bacteria binding to surfaces with Alk-S-spacers and no antibody coating was higher than in the presence of antibodies, showing the difficulties of the protocol based on Alk-S-spacers and the tendency to non-specific binding. Contrariwise, for OH-PEG-S-spacers the specific binding of bacteria was much stronger compared to unspecific physical adsorption, which was nearly zero. The promising results for OH-PEG-S-spacers could be accounted to the general PEG properties. Many studies have shown their remarkably anti-fouling characteristics. They are known to be chemically inert and to prevent protein attachment, like e.g. antibody adsorption.[224] Several theoretical ideas have been raised for modeling and explaining the protein resistance of a grafted PEG surface.[225] Eventually, the combination of the low interfacial energy of PEG with water [226] and its steric stabilization effect are responsible for the protein-resistant character of PEGylated surfaces.[227,228] Due to these reasons in the following experiments OH-PEG-S-spacers were employed.

In the next step, the impact of different types of antibodies and the bacteria's vitality in conjunction with the aforementioned spacer molecules was investigated.

4.4.2 Impact of Antibody Type and Bacteria's Vitality

As already described in section 4.2.3 – "Bacteria Binding by APTES and BMPS", the type of employed antibodies can have an outstanding impact on the adjacent bacteria binding experiments. Although in principle all surface antigens can be targeted to achieve immobilization, its efficiency can vary significantly.[229] Furthermore, the interaction of OH-PEG-S-spacer, different antibody types and the vitality of the bacteria should not be underestimated, and were therefore investigated.

Three different antibodies specific against *E. coli*, namely AbE1, AbE2 and AbK99, were applied to surface coated with a 1:1 ratio of AE-S and OH-PEG-S. Furthermore, blank samples with

no antibodies bound to the silanes was prepared. Eventually the surfaces were incubated with dead or living bacteria and the surface coverage determined, as already described. The results are depicted in Figure 4.18.

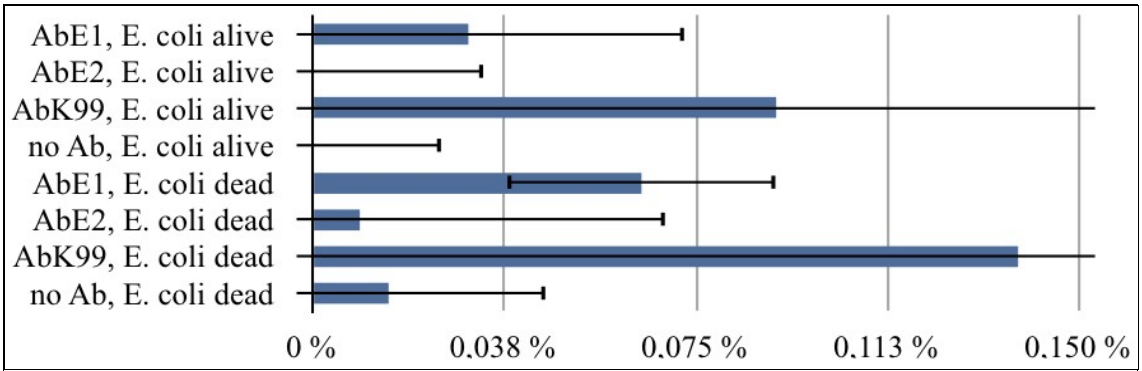

Figure 4.18 Correlation between the type of antibodies immobilized by active-ester-chemistry, the vitality/mobility of the bacteria and the difference in SCR of 2 – 3 µm² particles after and before incubation.The spacer was OH-PEG-S

As in section 4.2.3 a significantly higher binding of dead compared to living *E. coli* could be observed for all antibodies and also for the blank samples. Apart from that, the results differ strongly between different antibody types. The highest surface coverage and hence bacteria binding capacity was again observed for AbK99, which was therefore used for the adjacent experiments. This significantly stronger binding ability can be explained with the epitope of AbK99, which is the *E. coli* pili K99. These flexible hairlike appendages extent up to several micrometers from the cell and can hence presumably be better bound by antibodies on the surface.

In the final experiments before the application in inverse opals the specificity of the antibodies and the associated surfaces for *E. coli* was investigated.

4.4.3 Specificity of Detection

To prove whether the antibodies surface is specific for the sought-after bacteria strain, in this case *E. coli*, corresponding surfaces were incubated with either the specific strain *E. coli* or alternatively with the bacterium *Proteus myxofaciens* (*P. myx.*). The corresponding results for surface coverage are depicted in Figure 4.19.

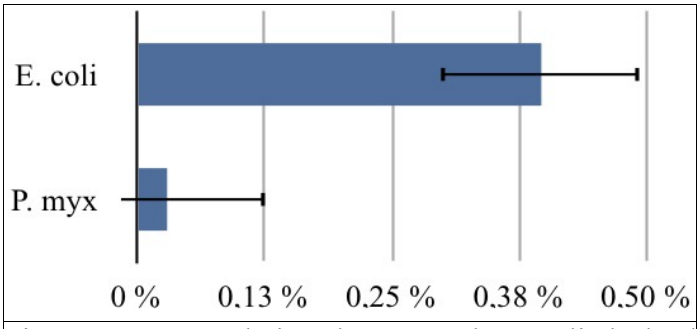

Figure 4.19 Correlation between the applied dead bacteria strain and the difference in SCR of 2 – 3 µm² particles after and before incubation. Anti-*E. coli* antibodies were immobilized on the surface.

It was evident that significantly more *E. coli* were bound to the anti-*E. coli* surfaces than *P. myx.* Hence, it could be stated that at least for this bacteria combination the surfaces are specific and could serve as a potential biosensor if combined with an adequate detection method.

With theses results it seemed to be sought-after to go one step further and coat inverse opals, which was the original idea from the beginning. Before however, it was necessary to study the fabrication and especially the tuning of several properties of the inverse opals in more detail to generate eligible structures. The corresponding experiments are presented in the following sections.

4.5 Inverse Opals Dimensioning

As described in section 1.6.1 – "Label-free Detection, inverse opals possess multiple properties, which make them perfectly applicable in biosensor surfaces. They are, for instance, easily tunable in size and material, and provide a superior specific surface area and homogeneity.

Before functionalizing an inverse opal structure with antibodies, it was necessary to investigate how the measure of such structures could be influenced. Obviously, the diameter and hence the volume of a single cavity could be determined by the size of the employed polymer precursor particles. Hence for the applied PS-MS, the inner diameter of the cavity accounted 10 µm.

The next parameter to be tuned was the diameter of the openings between two adjacent cavities in the final hexagonal crystal. It was found that it could be controlled by the time the dried PS-MS crystals were tempered at the glass transition temperature T_G of polystyrene (110°C). In Figure 4.20

the difference between no annealing and 75 min annealing is presented in two according SEM-images.

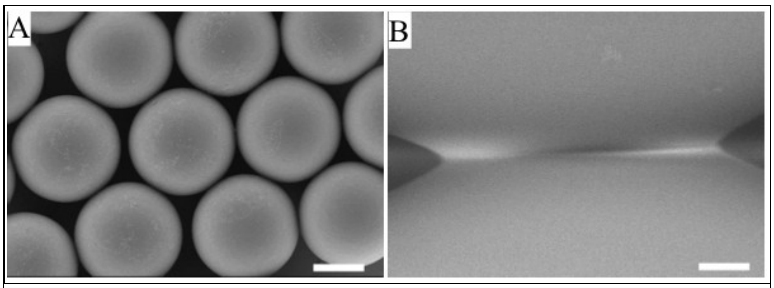

Figure 4.20 SEM images of 10 µm PS-MS heated for 0 min (A) and 75 min (B) at T_G. (Scale bars: 50 µm (A) and 500 nm (B))

It is evident that the single particles had a very small contact area or stayed slightly away from each other, if the crystals were not tempered. Possible reasons for this phenomenon could be, for instance, a thin remaining water layer, surface charges, very long molecules extending from the surface, surfactants remaining from the former suspension after the drying process or combinations thereof. In this state an adjacent incubation with an aqueous solution of nanospheres would have led to a decomposition of the structure. On the other hand, an overly long time of the needed tempering would have destroyed the spherical structure of the precursor, preventing the formation of the inverse opals. In order to optimize the contact length between PS-MS, a systematic investigation of the correlation between the tempering time and the contact length, i.e. the diameter of the openings, was performed and is depicted in Figure 4.21.

In first order, the rise can be considered as linear. Because the focused *E. coli* bacteria have a diameter of approximately 1 µm, openings between 2 and 3 µm would be large enough for letting them pass. Therefore an average time of 30 min was chosen, which also proved to be long enough to prevent the decomposition of the crystals during the subsequent contact with the aqueous nanospheres suspension. Hence about 2.7 µm interconnecting openings could be established.

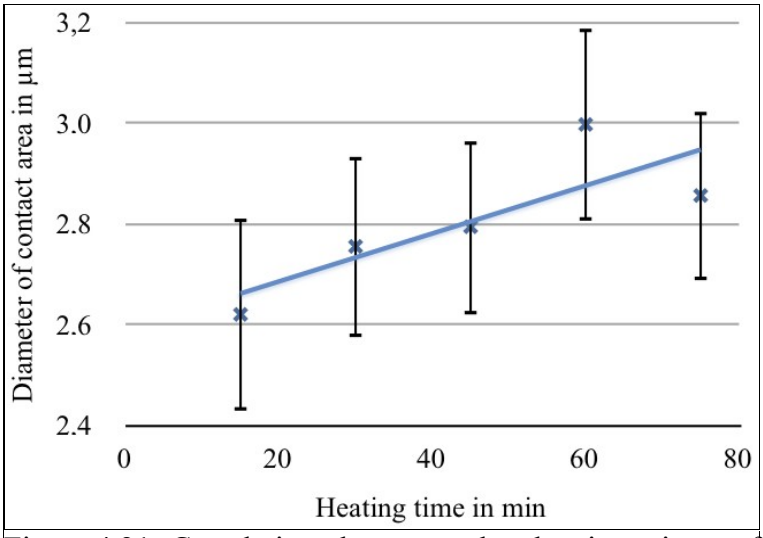

Figure 4.21 Correlation between the heating time of 10 µm PS-MS colloidal crystals at 110 °C and the particles' contact area diameter.

The third and last parameter to be tuned was the diameter of the top openings of the inverse opals. In the final sensor material this dimension would be responsible for a potential size-exclusion effect. Hence it had to be large enough for the bacteria, but at the same time small enough to still maintain the structure of connected cavities instead of just adjoined hemispheres. The diameter of the top openings could be tuned by the amount of applied nanospheres. The corresponding dependence for the home-built trough is depicted in Figure 4.22.

It is obvious that the opening diameter first decreases with increasing volume of silica nanoparticles. Then it increases from a certain volume on, hence forming a minimum opening of a little bit more than 4 µm for about 15 µl of nanoparticles. The reason for this behavior can be explained as follows. If very few particles are applied the total area covered with them shrank due to, presumably, cohesion and surface tension effects, hence leaving the outer part of the PS-MS crystal uncovered. During pyrolysis, these uncovered PS-MS particles vanished and in the middle a small circle of inverse opals was left over. With increasing amount of nanospheres this circle increased until it filled the whole trough. From this volume on the top opening diameter shrank with further increasing volume of particles.

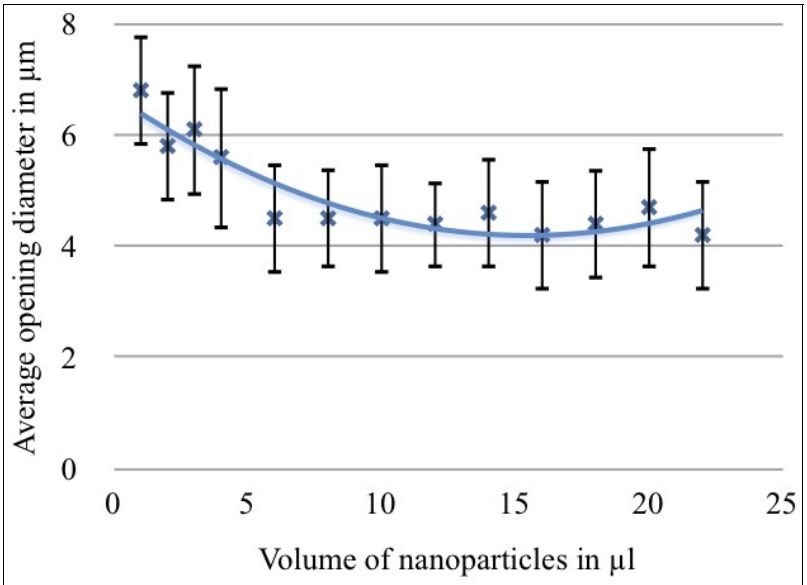

Figure 4.22 Correlation between the volume of nanoparticles infiltrating the PS-MS crystal and the average diameter of the openings after pyrolysis.

For a volume larger than approximately 15 µl the nanospheres enclosed the PS-MS increasingly more until finally a closed layer was established. But during pyrolysis the gaseous residues needed to get out and hence destroyed the finest parts of the structure, which were the top sides of the hollow spheres. If the nanospheres covered the structure completely and hence formed a kind of surface shells, the pressure inside the hollow spheres increased during pyrolysis until an actual "explosion" occurred. From this point on the diameter of the top openings could not be determined any more, because irregular structures were left over. This explains why the curve does not extend beyond 22 µl, which is approximately the point where a total coverage of the PS-MS was achieved. For further experiments the smallest possible diameter for top openings of about 4.2 µm was exploited.

After the critical values for the inverse opal fabrication were determined, the first experiments with coated structures were accomplished and are described in the following section.

4.6 Inverse Opals Functionalization

As the final step to prove the feasibility of a silica inverse opal structure capable of binding bacteria specifically by an antibody-antigen interaction, the before generated structures had to be functionalized. Hence, inverse opal structures with cavity diameters of 10 µm, interconnecting

openings of approximately 2.7 µm and top openings of about 4 µm were fabricated and coated with a 1:1 ratio of AE-S and OH-PEG-S, as described in the previous sections. Subsequently, multiple of these substrates were incubated with AbK99 solutions of different concentrations. Eventually, dead *E. coli* (OD_{600} = 0.1 D) were applied and the difference in the surface coverage (SCR) after and before the incubation determined. The corresponding results are depicted in Figure 4.23.

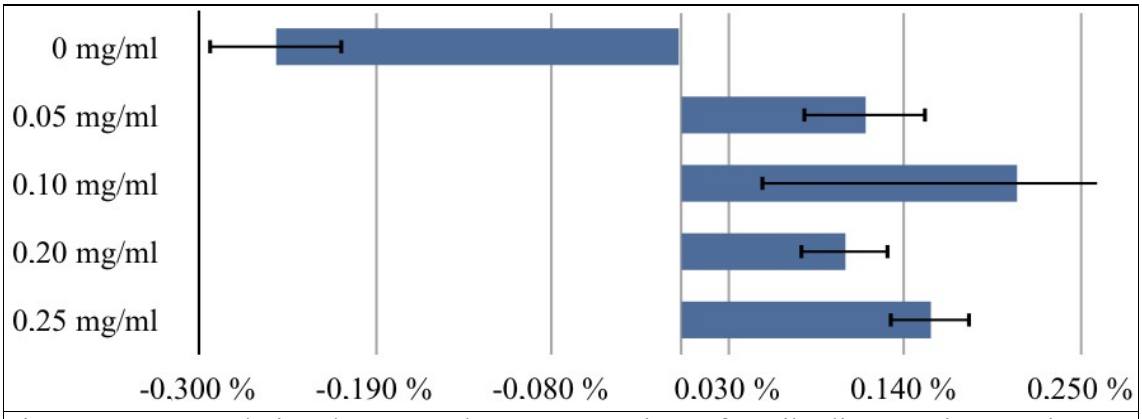

Figure 4.23 Correlation between the concentration of antibodies coating an inverse opals structure and the difference in SCR of 2 – 3 µm² particles after and before incubation.

For the evaluation of *E. coli* bound to inverse opals, the previously employed evaluation method, i.e. the determination of the coverage degree by analysis of phase contrast images, reached its limits. Due to reflection and refraction of the inverse opals, shadows and other dark artifacts occurred which were hard to distinguish from bacteria.

In Figure 4.23, the surfaces coated with no antibodies attracted attention. The negative value can be interpreted in a way that more bacteria were bound before the incubation than thereafter. Consequently, it could be concluded that the rinsing before the first taken images was not intensive enough but the incubation with pure buffer and the following washing steps removed existing impurities. Hence it is assumed that the AE/OH-PEG-S surfaces were antifouling in the way that only unspecific physical adsorption of bacteria occurred which could be removed by intensive rinsing.

In contrast to these observations, the antibody-coated surface showed a clear specific binding of bacteria. Nevertheless, partially wide error bars emerged and no clear correlation between the concentration of applied antibodies and the surface coverage and hence number of bound bacteria

was observable. Possibly, excluding the value for 0.10 mg/ml antibody solution and taking the error bars into account, a slight increase of bacteria binding for increasing concentrations could be seen. A possible reason for this indistinct relation could be saturation effects of antibody binding to the surface. It is possible that all binding sites on the surface were already covered for lower concentrations of antibodies and that an increase did not affect the amount of bound antibodies and hence bacteria. In addition, if not all binding sites were occupied for lower concentrations, a very high concentration of antibodies in solution and hence bound to the surface could lead to steric hindrance. The antibodies were bound tight to each other and to the surface, and the Fab binding sites were not longer accessible for their epitopes or at least the binding was reduced.

To visualize the inverse opal structures loaded with specifically bound bacteria, the incubated samples were subsequently dried and investigated by SEM. Some of the corresponding images are depicted in Figure 4.24. Because electrons can not pass through glass as easy as photons, the almost closed cavities are opaque for this technique. Hence it was necessary to look for inverse opals which surface shells had been removed. *E. coli* bound to the curved bases of hexagonal inverse opals are depicted by white arrows in Figure 4.24A–C. The bacteria adapted to the curved substrate decorated with antibodies, and are likely to be bound by antibody-antigen interaction. Furthermore, it was visible that no *E. coli* were bound to the surrounding substrate. Figure 4.24D shows the top view of an intact inverse opal with an *E. coli* visible in the middle of the opening. Hence is could be concluded that the functionalization of inverse opals by anti-*E. coli* antibodies was successful and that the corresponding bacteria could be bound to the curved structures of the hexagonal patterns by antibody-antigen interaction.

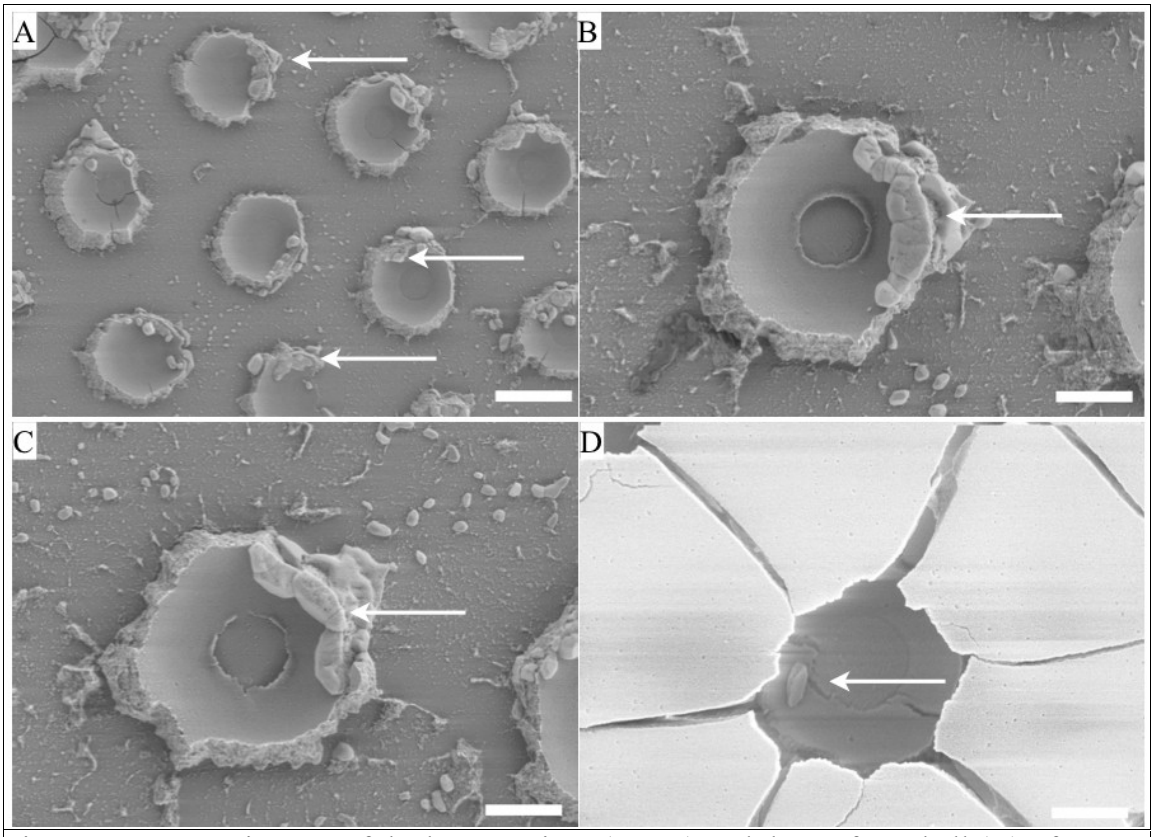

Figure 4.24 SEM images of the bottom piece (A – C) and the surface shell (D) of 10 µm inverse opals functionalized by active ester silanes with antibodies against *E. coli,* incubated with this bacteria strain and dried at room temperature. The bound bacteria are labelled by white arrows. (Scale bars: 5 µm (A) and 2 µm (B – D))

4.7 Conclusion and Outlook

In order to build up a "Label-free Detection of Microorganisms in an Integrated Biosensor Array", iopals were used for the first time to construct a new bacterial sensor with immobilized antibodies. The applicability of the employed antibodies to bind to the exterior parts of *E. coli* cells could be demonstrated. Subsequently, several methods for the immobilization of these antibodies to glass surfaces, like APTES/GA, APTES/BMPS, EDC/S-NHS, EDC/PFP, streptavidin/biotin or AE-S/OH-PEG-S, were analyzed and the results of corresponding experiments during this thesis presented. Thereby a general problem constituted the non-specific protein, i.e. antibody, adsorption. The antibody molecules were not only bound to the glass substrate by the intended covalent surfaces chemistry but also adhered due to non-specific interaction forces. This phenomenon has already been described in the literature as well.[230] Therein it has been determined by enzyme-linked immunoassays that for the immobilization of antibodies by aminosilane and glutaraldehyde, as

much as 15% of the measured response must be attributed to non-specific protein/surface interactions, even after copious washing with detergents. Hence, it can be assumed that during further steps of attended binding of bacteria, non-specific binding will not be preventable. Furthermore, the aim of binding antibodies covalently, and more effectively than with physical adsorption, could not be achieved that way.

The same accounted for the EDC/S-NHS/PFP approaches. Although a non-specific binding of the secondary antibody Ab-Cy2 could be excluded, the immobilization of the primary antibody AbE1 proceeded in an incomprehensible way and not according to the protocol. The most likely explanation for these observation was again non-specific binding of the chemical preliminary stages or of polymerized antibody conglomerates. Because also the chemical protocols for BMPS and biotin/streptavidin resulted in nonspecific adsorption of bacteria to the surface, the application of aminosilanes like APTES for the covalent immobilization of antibodies must be seen as problematic. On the one hand, the nonspecific binding of such surfaces is enormous, on the other hand, the achieved immobilization does not appear to be significantly better compared to nonspecific physical adsorption.

A specific antibody binding could be achieved by the application of the active ester silane AE-S. Together with the employment of a spacer molecule based on polyethylene glycol, OH-PEG-S, a very good covalent binding of antibodies could be achieved, while at the same time preventing nonspecific binding. Thereby the ratio between AE-S and OH-PEG-S could be subject of future studies. In the presented work a value of 1:1 was used but experimental data showed that values up to 1:10 may be sought-after too.

Although the specific binding of the antibodies to the exterior of the bacteria cell and their covalent chemical binding to the glass substrate can be assumed, a binding of the bacteria to the surface is not inevitable. Besides for AbK99, nothing is known about the antibodies' epitope and whether this is extending enough from the bacteria cell wall to be bound by the immobilized antibodies. For the continuation of this project, the search for appropriate antibodies and hence bacteria epitopes like pili and fimbriae for all bacteria to be detected is essential.

In addition, it could be shown that the binding of dead *E. coli* is superior to living bacteria. This must be taken into account if the detection and hence addressing the binding of living organism is sought-after in future projects. Furthermore, it became apparent that it will be essential for future studies to establish new automated evaluation methods, for instance based on a Fabry-Pérot

interferometer or surface plasmon resonance. The simple manual analysis of surface images taken by phase contrast microscopy is too error-prone and slow for a multiplicity of samples and high-throughput automation.

Taken together, the presented results show the proof-of-principle of specifically binding bacteria by antibodies to inverse opal structures. They open the way towards different possible future projects, finally leading to the potential sought-after biosensor for pathogens.

5 2D Array-Patterning of Antibody Annuli

The following section represents an excerpt of a manuscript already published during this thesis redaction [87] together with results unpublished until now.

First, the formation of the colloidal crystal templates is briefly introduced in section 5.1. Subsequently, the process of protein patterning around the nano-spheres and the resulting antibody annuli are described in sections 5.2 and 5.3, respectively. Eventually, the working antibodies and control experiments are demonstrated in sections 5.4 and 5.5.

5.1 Template Formation

In order to create a template for the later antibody patterning, a monolayer of (PS-MS) with large crystalline subareas, as shown in Figure 5.1, was generated on a glass slide substrate. It formation is described in section 2.2 – "Colloidal Crystals". Antibody annuli patterns were fabricated by this precursor and finally tested.

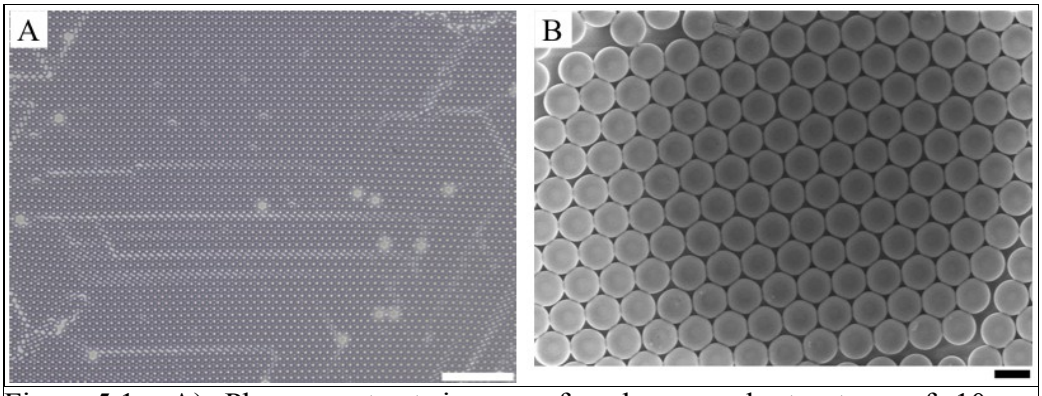

Figure 5.1 A) Phase contrast image of a hexagonal structure of 10 µm polystyrene microspheres (PS-MS). B) SEM image of PS-MS. The structure was annealed for 30 min at 100 °C for connecting the particles. (Scale bars: 100 µm (A) and 10 µm (B))

5.2 Protein Patterning

For the purpose of cleaning, as the very first step all potentially existing impurities on the glass surface were removed by submerging the substrates in piranha solution, as described in section 2.1.1 – "Preparation of Silane-Functionalized Glass Surfaces".

A hexagonal structure of annuli made of specific antibodies (AbE1) against *E. coli* was created as depicted in Figure 5.3. The selected feature size, 10 µm, permits examinations with optical microscopic techniques. Furthermore structures of 1 and 50 µm respectively PS-MS were produced, as depicted in Figure 5.4.

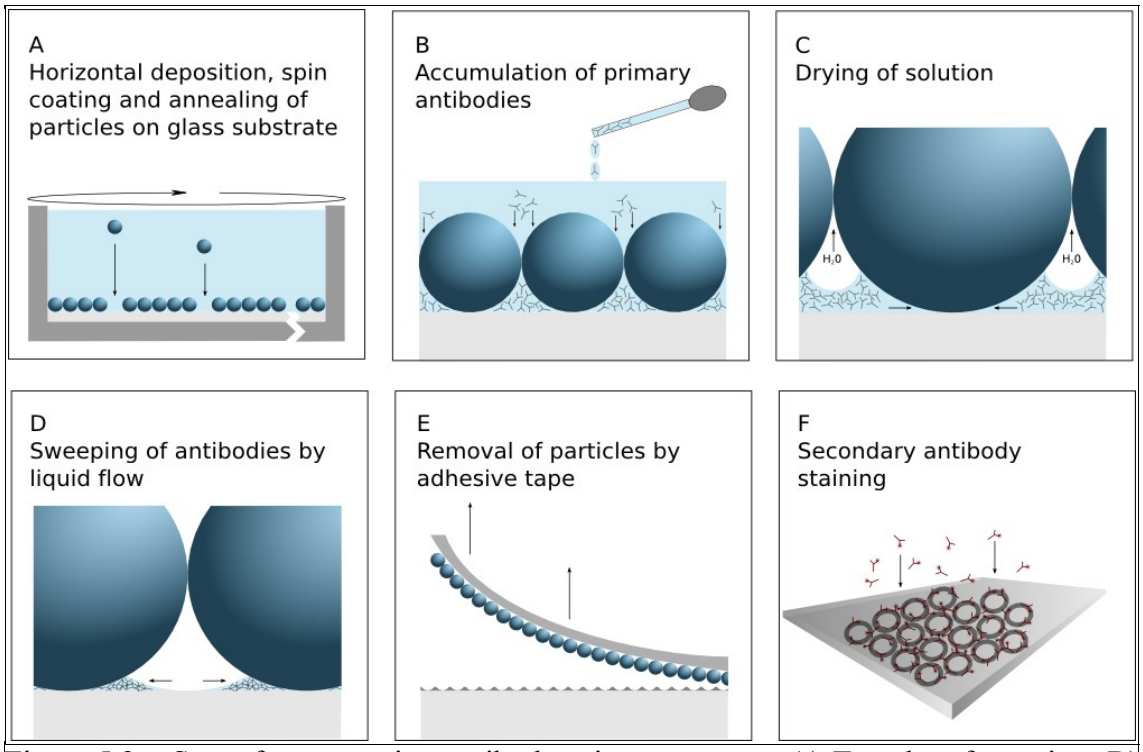

Figure 5.2 Steps for generating antibody microstructures: A) Template formation. B) Applying of antibody solution. C) Drying of solution. D) Sweeping of antibodies around microspheres (PS-MS). E) Template removal. F) Staining of annuli microstructures.

For the preparation of the antibody annuli structures, the annealed PS-MS samples were placed in a petri dish and incubated with equal amounts of AbE1 or AbE2 in varying volumes of either phosphate buffered saline (PBS) or a 0.1 vol% solution of the surfactant Tween 20® in PBS (TPBS, Figure 5.2B). Hence different concentrations of the antibody solution could be achieved. As the

solvent was evaporating (Figure 5.2C), the antibodies were swept by the liquid flow into the area which contains more liquid and hence around the PS-MS (Figure 5.2D). Similar behavior of nanoparticles was quantitatively analyzed recently.[231] After drying, the microparticles were peeled off with the aid of adhesive tape (Figure 5.2E) and the final microstructure constituted of specific antibodies against *E. coli* was achieved. This pattern could be further visualized by, for instance, a fluorescent secondary antibody (Ab-Cy3) against the primary one (Figure 5.2F), which then could be observed with a fluorescent or Confocal Laser Scanning Microscope (CLSM). The structures were examined by AFM with data shown in the following section.

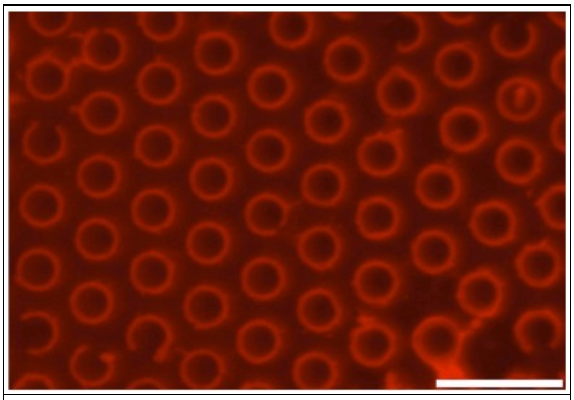

Figure 5.3 Fluorescence microscope image of a hexagonal structure of AbE1 annuli labeled with Ab-Cy3. As the template, if not otherwise identified, served always 10 µm PS-MS. (Scale bar: 20 µm)

It has been shown that under laboratory conditions of about 40 % humidity antibodies show motion on surfaces and the motion could only be eliminated after desiccating the samples for one week or more to remove surface-bound water layers.[232] This feature of antibody movement under humid conditions was extensively exploited in the present work. The drops of antibody solution on the PS-MS-treated glass slides were dried at ambient lab conditions (approximately 24 °C, 24 % relative humidity, 7 hPa water vapor pressure) or alternative nearly zero humidity for times ranging from one up to six days before the PS particles were removed and the second antibody was applied. At the higher humidity range and for up to three days the samples could be identified as wet by bare eye since a water layer was still apparent, but even after four days, when there was no more water layer visible, no structures were observable under the fluorescence microscope after staining with

Ab-Cy3. The same phenomenon was found when the samples were dried fast in a desiccator within several hours at room temperature. Higher temperature (60 – 70 °C) also did not lead to the expected results, which could however be explained by an occurring heat denaturation of the antibodies, i.e. proteins.

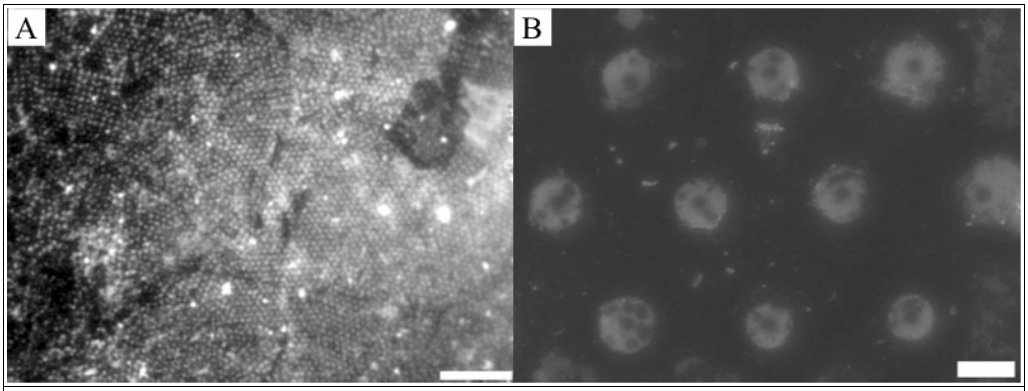

Figure 5.4 Fluorescence microscope images of hexagonal structures of AbE1 annuli labeled with Ab-Cy3. As the template served 1 µm (A) and 50 µm (B) PS-MS. (Scale bars: 10 µm (A) and 20 µm (B))

The following conclusions were drawn concerning the movement and adsorption of the antibodies to the glass surface: The evaporation rate was an important factor in the formation of the antibody annuli; therefore, both temperature and relative humidity played important roles. While raising temperature was not a favorable means due to the likely consequence of protein denaturation, speeding up the evaporation by reducing humidity may also led to the condition where the antibodies could no longer be completely transported by the fast retreating solvent. To overcome these issues it was necessary to dry the samples at temperatures below the denaturation point and at appropriate humidity values (20 – 30 %). This, in turn, required longer drying time to yield well-bound antibody structures. It was found out that at the aforementioned conditions a minimum time of six days was necessary for obtaining stable structures. Shorter drying time or lower humidity led to unstable antibody topologies which then, for instance, dissolved during water contact.

It was also observed that both the solvent and the antibody concentration have a strong impact on the protein arrangement in the following drying process. When the antibody suspension (10 mM PBS and a concentration of 50 µg/ml) without Tween20® was applied, no formation of antibody annuli was observed, as depicted in Figure 5.5A. Instead a structure of non-fluorescent partially connected ordered black dots on a red background was visible. Because fluorescent secondary

antibody Ab-Cy3 specifically binds to the primary, one could assume that the latter was coated homogeneously all over the sample. Only the areas which were protected by the PS-MS stayed free of antibodies and therefore showed no fluorescence signal. It was concluded that the availability of a surfactant like Tween20® was crucial for the arrangement of antibodies into annuli structures during the drying process. There were two possible reasons: Firstly, the protein mobility on surface was increased with the presence of the surfactant. Secondly, the capillary linkage between the template spheres broke earlier with the presence of surfactants owing to the reduced surface tension, which also allowed the formation of the discrete ring structure.

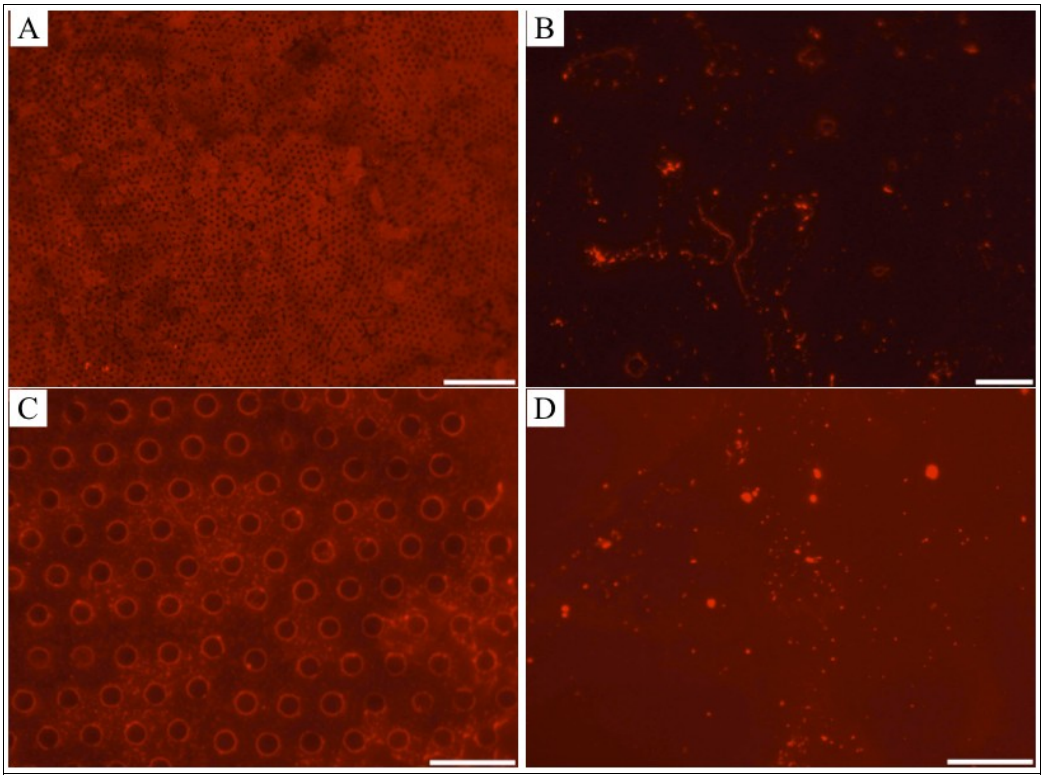

Figure 5.5 Fluorescence microscope images of structures treated with antibody solutions of different solvents, concentrations and antibodies: A) Sample treated with AbE1 solved in PBS instead of TPBS. The antibodies (red fluorescence) are coated over the whole sample, only the places where the polystyrene microspheres (PS-MS) were sitting (black dots) are free. B) Sample treated with an AbE1 concentration of 6,7 µg/ml instead of 50 µg/ml in TPBS. Almost no structure was visible. C) Sample treated with an Ab1.1 concentration of 500 µg/ml instead of 50 µg/ml in TPBS. Not all antibodies have moved around the spheres hence a strong background signal is still visible. D) Sample treated with 50 µg/ml AbE2 instead of AbE1. No structure was visible. Scale bars: 20 µm. (Scale bars: 100 µm (A) and 20 µm (B – D))

To investigate the influence of the antibody concentration on the structure forming, concentration used previously of 50 µg/ml antibodies in TPBS (Figure 5.3) was decreased to 6.7 µg/ml and increased up to 500 µg/ml respectively. The resultant fluorescence images are shown in Figure 5.5B and Figure 5.5C. In the former case, the concentration was apparently too low to cause any structure forming around the PS-MS. Only very few and pale annuli were visible through fluorescence imaging, but no array structures could be discerned. In the latter case, the exceedingly high concentration of antibodies led to a strong background fluorescence though patterns were discernible. This suggested that the amount of antibodies that could be transported by the solvent during the drying process was limited. If the amount of antibodies exceeded a specific limit, then it was no longer possible for the solvent to transport all of them to the edge of the PS-MS. The residual proteins were deposited in the space between the particles, hence increasing the noise-to-signal ratio.

Following that, the impact of antibodies obtained by different suppliers and hence different versions of antibodies against *E. coli* K12 was investigated. Figure 5.5D shows a fluorescence microscope image of a sample with an exchanged antibody after staining with Ab-Cy3. Instead of the previously used AbE1, another antibody (AbE2) at the working concentration of 50 µg/ml in TPBS was applied for the incubation step of the PS-MS. No annuli, not to mention any crystalline structures, were visible over the whole sample. Although AbE2 was also targeting against *E. coli* K12, it did not show the same annuli structure forming property. Since most of the structure of IgG antibodies was equal between different types, the solvent in which the antibody is offered was considered to be crucial. Unfortunately the explicit composition of the obtained antibody solutions was unknown.

In summary, it was necessary to dispense the antibodies in the appropriate solvent which should compromise a surfactant to modify the surface tension and the protein surface. Also the protein concentration should be fine-tuned in order to obtain defined structures as well as a high signal to noise ratio. In the experiments presented here the optimal solvent was a 0.1 vol% concentration of Tween 20® in PBS and an antibody concentration of 50 µg/ml.

5.3 Antibody Annuli Structures

The topographical properties and structure of the antibody annuli were observed by AFM, as shown in Figure 5.6 and Figure 5.7. Because no labeling is necessary for this technique, the unaltered

topology of the primary antibodies without any potential corruption by a secondary antibody could be observed. In Figure 5.7A the almost perfect hexagonal structure of seven annuli is presented. The distance between the neighboring rings was 10 µm, identical to the diameter of the MS-PS in the template. Figure 5.7B shows the cross section through three annuli in a line in Figure 5.7A. The annulus height was in the range of 25 – 40 nm. Because one IgG antibody had an extension between approximately 10 and 15 nm [171,172] it was assumed that layers of two or three antibodies were packed on top of each other in the structure. The lateral annuli thickness lay between 0.5 and 1 µm. Therefore, multiple antibodies were packed next to each other. The outer diameter of one annulus, as depicted in Figure 5.6 and Figure 5.7, lay between 3 and 3.5 µm and hence the inner diameter between 1 and 2 µm. Figure 5.6B shows that the inner shape of an annulus is, according to its origin, hemispherical. They therefore could serve as perfect attaching points for spherical objects like giant vesicles or cells in further studies. The AFM images clearly show that the surface around the annuli was smooth in spite of some minor impurities, and therefore the signal-to-noise ratio could be high. This was especially useful for selective binding of specific antigens from a mixture.

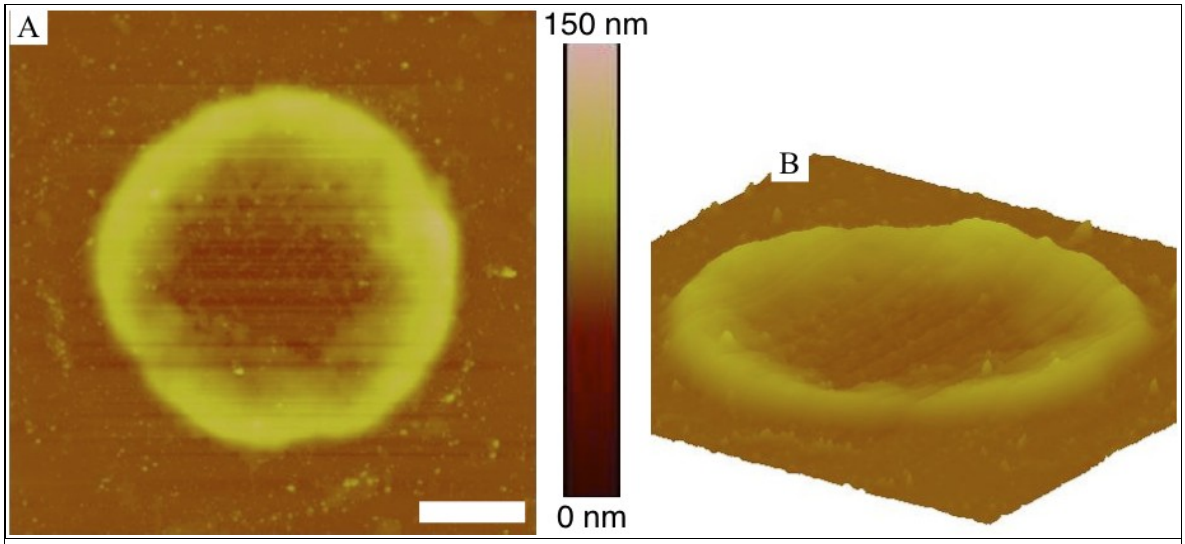

Figure 5.6 AFM images of a single antibody (AbE1) annuli. (Lateral scale bar: 1 µm, height scale bar applies to all AFM images throughout the article.)

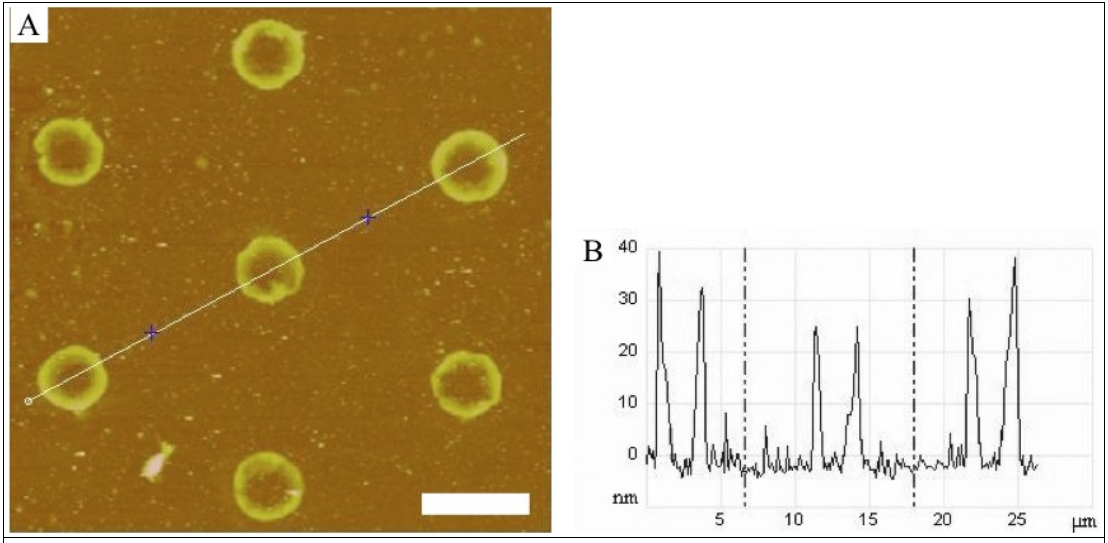

Figure 5.7 A) AFM image of a hexagonal structure of antibody (AbE1) annuli. B) Cross section of (A) along the white line. Dashed lines represent blue crosses in A. (Scale bar: 5 µm)

5.4 Proteins Bound to Annuli Structures

To demonstrate the versatility of this protein patterning technique, an array of annuli with a monoclonal antibody (AbGFP-DL) against the Green Fluorescent Protein (GFP), labeled with DyLight™ 549, was created. The concentration and minimum time for drying were the same values as had been characterized before for being optimal (50 µg/ml in TPBS, more than six days at ambient conditions). The corresponding fluorescence image is depicted in Fehler: Referenz nicht gefundenA. Hexagonal structures were created as described before. In the next step the surface was incubated with a solution of 10 mg/ml enhanced Green Fluorescence Protein (eGFP) in PBS over night, rinsed several times with PBS and again visualized with a fluorescent microscope (Fehler: Referenz nicht gefundenB). The same hexagonal structure as for the antibody was visible for the fluorescent protein. In Fehler: Referenz nicht gefundenC the superposition of Fehler: Referenz nicht gefundenA and Fehler: Referenz nicht gefundenB and therefore the two dyes is shown. The antibody structures clearly coincide with the protein pattern – its antigen. Therefore, it is concluded that the antibodies are still able to bind to their antigens after the patterning process, and their full functionality is well preserved.

With these experiments it could also be show that this new patterning process is not limited to a special type of antibody. This phenomenon is ascribed to the comparatively small structural differences within the IgG family.[233] The replacement by other monoclonal and polyclonal IgG

antibodies is possible and can, under the appropriate conditions, easily be used to produce 2D-arrays of annuli structures of a large variety of antibodies.

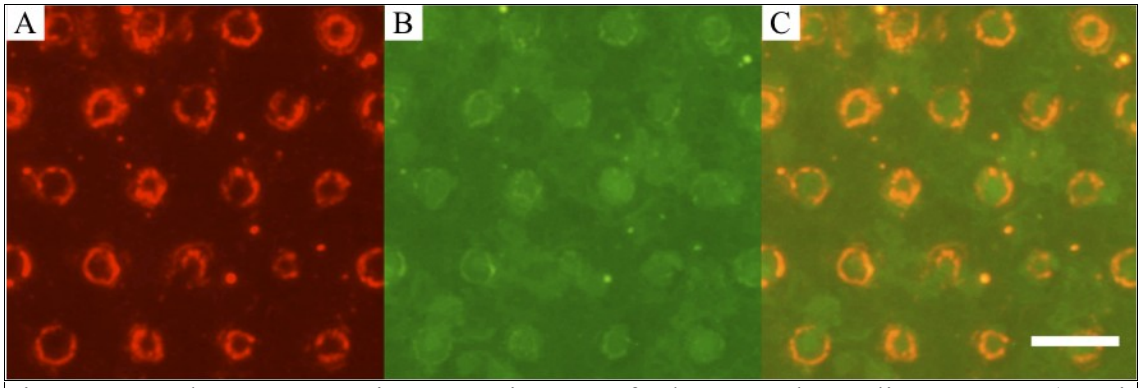

Figure 5.8: Fluorescence microscope images of a hexagonal annuli structure. A) anti-GFP DyLight™ 549 labeled antibodies (AbGFP-DL). B) GFP bound to AbGFP-DL. C) Overlay of (A) and (B).)Scale bar: 20 µm)

5.5 Negative Control for Specific Binding

As a negative control test Ab-Cy3 was substituted with a nonspecific Donkey anti-Mouse antibody (AbX-FITC). In this combination of primary and secondary antibody the formed structures showed no fluorescence signal after processing (data not shown).

Because Ab-Cy3 after processing still binds to AbE1, as depicted in the fluorescent images, it can be inferred that the epitope binding motive of the second antibody on the first is not degraded during the proceedings, and therefore the quaternary structure of this epitope region in AbE1 is likely to be preserved. Merkel et al. have shown that in general the functionality of immobilized proteins appears to be robust to a variety of immobilization strategies, at least qualitatively.[234] According to this, it is concluded that the epitope binding motives of AbE1 remain unaltered and thus the antibodies are able to bind to their corresponding antigens.

6 Structured Antibody Surfaces for Bio-recognition

The following section represents an excerpt of a manuscript submitted during this thesis redaction (cf. section 10.2 – Submitted Manuscripts) together with until now unpublished results.

The multi-scale detection function of the biomolecular nano-ring arrays, introduced in the last section, is reported. They served as a versatile sensing platform, i.e. for the detection from molecules to whole cell organisms, owing to the hierarchical structural features. Two examples, covering both prokaryotes and eukaryotes systems and ranging from single molecules like integrin to whole cells like *E. coli*, were used in the following sections to demonstrate the advanced bio-recognition functions of this structured antibody surface by fully utilizing the ordered arrangement, the geometrical advantage of nano-rings in capture (section 6.1 – "Bacteria Whole-Cell Sensing") and the protein molecular recognition function as a platform integration with synthetic biology (section 6.2 – "Cellular Mimics by Integrin Functionalized Lipid Vesicles").

6.1 Bacteria Whole-Cell Sensing

In this section, a selective bacterial detection by the structured antibody surface from a crude mixture of different bacterial species is described.

Recent finding on the immobilization of bacteria cells [97] led to the hypothesis that the binding of bacteria to an antibody coated surface could also be heavily influenced, and maybe improved, by the surface structure. As already shown in sections 5.2 and 5.3, it is possible to pattern antibodies in a nano-ring/annulus-shaped fashion and that the proteins having undergone this process retain their functionality.[87] In the context of bacteria whole-cell sensing, the first question to address was whether it is possible to bind bacteria to this structured antibody nano-ring arrays against the specific strain. The second question was whether these structured patterns improve the binding capabilities of the substrate compared to non-structured "flat" surfaces. The primary concept of binding bacteria by antibodies to a curved surface is depicted in schematic scale in Figure 6.1. The proteins are preferably immobilized by their Fc end to the substrate (light blue), presenting the Fab terminus, the recognition fragment, to the solution from where the bacteria, e.g. *E. coli*, to be captured.

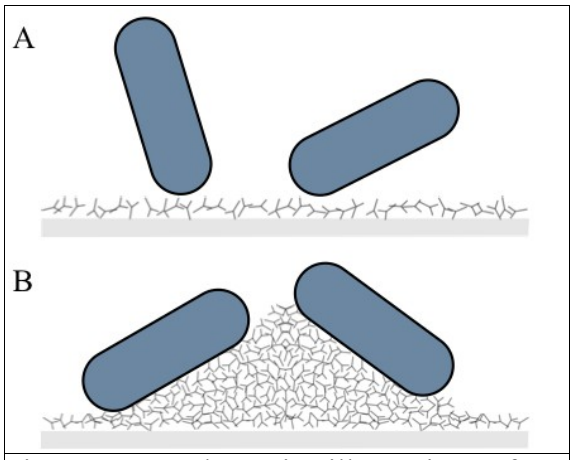

Figure 6.1 Schematic illustration of *E. coli* bound to a planar antibody surface (A) and to an annuli-structured antibody surface (B). (Not to scale)

6.1.1 Bacterial Binding to Antibody Annuli

In Figure 6.2 *E. coli* K12 bound to AbE1 annuli against this bacteria strain are shown. The structures were constituted by 50 µm PS-MS. The diameter of an AbE1 annulus was on the order of 10 to 15 µm. In Figure 6.2A the phase contrast image clearly shows the hexagonal pattern of bacteria bound to the annuli antibody structures emerging from 50 µm PS-MS. In Figure 6.2C a single ring-like annulus from 50 µm PS-MS is shown. The bacteria were stained with DAPI fluorescence dye and imaged by fluorescence microscopy. The images clearly show that the bacteria were captured on the AbE1 annuli.

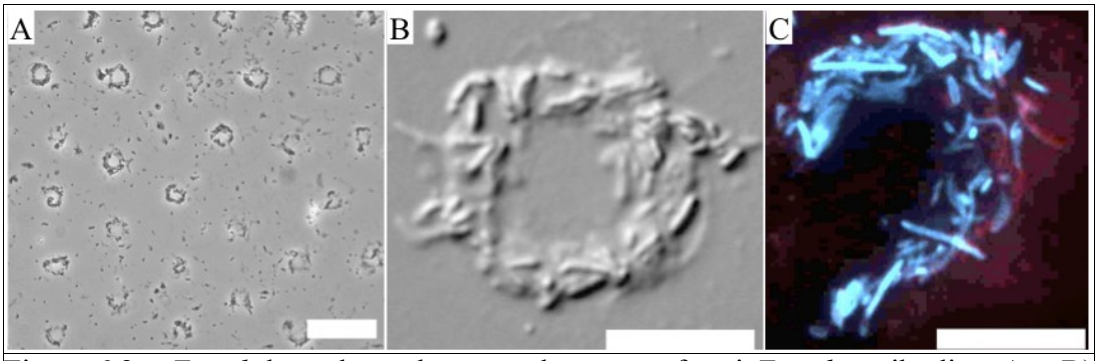

Figure 6.2 *E. coli* bound to a hexagonal pattern of anti-*E. coli* antibodies. A + B) Phase contrast images. C) Fluorescence image, bluish *E. coli*, stained with DAPI, reddish antibodies, stained with Ab-Cy3. (Scale bars: 50 µm (A) and 10 µm (B+C)

6.1.2 Comparison between Annuli- and Non-structured surfaces

In order to verify whether these antibody structures were still specific for their actual antigen and whether the arrangement of antibodies in a curved topography could improve the binding of the bacteria, comparative experiments were carried out. Figure 6.3 shows the results of a test in which three different bacteria strains were applied to a pattern of anti-*E. coli* antibodies. For each image the number and average size of particles were determined by image analysis software. In Figure 6.3A a phase contrast image shows a hexagonal pattern of anti-*E. coli* antibodies incubated with a mixture of *Proteus myxofaciens* (*P. myx*) and *Klebsiella planticola* (*K. pla*) (optical density $OD_{600} = 0.1$) and rinsed afterwards. In this case the bacteria strains are not specific for the antibodies. One can clearly see the individual annuli and that only few single particles are present. Most of the bacteria did not bind to the antibody structures and were rinsed away. Therefore it is concluded that the nonspecific binding is marginal.

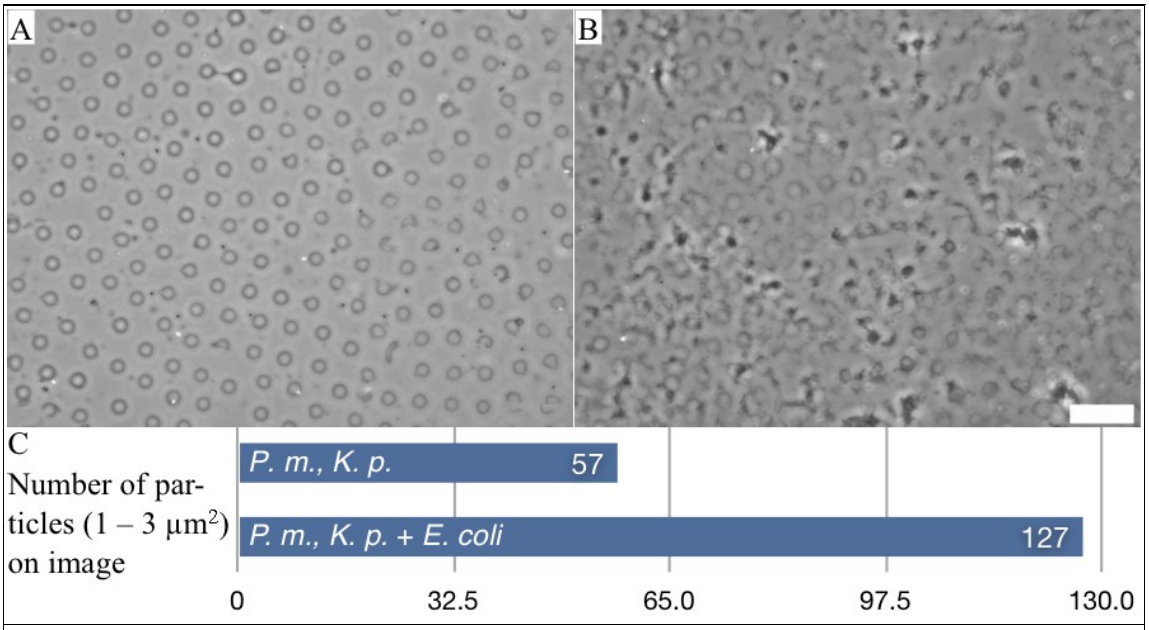

Figure 6.3 A) Phase contrast image of a hexagonal pattern of AbE1, incubated with a solution of *P. myx.* and *K. pla*.. B) Phase contrast image of a similar surface but incubated with *E. coli* in addition to the aforementioned bacteria. (Scale bar: 20 µm) C) Relation between the number of particles in the size between 1 and 3 µm² on an anti-*E. coli* antibodies surface and the applied bacteria strains.

In the comparison experiment, in addition to the two other bacteria strains, *E. coli* was added at the same concentration. After applying the bacteria mixture, incubating and rinsing, the antibody annuli array structures became hardly discernible as shown in Figure 6.3B. Contrary to the case above, a large amount of small particles, i.e. bacteria, are randomly distributed on the surface. Although not strictly following the annuli contour, many particles, most likely the *E. coli*, bound to the antibody structures under a close examination. The amount of particles and their size in the two images are compared in Figure 6.3C. On comparable substrates the number of particles in the size of bacteria (1 – 3 µm^2) is more than twice as high (127 compared to 57) after rinsing if the specific bacteria, i.e. *E. coli*, are present in the solution.

To prove that the annuli-patterned substrate is superior over a normal "flat" substrate incubated with antibodies and dried afterwards, the experiment was repeated on a flat glass slide coated by physical adsorption with the same kind of antibodies as in Figure 6.3. The corresponding image is depicted in Figure 6.4. Figure 6.4C shows that less (1/3 – 1/2) specific and non-specific binding occurs when particles are bound to the flat surface compared to the annuli-structured one. The higher binding capacity of the annuli-structured surface can be exploited in a potential biosensor.

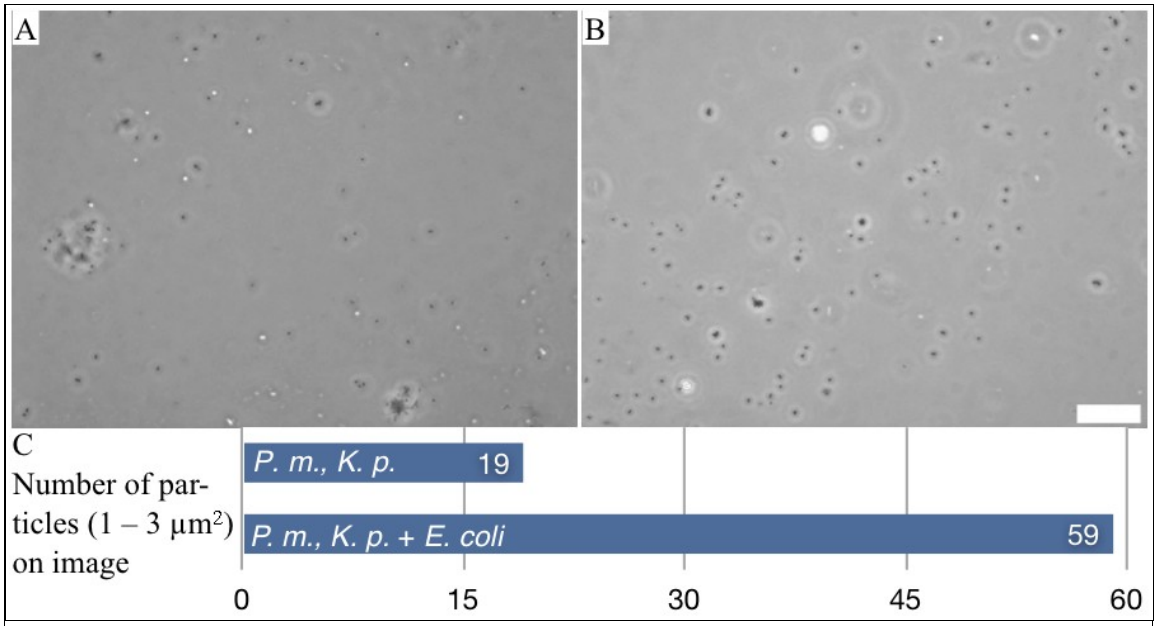

Figure 6.4 A) Phase contrast image of a planar glass slide coated with AbE1 and incubated with a solution of *P. myx.* and *K. pla.*. B) Phase contrast image of a similar surface but incubated with *E. coli* in addition to the aforementioned bacteria. (Scale bar: 20 µm) C) Relation between the number of particles in the size between 1 and 3 µm^2 on a planar anti-*E. coli* antibodies surface and the applied bacteria strains.

This study shows that the antibody-annuli-patterned surface can function as an effective detector device for bacteria in a mixture solution, since the specific capture of bacteria has been significantly improved owing to the geometrical feature of the annuli. The study also corroborates that the specificity of the antibodies immobilized in two-dimensional annuli arrays was unscathed during the surface preparation and the following detection procedures.

6.2 Cellular Mimics by Integrin Functionalized Lipid Vesicles

The structured protein annuli can also be employed for the bio-recognition and enrichment of eukaryotic mammalian cells by integrin-mediated cell adhesion.

Integrins present an important family of transmembrane proteins specifically responsible for the mediation of cell surface adhesion and binding to the extracellular matrix.[235] They are involved in mechanical interactions and in signal transduction processes inside cells. Furthermore, they present an interesting class of transmembrane proteins appearing in different kind of physiological as well as pathophysiological processes and are known as potential targets for drug development.[236] Integrins are heterodimeric and consist of two, non-covalently bound subunits, alpha and beta respectively.[237] One integrin species, the vitronectin receptor $\alpha_v\beta_3$, is especially involved in tumor metastasis and tumor-related angiogenesis.[238] The investigation of the interactions between such transmembrane proteins and their potential ligands is of great importance. In particular, the development of methods to prepare substrates having ligands immobilized in controlled densities and patterns and wherein the ligand–receptor interactions between cell and substrate are well-defined is sought.[239] Our technique therefore provides a toolbox to investigate the interplay between integrin and its ligand, which underpins the major scientific effort of elucidating the complex biological pathways associated with cell membranes.

Cell culture models are widely exploited for integrin-ligand drug screening.[240,241] Although bearing some advantages, the number, location and state of the integrins in the cell membrane can hardly be controlled, hence resulting in poor reproducibility. The implications of using cell-free binding tests are however problematic since integrins, as membrane proteins, need a cell membrane environment for their native conformation and the purified integrins are hardly functional. Moreover, the incorporation of membranes may be crucial for the protein-ligand interaction of membrane proteins. To overcome these intrinsic problems, a cellular membrane mimic system, where native transmembrane receptors were incorporated into artificial phospholipid bilayers on

biosensor devices, was developed for the first time in 2006.[242] This technique was one step further improved by incorporating intact $\alpha_{IIb}\beta_3$ integrin molecules in giant unilamellar vesicles (GUVs) in the range of 20 – 40 µm instead of planar bilayers, hence creating artificial integrin-functionalized phospholipid quasi-spheres.[243]

In contrast to the present binding assays [244,245], an alternative is presented in this work: An *in vitro* assay, enabling characterization of both native and synthetic integrin ligands. The approach is expected to be capable of providing quantitative conclusions about the interplay between integrin and its ligands by, for instance, the intensity of a fluorescence signal arising from binding events to the antibody-structured surface. Both concepts, a cellular membrane mimic system for ligand-binding studies and the incorporation of integrins in vesicles are brought together in the second part of the presented work. Integrin $\alpha_v\beta_3$ was incorporated into large unilamellar vesicles (LUVs) [191] (diameters 60 – 100 nm) consisting of a phospholipid bilayer and specifically bound to annuli antibody structures where the antibodies were specific for the integrin $\alpha_v\beta_3$. In brief, multilamellar vesicles were repeatedly extruded under moderate pressure through polycarbonate filters (100 nm pore size). These spherical vesicles were bound to and defined by the array of antibody nano-rings. The secondary vesicle structures were observed by means of atomic force, phase contrast as well as fluorescence microscopy.

6.2.1 Assembly of Integrin $\alpha_v\beta_3$ in 100 nm Vesicles

The antibody annuli were used so far to bind whole bacteria, on which the actual antigen is unknown. As the next step, a specific protein was utilized, against which the antibody annuli are specific. Two questions were addressed in this part of the presented work: it was examined, firstly, whether it was possible to incorporate human integrin $\alpha_v\beta_3$ into the 1,2-dioleoyl-sn-glycero-3-phosphocholine (DOPC) 100 nm vesicles. Secondly, whether the inserted integrins have kept their physiological structure during vesicle preparation and could bind specifically to an annuli structure made of antibodies against this protein. The answer of the first question brought us to an integrin binding assay as well as a model for the binding of cells containing integrin in their outer membrane. The schematic in Figure 6.5A depicts a DOPC-vesicle with on average three integrated integrin molecules. Figure 6.5B and Figure 6.5C illustrate the question already raised for the bacteria study: Will the vesicles show enhanced binding to the structured surface compared to “flat“ surfaces?

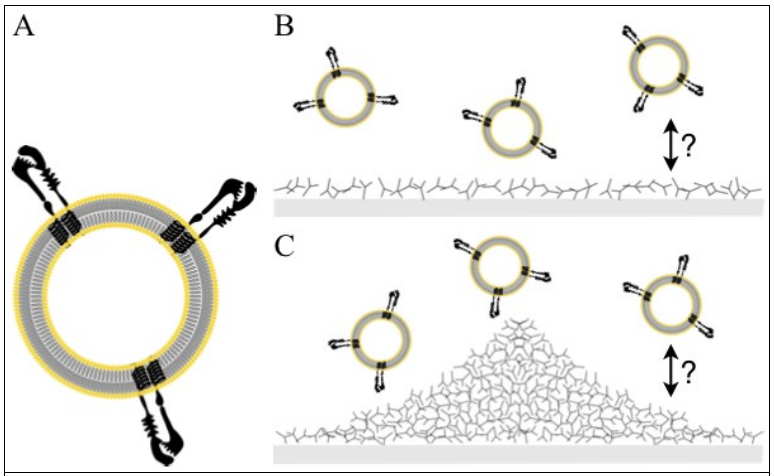

Figure 6.5 A) Schematic illustration of a vesicle with three incorporated integrin molecules. B) Integrin vesicles inter-acting with a planar antibody coated surface. C) Integrin vesicles interacting with a structured antibody surface. (Not to scale)

6.2.2 Integrin Functionality

In order to investigate the orientation and conformation of the incorporated integrins, human integrin $\alpha_v\beta_3$ was selected for constituting the nanoring structures because of its resolved specificity to human integrin. The height of the antibody annuli was measured by AFM after constitution, i.e. before incubation, and after pipetting a small amount of integrin vesicles on them. To check for unspecific binding to the antibody structures, the surface was incubated with vesicles without integrin. Examples for the results are shown in Figure 6.6. Figure 6.6A shows the AFM-image of antibody annuli incubated with vesicles without integrin and Figure 6.6B incubated with vesicles with integrin. Height profiles were extracted from the white lines and are depicted in Figure 6.6C. One can clearly see that the topography after the incubation with integrin vesicles is approximately 100 nm higher compared to the pure structures.

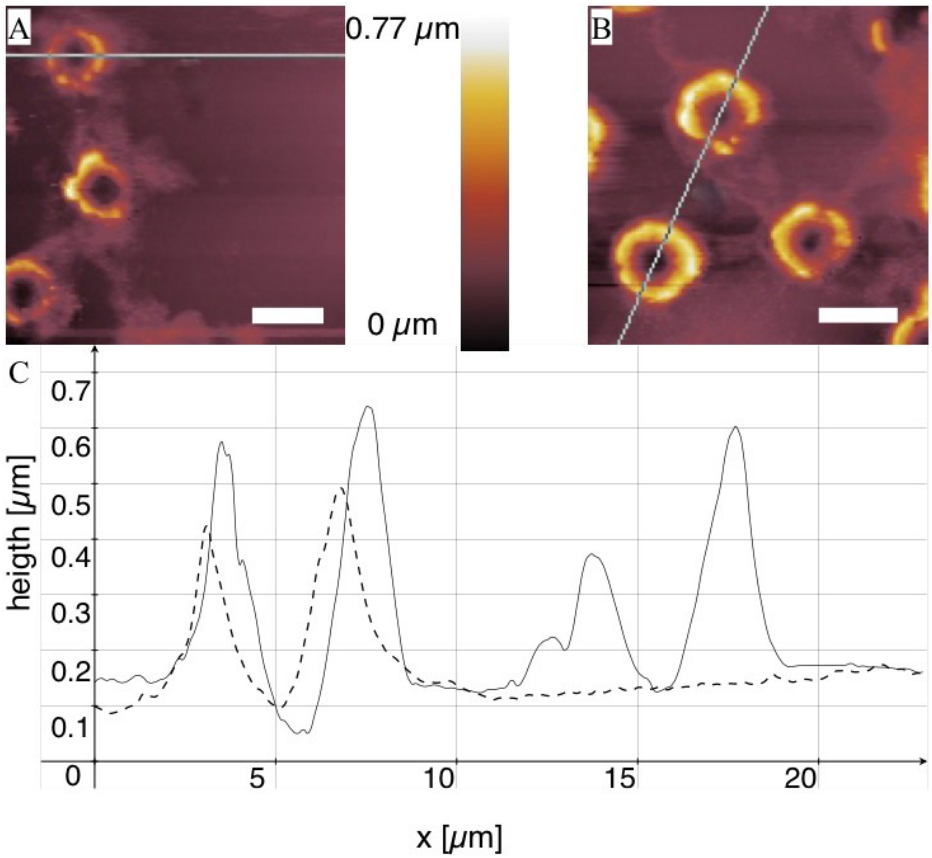

Figure 6.6 AFM images of annuli antibody surface, incubated with vesicles without integrin (A) and with integrin (B). C) Height profiles along the indicated lines: A) dashed, B) continuous. (Scale bars: 5 µm)

The mean values of several analogous experiments and an additional comparison with surfaces incubated with pure vesicles without any integrin are depicted in Figure 6.7. Although the error due to the limited number of annuli is fairly high, a clear distinction between integrin and non-integrin vesicles as well as the pure antibody structures can be made. The topography of the antibody annuli is about 100 to 150 nm higher compared to the two other cases if proteoliposomes are applied. Furthermore the height difference is in good agreement with the diameter of the applied vesicles. This accordance means that the vesicles are only bound to the antibody structures if integrin molecules are present in the double layer. It is assumed that the proteins are bound to the antibody structures and are therefore in a physiological conformation.

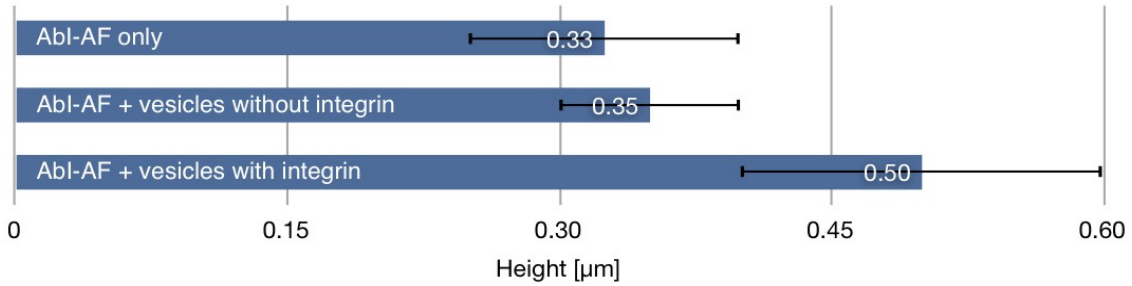

Figure 6.7 Average height of AbI antibody annuli structures (top), incubated with vesicles without integrin (middle) and with integrin (bottom). Measured by AFM.

An additional test was conducted to further prove the specific binding of vesicles to the antibody annuli. A fluorescent dye was included in the vesicle membranes and the signal intensity was measured for the three aforementioned cases. The corresponding graphs are presented in Figure 6.8. The wide error-bars were probably caused by the small amount of fluorescent molecules incorporated in the vesicle membranes and the limited sensitivity of the utilized microscope relatively high. But nonetheless the trend is consistent to the AFM height evaluation, showing a stronger signal for vesicles with integrin than without.

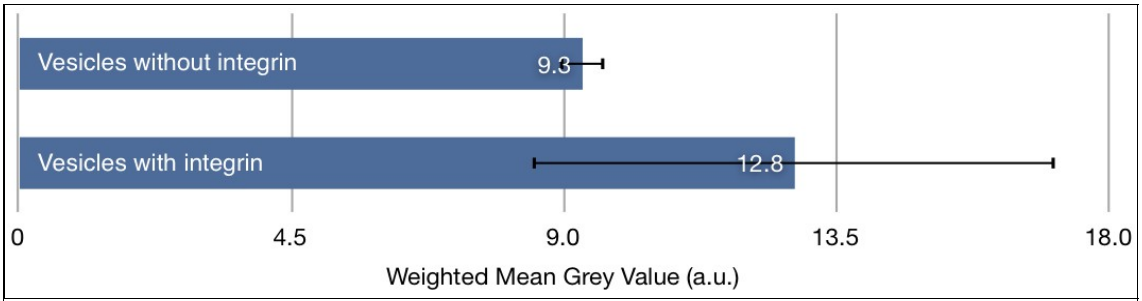

Figure 6.8 Average mean grey value (higher = brighter) of antibody annuli surfaces incubated with vesicles stained with a fluorescence dye (DiD648, top) and the same vesicles with additionally incorporated (bottom). Measured by fluorescence microscopy.

6.3 P19 Cells Bound to Annuli Structures

Subsequent to bacteria and integrin vesicles, it was finally tested whether it is possible to bind P19 embryonal carcinoma cells to the AbI-AF annuli pattern. It is known that P19 cells carry integrin $\alpha_v\beta_3$ on their membrane.[246] Hence these cells represent a reasonable continuation to the previous

experiments with integrin vesicles and it was sought-after to find out whether their adhesion to surface is affected by the anti-integrin antibody annuli.

The cells were cultivated without any antibiotics over several days by another group member until they had reached a concentration of approximately 10^5 and 10^6 cells per milliliter. Subsequently, antibody annuli structure of 10, 20, 50 and 100 µm were incubated with four milliliters of the P19 suspension for 5, 24 and 48 hours. Three typical images of the results are depicted in Figure 6.9.

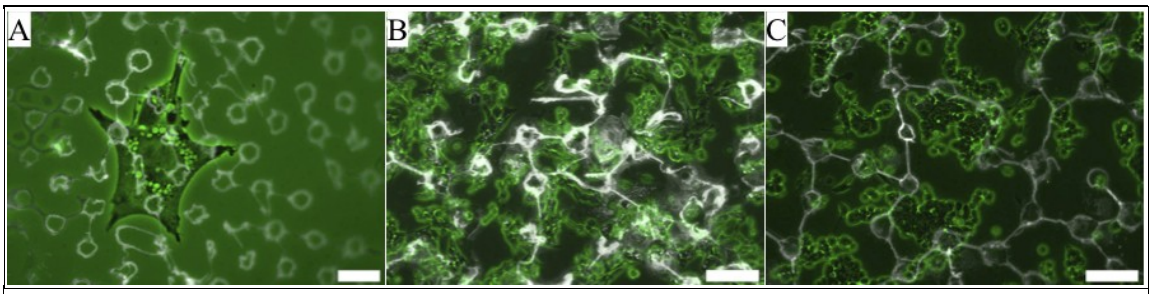

Figure 6.9 P19 cells (phase contrast, green colored) incubated on AbI-AF (fluorescent, grey colored) annuli pattern of different sizes. (Scale bars: 20 µm (A) and 100 µm (B + C))

It is evident that no pattern of P19 cells was visible nor was any other structure of the underlying antibody annuli adopted by the cells. The same accounted for other sizes of antibody structures, incubation times and concentrations. Therefore, it is concluded that the pattern of anti-integrin $\alpha_v\beta_3$ antibody was not able to influence the surface adhesion and growing of the P19 cells. Possible explanations could be that the integrins on the membrane of the cells were neither bound to nor effected by the antibodies. Because in previous experiments this mere binding was observed, it is also possible that the binding of single integrin molecules in the membrane did not effect the growth and development of the P19 cells in a way that the results are microscopically visible.

6.4 Circular Antibody Structures

In contrast to the readily described annuli and in order to achieve circular structures completely filled with antibodies against *E. coli* another proceeding was developed. It included no drying step, hence the arrangement of the antibodies is not induced by the retreating solvent. Rather the area around the microparticles was passivated. Compared to microspot printing our technique allows the

production of large-scale spots in a very simple „bench-top“ process without the need for sophisticated equipment like, for instance, a microarray printer, therefore being cheap and timesaving.[247]

As the first step, a monolayer of microparticles in the size of 10 µm was again deposited on a cleaned glass slide by horizontal deposition. The area around the microspheres was subsequently activated by very shortly dipping the substrate in boiling piranha solution. Thereby timing was crucial. An overly long incubation of the polystyrene template in the boiling acid caused a complete displacement of the spheres and therefore destruction of the structures.

After activating the hydroxyl groups the surface was in the next step passivated by means of the silane Methoxytriethyleneoxypropyltrimethoxysilane (MTMS), which has a structural property $(O\text{-}C_2H_4)_n$ similar to that of polyethylene glycols (PEGs) and was commercially available. As mentioned above, PEGs are known to be chemically inert and especially to prevent protein attachment, like e.g. antibody adsorption. Although the PEG-derivate used in this study was significantly shorter compared to the one examined by Sofia et al.[224] (with molecular weights in the range of several thousand up to 20,000 Da), the results showed a significant blocking of the protein adsorption on the areas passivated with PEG silanes.

Subsequently to the passivation step the residual microparticle template was dissolved and washed away, uncovering non-passivated circle spots, which were filled with physisorbed antibodies subsequently: The sample was immersed overnight in an AbE1 solution, rinsed and incubated for another night with Ab-Cy3. The results are depicted in Figure 6.10.

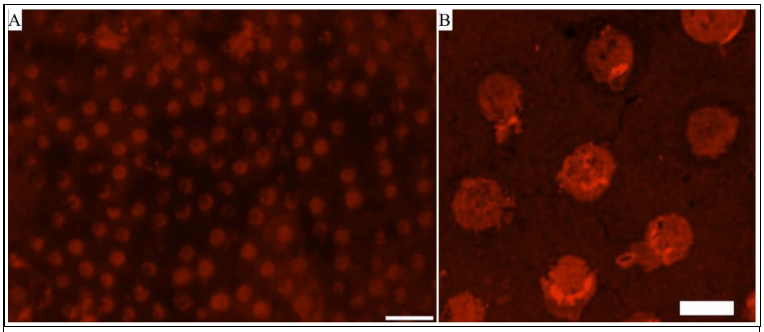

Figure 6.10 CLSM images of circular antibody structures. (Scale bars: 20 µm (A) and 5 µm (B))

It can be clearly seen that red spots were evenly distributed over a dark background and partially formed a hexagonal pattern. There were two types of red circles, namely fully filled red circles and ring-like red circles. The red fluorescence implied the specific binding of the secondary to the first antibody, which was selectively deposited on the areas protected by the PS.MS spheres from PEGylation. The dark areas in the incomplete red circles or the ring-like circles suggested that no antibodies were bound. A possible explanation for this can be that the particles only partially touched the bottom which could be caused during template formation where the microspheres did not achieve perfect hexagonal ordered crystals. A possible explanation for the residual signals could be impurities in the antibody solution as well as density and concentration heterogeneity during immersing of the samples.

On the other side, when the surface was not treated with MTMS, the inverse structure could be observed (data not shown). The antibodies were physisorbed to the whole glass surface. That means if the spheres are dissolved before applying AbE1 almost the entire glass slide showed a fluorescent signal after staining with Ab-Cy3. If the antibodies however are applied without dissolving the spheres before, one can observe dark dots (where the particles where sitting) on a bright (fluorescent) background after the staining (data not shown).

6.5 Conclusion and Outlook

In this section a new and facile approach for patterning large-scale 2D arrays of ordered antibody annuli with a preserved protein functionality and tunability in size and shape was presented. The distance between the created annuli could easily be tuned by using templates of appropriate polystyrene microspheres (PS-MS). Particles of sizes between 1 and 100 µm were studied but different ones should be readily applicable.

The patterning of large area nanoscale ring structures, dots, rods and microwire networks, respectively, by a similar attempt has already been described for carbon nanotubes [248], iron [249] and gold nanoparticles.[250,251] Here it was demonstrated that this approach could be expanded further from hard to soft matter. Antibodies, as a class of much more complex nanoparticles featuring bioactive functionalities, could also be patterned into hexagonal arranged annuli arrays with a high robustness as well as active bio-functionality. To obtain a template for protein patterning, glass substrates were covered with a crystalline monolayer of micrometer-sized polystyrene spheres. After detaching the template, the resulting antibody patterning was investigated by atomic force,

confocal and fluorescence microscopy. To study the protein drying, migration and arrangement processes, antibodies against *Escherichia coli* K12 and enhanced Green Fluorescent Protein (eGFP) were used as model systems. The integrity of the primary antibodies in the ring structures appeared to be well-preserved during the patterning procedures, hence remaining effective in binding their specific antigens. The structures showed robust properties without any sign of degradation after rewetting by, for instance, the aqueous secondary antibody solution. So it can be concluded that the proteins, although still showing bioactivity, are strongly bound to the substrate and connected with each other simply through the drying procedure. The produced antibody annuli structures replicated the hexagonal alignment from the colloidal template and consisted of two to three layers of antibodies.

With this approach, the drying lithography method [250] was taken one step further in terms of structure versatility and bio-compatibility, whereas in particular the latter opens up new avenues for constructing supramolecular architectures with cellular compositions for sensing applications. This facilitated the subsequent demonstration of the validity of this novel technique for further applications.

The ordered antibody-annuli surfaces, created in the presented work, provided a new sensing platform that could address antigens of several orders of magnitude – ranging from single molecules like integrin to whole bacteria cells like *E. coli*. In addition to exploiting the singular biochemical specificity and sensitivity of antibodies for a multiplicity of molecules, the physical shape and size of the surface features were employed by the creation of ordered annuli-shaped antibody pattern for cellular and vesicular attachment. By positioning antibodies in a three-dimensional curved topography, the physical shape and dimensions of an antibody surface resulted in an enhanced specific binding capability of analytes.

Contrariwise, for the binding of P19 cells to antibody annuli no clear results could be observed. Therefore, it is concluded that other cell lines and maybe different membrane proteins needed to be investigated for their application in binding eukaryotic cells to an antibody pattern in a defined way.

Eventually, filled spots of antibodies could be prepared by passivating the area around the microspheres with a silane showing structural characteristics similar to PEGs. After the detachment of the PS spheres the primary antibodies were applied and physisorbed to the silane-free surface.

It was shown that the solvent of the antibodies played a major role in the arrangement into annuli and hence exclude some of the commercially available antibodies from this technique.

Hence, the capability of a specific antibody to be applicable must be examined as the case arises. This may be a problem if there will be only one specific antibody available but can be overcome by, for instance, putting further efforts in the cleaning or exchange of the antibody solution.

In summary, a facile and versatile „bottom-up“ strategy for generating large area microarrays of different mono- as well as polyclonal antibody annuli was presented. It could be employed as a surface technology toolbox in the micrometer regime, for structured bioactive surfaces which can be applied in, for instance, biochemistry, molecular biology and materials science. Owing to its relative simplicity this framework should easily be extendable to other antibodies and proteins as well. The additional structuring of surfaces with a hexagonal patterning of antibody annuli can enable annuli-shaped antibody-based microarray sensors. The approach may be used for methods requiring hexagonal arrangements of vesicles, cells and other microsize biological objects and thereby assist well-established methods like cell culture and future cell-free *in vitro* assays.

7 Size Exclusion Filters

Starting with section 7.1 the process of nano-filter fabrication including occurred problems and adequate solutions are elucidated. Following that, the trials to get rid of cracks and to find a suitable substrate material are presented in sections 7.2 and 7.3, respectively. Eventually, in section 7.4 the first results of bacteria applied to the generated structures are demonstrated.

7.1 Fabrication Process

As described in section 1.6.4 – "200 nm Size Exclusion Filters for Nano-Filtration", 200 nm filtrations are frequently referred to as "sterile filtration". The aim of this project was to achieve 200 nm filters in an extremely flat way for application in an optical read-out system.

To achieve a pore size of approximately 200 nm, much smaller particles compared to the already described 10 µm PS-MS had to be used. Because the diameter of the contact area between two equal polystyrene particles, and hence the smallest dimension in the according inverse opals, is approximately one fifth of their diameter after annealing (cf. section 4.5 – "Inverse Opals Dimensioning"), 1 µm PS-MS seemed to be reasonable for the construction of 200 nm pores.

In the beginning, it was tried to generate inverse opals by sequential deposition of 1 µm PS-MS and 7 nm silica nano-particles in ultrapure water in a PTFE trough, as described in section 2.3.1 – "Sequential Deposition". The resulting structures before and after pyrolysis are depicted in Figure 7.1A and Figure 7.1B, respectively.

It is obvious that only parts of the substrate were covered with particles, which made the structure intrinsically unfeasible as a filter. This was also visible by eye because large "insular" structures were formed. A simple increase in the volumes, until the whole surface would have been covered by inverse opals, would have led to, amongst others, too much particle layers, which would be not applicable in a potential filter for liquids, due to an increase in pressure.

Therefore the next idea was to substitute the ultrapure water with a surfactant like T20, in order to decrease the surface tension and facilitate the formation of a homogenous liquid layer above the substrate. The corresponding SEM images are depicted in Figure 7.1C and Figure 7.1D, respectively. Sponge-like structures with very small cavities in the order of tens of nanometers were formed. The reason for this behavior stayed unclear and the formed structures showed several

distinct disadvantages. On the one hand, an unneeded small porosity for the purpose of bacteria filtering was generated, potentially leading again to an increase in pressure. On the other hand, the number of “layers” and the roughness of the surface – which was sought-afterto be as flat as possible – seemed to be uncontrollable.

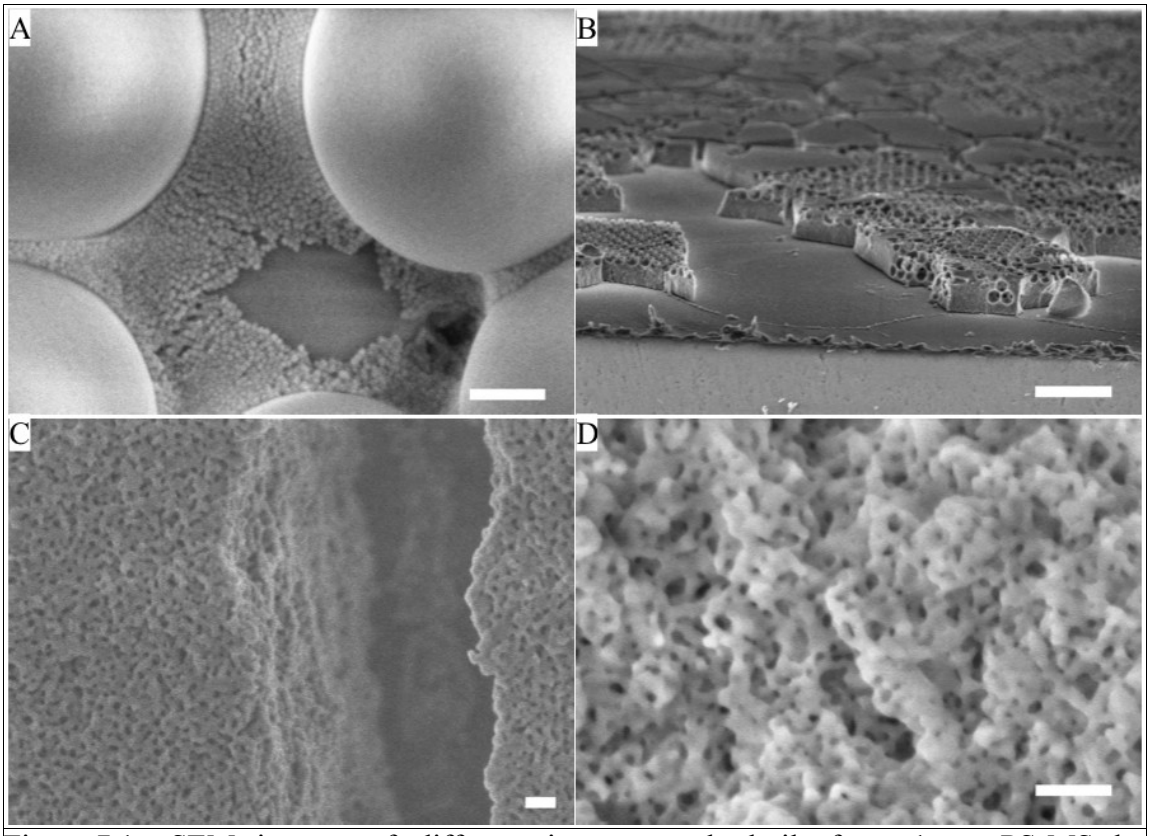

Figure 7.1 SEM images of different inverse opals built from 1 µm PS-MS by sequential deposition in a PTFE trough. A + B) PS-MS suspended in ultrapure water. C + D) PS-MS suspended in T20. (Scale bars: 200 nm (A,C,D) and 5 µm (B))

All those drawbacks made the sequential deposition in a PTFE trough to appear unfeasible for the sought-after filter application. Hence, it was switched to the second possibility – the sequential vertical deposition, as likewise described in section 2.3.1 – “Sequential Deposition“. The resulting structures are depicted in Figure 7.2.

One can clearly see that the fabricated inverse opals were of better order and hence quality. SEM images show a perfect crystalline arrangement and defined number of layers. Furthermore, in

Figure 7.2 the generated connecting openings between two hollow spheres with the required diameters of about 200 nm, are clearly visible.

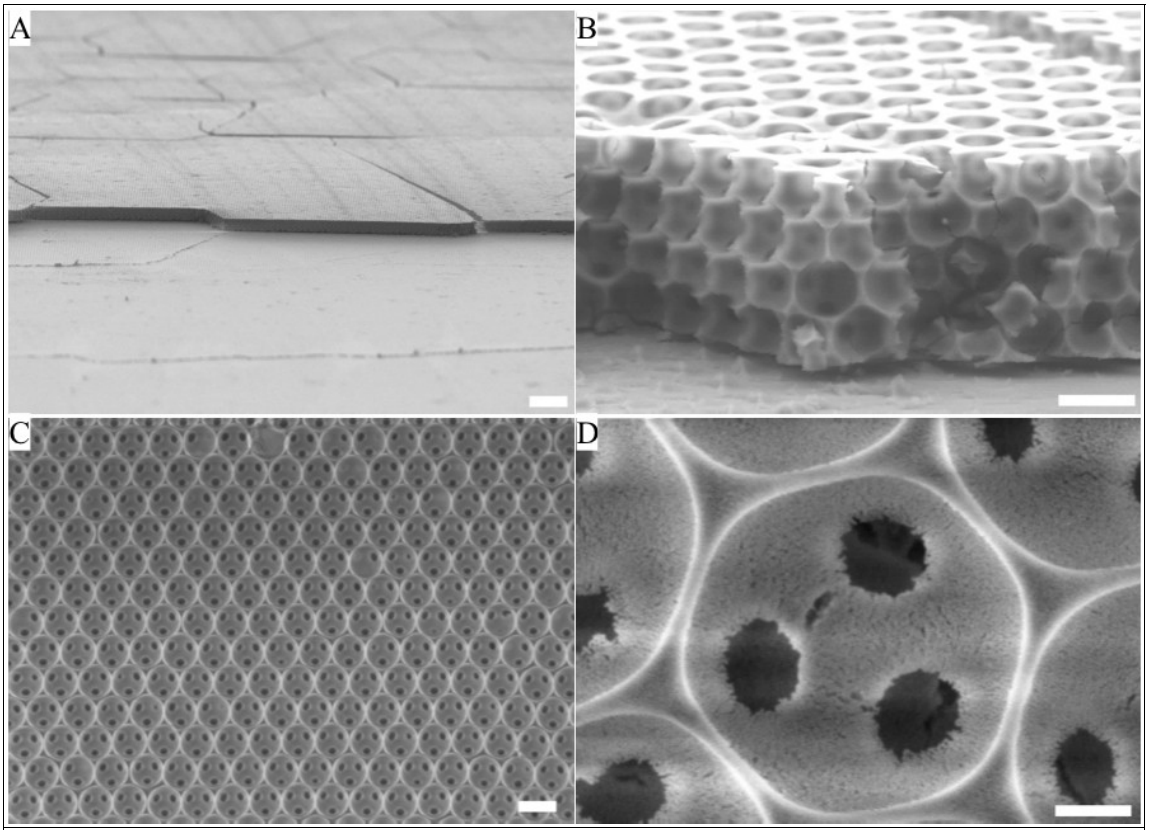

Figure 7.2 SEM images of different inverse opals built from 1 µm PS-MS by vertical co-deposition. A + B) side view. C + D) top view. (Scale bars: 10 µm (A), 1 µm (B + C) and 200 nm (D))

Nevertheless, also this fabrication process revealed one phenomenon making the obtained structures inappropriate for potential filter applications. Fine cracks could be observed along the growth direction of the polystyrene and silica particles, as depicted in Figure 7.2A. The reason for them is the release of the stress accumulated in the lattice due to shrinkage of the water layer around the spheres during the drying process.[130,252] The spacing between the cracks was about several micrometers.

To overcome these issues, two “anti-crack approaches” were accomplished and are described in the next sections.

7.2 Anti-Crack Approaches

SEM images showing the incidence of typical cracks during inverse opals construction are depicted in Figure 7.3. It was visible that they were evenly distributed over the whole substrate with a distance between two parallel cracks of about 10 – 20 µm and a width of the cracks of about 1 – 2 µm.

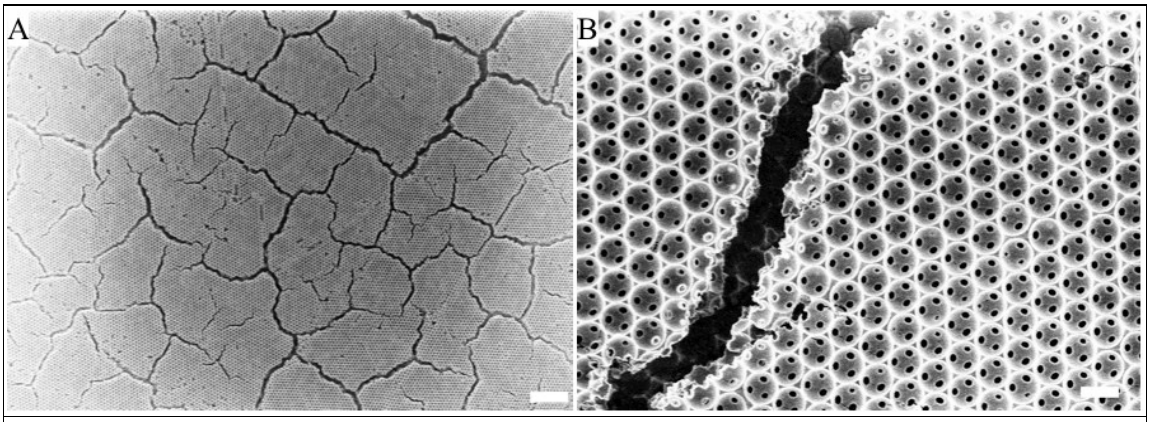

Figure 7.3 SEM images of 1 µm inverse opals, showing multiple cracks. (Scale bars: 10 µm (A) and 1 µm (B))

In order to dispose them and make the structures appropriate for a potential application as a filter for bacteria, two approaches were pursued. On the one hand three thin layers of inverse opals were generated on top of each other. On the other hand, instead of using 7 nm silica nano-spheres, the sol-gel precursor tetraethyl orthosilicate was used as the filling material. It has been recently shown that with this approach large-area, highly ordered, crack-free inverse opals film can be fabricated.[139]

7.2.1 Multilayer Assembly

The first approach to overcome the emergence of cracks in the crystal and hence to make the created inverse opal structures suitable as a filter element for bacteria, was not to avoid them but rather the consequence of their existence, which was a connecting passage from one side of the substrate to the other without the liquid passing through the inverse opal cavities.

Therefore, three thin layers of inverse opals were deposited one after another on top of each other, each showing a thickness of 1 – 3 µm. With every additional layer the probability of end-to-

end cracks decreased and the defects changed from lines to points and eventually disappeared, as depicted in Figure 7.4.

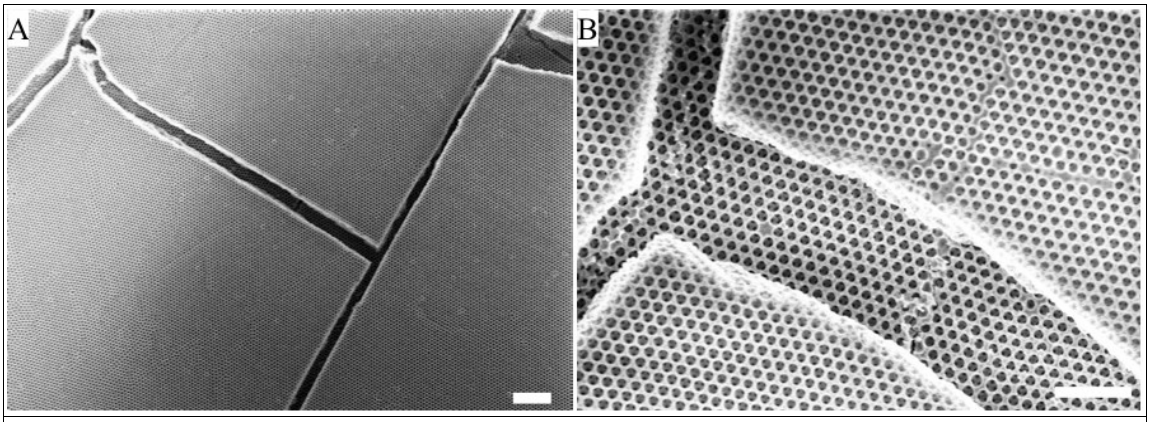

Figure 7.4 SEM images of 1 µm inverse opals, showing two layers on top of each other. (Scale bars: 10 µm (A) and 5 µm (B))

Before the deposition of the next layer of inverse opals, each layer was tempered and afterwards assembled again in the vertical deposition instrument. Hence, for three layers three steps of tempering and vertical deposition were necessary. Consequently, the whole process was time-consuming and had the risk of losing parts of the structure in between, hence leading to only very small intact filters. Therefore, another optimization step for avoiding cracks was necessary. It was found in a sol-gel process and is described in the next section.

7.2.2 Co-assembly with Sol-Gel Precursor

According to Hatton et al. avoidance of cracks during the fabrication of inverse opals can be achieved by exploiting such a sol-gel precursor.[139] They generated multilayered composite colloidal crystal films by evaporative deposition of polymeric colloidal spheres suspended within a hydrolyzed silicate sol-gel precursor solution. The co-assembly of a sacrificial colloidal template with a matrix material avoided the need for liquid infiltration into the colloidal crystal and minimized the associated cracking and inhomogeneities of the resulting inverse opal films. The resulting SEM images are depicted in Figure 7.5.

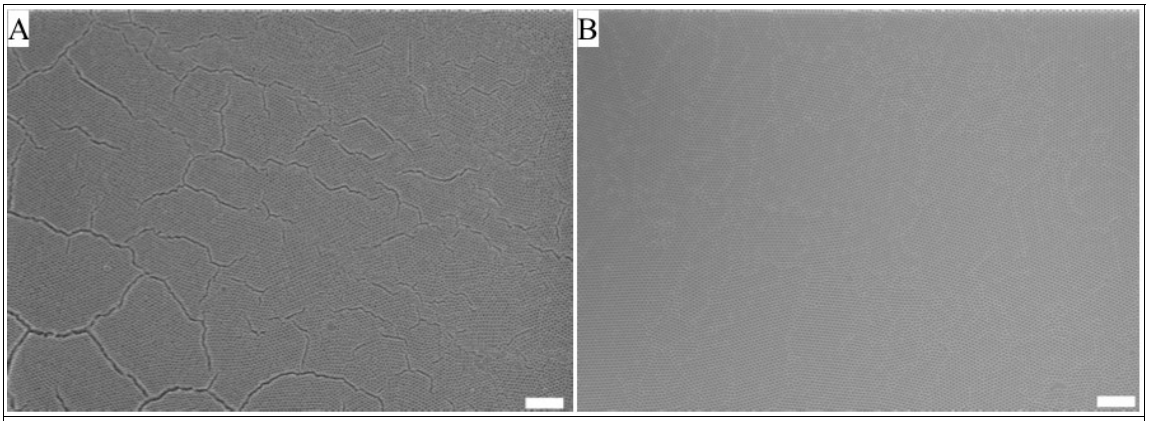

Figure 7.5 SEM images of 1 µm inverse opals built by co-assembly with a sol-gel precursor. For details see text. (Scale bars: 10 µm)

On parts of the substrate cracks were still visible, as depicted in Figure 7.5A (bottom left corner). But on other areas the glass slide was almost crack-free, as depicted in Figure 7.5A and B. Hence this approach seemed to be promising but also needed further parameter improvement with the perspective that more reproducible and larger substrates could be produced.

In order to transfer the filter structures from a flat glass slide to a usable filter system, it was necessary to find an appropriate porous substrate material. This material should be at the same time capable to support the filter and prevent it from breaking, and flat enough for the potential detection system. A potential solution is described in the next section.

7.3 Recrystallized Silicon Carbide Substrates

To use the fabricated structures as a potential filter, a porous substrate capable of providing a basement-like structure for the adjacent deposition of 1 µm inverse opals produced by one of the previously described methods was required. It needed to be mechanically stable but at the same time as thin as possible to keep the need pressure as low as possible. Furthermore, a porosity and surface structure which facilitated the deposition of crystals and which was applicable in a vertical deposition instrument was essential.

First attempts with a perforated adhesive tape failed due to the large diameter of the openings and the intricate production process by CO_2-laser treatment. Alternatively, samples of a recently developed recrystallized silicon carbide material were provided by the University of Applied Sciences Koblenz and showed some remarkable properties. The porous ceramic material was available in the sought-after geometry, including a thickness of 700 µm, and it showed a porosity of

50 %, a tunable pore size between 1 and 12 µm and a narrow pore size distribution of 80 – 90 %. Hence together with our 200 nm inverse opal material a good filtrating material seemed to be accessible.

Small rectangular plates were mounted in the vertical deposition instrument and, by co-deposition, coated with 1 µm PS-MS crystals encapsulated with 7 nm silica nano-spheres. Afterwards the structures were pyrolyzed as described before and analyzed by SEM. The resulting image are depicted in Figure 7.6.

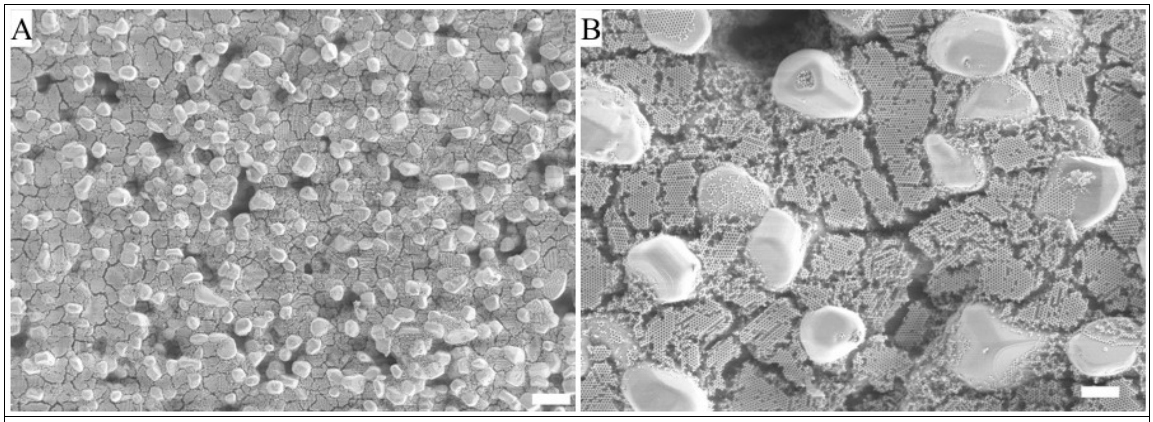

Figure 7.6 SEM images of 1 µm inverse opals (3 wt% solution) on a recrystallized silicon carbide substrate. For details see text. (Scale bars: 50 µm (A) and 10 µm (B))

Depending on the concentration of PS-MS, which ranged from 0.75 to 3.0 wt%, the silicon carbide substrates were covered to different degrees. Till 2 wt% only partially samples, but for 3 wt % an almost closed structure could be achieved. Nevertheless, a considerable formation of cracks could not be avoided again. Furthermore, the images clearly show that the structure was due to the underlying substrate not as flat as needed. The 1 µm inverse opals were deposited between the larger, 10 – 20 µm sized ceramic “nuggets”, which overhung. Hence it was concluded that this approach also needed further improvement in the way of substrate preparation, i.e. seediness, and deposition of inverse opals, i.e. amount of particles, to obtain a smoother surface.

At this point, the structure’s ability to serve as a filter for bacteria still needed to be verified and is demonstrated in the next section.

7.4 200 nm Bacteria-Filters

To prove that the fabricated inverse opal structures were in fact capable of filtering bacteria and other substances with a size of 1 – 3 µm, a solution of *E. coli* was applied.

At first, the bacteria were cultivated in LB-medium over night, as described in section 2.5.3 – "Cultivation for Experimental Use". On the next day the bacteria solution was diluted in PBS until an OD_{600} value of 0.1 was achieved (approximately 1/20 of the primary solution). Afterwards the bacteria were killed by heating the solution for 30 min to 90 °C. In the end, a drop was pipetted on the inverse opal structures, let dry again over night and the structures investigated by SEM the next day. The resulting images are depicted in Figure 7.7.

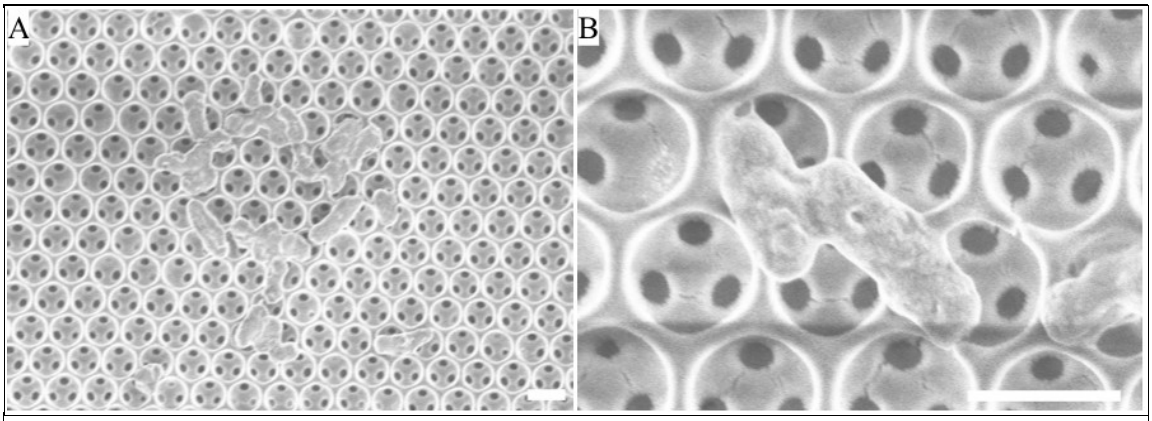

Figure 7.7 SEM images of 1 µm inverse opals with dried *E. coli* on top. (Scale bars: 1 µm)

In Figure 7.7A a circular conglomerate of several *E. coli* is displayed. In addition, in Figure 7.7B the different scales of inverse opals and bacteria are apparent. The latter are significantly larger than the top loopholes of the glass structure and compared to the openings to the underlying hollow spheres the *E. coli* exceed even more. Therefore the general filtering capability in terms of size exclusion was proved and the results were even promising for even smaller particles, either bacteria or organic and inorganic materials.

7.5 Conclusion and Outlook

In this chapter, inverse opals with a cavity diameter of 1 µm were generated. Due to the existence of several layers of inverse opals, the contact areas to the underlying colloidal crystals became

openings between hollow spheres during the fabrication process. These passages showed a size of approximately 200 nm, which is known to be a critical size in “sterile filtration”. It could be shown that the resulting inverse opals structures were capable of size-excluding *E. coli* bacteria.

In addition to this, several of the occurred problems were addressed like, for instance, the formation of unordered structures, only partially covered glass substrates, the development of cracks and the need of an adequate porous substrate as replacement of the aforementioned glass. With it, a further application of a another work group’s development could be shown too.

Contrariwise, also several problems occurred which still need further examination, like the reproducible fabrication of larger crack-free opal structures. Furthermore, the application of the inverse opals to the porous recrystallized silicon carbide substrate in a way that a flat surface is achieved, is still demanded for a very flat filter material. Finally the assembly of the complete material and its application for filtering “real” liquid samples still needs to be realized.

In conclusion, the proof of principle to use inverse opals as a potential filter material for “sterile filtration” were demonstrated but still additional work is needed to overcome the multifaceted problems. Nevertheless the idea is fascinating, since self-assembled opaline lattices of colloidal particles provide a simple but fast approach to produce size-controlled nanostructures over a large area. The first results were very promising and showed the ability of inverse opals to pave the way for a versatile filter application to be used in life and material sciences.

8 General Conclusion and Outlook

Several projects with intersecting topics were conducted in the course of this thesis. In the center is the detection of pathogens and bio-molecules. On the other hand, the structuring of surfaces was of key significance and a topic of this work.

In the first part, chapter 4 – "Label-free Detection of Microorganisms in an Integrated Biosensor Array, a new approach for binding antibodies covalently to glass by means of an active-ester-silane was tested. But this project revealed the intrinsic challenges of binding antibodies to glass in a defined way too. This is reflected by the huge amount of publications about oriented and functional immobilization of antibodies.[170,184,253] Nevertheless, the developed protocol paves the way for future studies on the binding of antibodies and hence bacteria to glass. But to implement this, it will be essential to concentrate on the surface chemistry and in parallel on the choice of applied antibodies. Although a large amount of mono- and polyclonal antibodies against a multiplicity of antigens are available, there is still a lack of antibodies specific against known proteins on the exterior of bacteria. For almost all commercially available antibodies against the examined *E. coli* strain K12, the specific type of epitope is unknown, because they are polyclonal. Since for the binding of bacteria to immobilized antibodies the type of addressed antigen and its accessibility is the crucial factor, more attention will have to be payed to this. This is also underlined by Suo et al.: "Our experiments demonstrate that in order to achieve efficient immobilization of living bacteria through immuno-binding, an appropriate ab-ag pair must be identified." They support a potential direction for a way out of this problem, presented also in the course of this thesis: "Fimbriae or pili, if present on the bacterial surface, are an excellent target antigen."[47,229] In this work, antibodies against the K99 pili of *E. coli* seemed to be superior to those with unknown epitope too. Nonetheless, not all bacteria strains to be addressed in potential biosensors show these structural features. Hence in the future, beside the search for other potential exterior antigens, it will be essential to think about other sensor concepts which combine antibody specificity and sensitivity with physical and structural properties of the sensor surface.

This approach was pursued intensively in the second part of the presented thesis, namely in the chapters 5 – "2D Array-Patterning of Antibody Annuli" and 6 – "Structured Antibody Surfaces for Bio-recognition". Therein the new developed "bottom up" technique for creating ordered annuli-shaped antibody patterns showed very promising results, including well-preserved functionality and

specificity of antibodies. Antigens ranging from single molecules like integrins to whole bacteria cells like *E. coli*. could be bound. In addition to this, the positioning of antibodies in a three-dimensional curved topography resulted in an enhanced specific binding capability. The technique pointed out to be at the same time comparatively facile and versatile in its appliance.

It is a promising way for upcoming bio-structured surface technologies to not only functionalize but also to modify the topography and hence physical structure of a surface, either by coating inverse opals or creating antibody annuli. It can establish a new toolbox for bio-active surfaces and be applied in, for instance, biochemistry, molecular biology and materials science and thereby assist well-established methods like cell culture and future cell-free *in vitro* assays.

The final part of this thesis, presented in chapter 7 – "Size Exclusion Filters" can assist the aforementioned detection concepts by providing an advanced way for fabricating nanometer-sized filter surfaces with a high degree of flatness and an extremely narrow size distribution.

By these concepts the presented thesis describes new paths and technologies for many parts of the process of biomolecule and pathogen detection – from filtering and specific binding to enrichment and detection. The initial goal of this thesis was to establish a new technique for the label-free detection of bio-molecules and bacteria on topographically structured antibody surfaces. It is achieved in a number of ways. At the same time, the presented work could also raise interesting new questions for future projects and hence corroborated Albert Einstein when he said "In the middle of every difficulty lies opportunity."

9 Bibliography

[1] Madigan, M., Martinko, J. & Parker, J. *Brock biology of microorganisms*. (2000).

[2] Wikipedia, keyword ”Mikroorganismus“, http://de.wikipedia.org/wiki/Mikroorganismus, retrieved October 2010.

[3] Ivnitski, D., Abdel-Hamid, I., Atanasov, P. & Wilkins, E. *Biosensors for detection of pathogenic bacteria*. Biosensors & Bioelectronics 14, 599-624 (1999).

[4] Maple, P., Hamilton-Miller, J. & Brumfitt, W. *World-wide antibiotic resistance in methicillin-resistant Staphylococcus aureus*. The Lancet 333, 537-540 (1989).

[5] *Annual epidemiological report on communicable diseases in Europe*. European Center for Disease Prevention and Control (2007)

[6] Korenromp, E., Scano, F., Williams, B., Dye, C. & Nunn, P. *Effects of human immunodeficiency virus infection on recurrence of tuberculosis after rifampin-based treatment: an analytical review.* Clinical Infectious Diseases, 101-112 (2003).

[7] McNamara, A. *Foodborne pathogens*. JOURNAL OF URBAN HEALTH 75, 503-505 (1998).

[8] Slutsker, L., Altekruse, S. & Swerdlow, D. *Foodborne diseases. Emerging pathogens and trends*. Infectious disease clinics of North America 12, 199 (1998).

[9] UNICEF and WHO report from October 2009, *Diarrhea: Why Children Are Still Dying and What Can Be Done.* http://whqlibdoc.who.int/publications/2009/9789241598415_eng.pdf, retrieved October 2010

[10] Klonsky, K. *E. coli in spinach, foodborne illnesses, and expectations about food safety.* Agricultural and Resource Economic Update: Giannini Foundation of Agricultural Economics 10, 1-4 (2006).

[11] Guentzel, J. L., Lam, K. L., Callan, M. A., Emmons, S. A. & Dunham, V. L. *Reduction of bacteria on spinach, lettuce, and surfaces in food service areas using neutral electrolyzed oxidizing water.* Food Microbiol. 25, 36-41, 10.1016/j.fm.2007.08.003 (2008).

[12] Donnenberg, M. & Kaper, J. *Enteropathogenic Escherichia coli*. Infection and Immunity 60, 3953 (1992).

[13] Gfeller, K. Y., Nugaeva, N. & Hegner, M. *Micromechanical oscillators as rapid biosensor for the detection of active growth of Escherichia coli*. Biosensors & Bioelectronics 21, 528-533, 10.1016/j.bios.2004.11.018 (2005).

[14] Linman, M. J., Sugerman, K. & Cheng, Q. *Detection of low levels of Escherichia coli in fresh*

spinach by surface plasmon resonance spectroscopy with a TMB-based enzymatic signal enhancement method. Sensor Actuat B-Chem 145, 613-619, Doi 10.1016/J.Snb.2010.01.007 (2010).

[15] Clesceri, L., Greenberg, A. & Eaton, A. *Standard methods for the examination of water and wastewater.* (1998).

[16] Byrne, B., Stack, E., Gilmartin, N. & O'Kennedy, R. *Antibody-Based Sensors: Principles, Problems and Potential for Detection of Pathogens and Associated Toxins*. Sensors 9, 4407-4445, Doi 10.3390/S90604407 (2009).

[17] Lazcka, O., Del Campo, F. J. & Munoz, F. X. *Pathogen detection: A perspective of traditional methods and biosensors*. Biosensors & Bioelectronics 22, 1205-1217, 10.1016/j.bios.2006.06.036 (2007).

[18] Kaspar, C. W. & Tartera, C. *Methods for Detecting Microbial Pathogens in Food and Water.* Method Microbiol 22, 497-531 (1990).

[19] Meng, J., Zhao, S., Doyle, M., Mitchell, S. & Kresovich, S. *Polymerase chain reaction for detecting Escherichia coli O157: H7*. International journal of food microbiology 32, 103-113 (1996).

[20] Jasson, V., Jacxsens, L., Luning, P., Rajkovic, A. & Uyttendaele, M. *Alternative microbial methods: An overview and selection criteria*. Food Microbiol. 27, 710-730, Doi 10.1016/J.Fm.2010.04.008 (2010).

[21] Brooks, B. W. *et al. Evaluation of a monoclonal antibody-based enzyme-linked immunosorbent assay for detection of Campylobacter fetus in bovine preputial washing and vaginal mucus samples*. Veterinary Microbiology 103, 77-84, 10.1016/j.vetmic.2004.07.008 (2004).

[22] Glynn, B. *et al. Current and emerging molecular diagnostic technologies applicable to bacterial food safety*. International Journal of Dairy Technology 59, 126-139 (2006).

[23] Fratamico, P. M. *Comparison of culture, polymerase chain reaction (PCR), TaqMan Salmonella, and Transia Card Salmonella assays for detection of Salmonella spp. in naturally-contaminated ground chicken, ground turkey, and ground beef*. Mol. Cell. Probes 17, 215-221, 10.1016/s0890-8508(03)00056-2 (2003).

[24] Mullis, K. *et al. SPECIFIC ENZYMATIC AMPLIFICATION OF DNA INVITRO - THE POLYMERASE CHAIN-REACTION*. Cold Spring Harbor Symp. Quant. Biol. 51, 263-273 (1986).

[25] Crowther, J. ELISA: theory and practice. (Humana Pr Inc, 1995).

[26] Cohen, A. E. & Kerdahi, K. F. *Evaluation of a rapid and automated enzyme-linked fluorescent immunoassay say for detecting Escherichia coli serogroup O157 in cheese*. Journal of AOAC International 79, 858-860 (1996).

[27] Kumar, R., Surendran, P. K. & Thampuran, N. *Evaluation of culture, ELISA and PCR assays for the detection of Salmonella in seafood*. Lett Appl Microbiol 46, 221-226, Doi 10.1111/J.1472-765x.2007.02286.X (2008).

[28] Mine, Y. *Separation of Salmonella enteritidis from experimentally contaminated liquid eggs using a hen IgY immobilized immunomagnetic separation system*. Journal of Agricultural and Food Chemistry 45, 3723-3727 (1997).min

[29] Baker, G., Dunn, S. & Holt, A. Handbook of neurochemistry and molecular neurobiology: Practical neurochemistry methods. (Springer Verlag, 2007).

[30] Chen, J. & Griffiths, M. W. *Salmonella detection in eggs using Lux(+) bacteriophages*. J Food Protect 59, 908-914 (1996).

[31] Wermuth, C., Ganellin, C., Lindberg, P. & Mitscher, L. *Glossary of Terms Used in Medicinal Chemistry (IUPAC Recommendations 1997*. Annual Reports in Medicinal Chemistry 33, 385-395 (1998).

[32] Ko, S. & Grant, S. *A novel FRET-based optical fiber biosensor for rapid detection of Salmonella typhimurium*. Biosensors and Bioelectronics 21, 1283-1290 (2006).

[33] Lucarelli, F., Marrazza, G., Turner, A. & Mascini, M. *Carbon and gold electrodes as electrochemical transducers for DNA hybridisation sensors*. Biosensors and Bioelectronics 19, 515-530 (2004).

[34] D'Souza, S. F. *Microbial biosensors*. Biosensors & Bioelectronics 16, 337-353 (2001).

[35] Nayak, M., Kotian, A., Marathe, S. & Chakravortty, D. *Detection of microorganisms using biosensors-A smarter way towards detection techniques*. Biosensors & Bioelectronics 25, 661-667, 10.1016/j.bios.2009.08.037 (2009).

[36] Gopel, W. & Heiduschka, P. *Interface Analysis in Biosensor Design*. Biosensors & Bioelectronics 10, 853-883 (1995).

[37] Rich, R. L. & Myszka, D. G. *Survey of the year 2006 commercial optical biosensor literature*. Journal of Molecular Recognition 20, 300-366, Doi 10.1002/Jmr.862 (2007).

[38] Owen, V. *Market requirements for advanced biosensors in healthcare*. Biosensors & Bioelectronics 9 (1994).

[39] Willardson, B. *et al. Development and testing of a bacterial biosensor for toluene-based environmental contaminants*. Applied and environmental microbiology 64, 1006 (1998).

[40] Bae, Y., Oh, B., Lee, W., Lee, W. & Choi, J. *Detection of insulin-antibody binding on a solid surface using imaging ellipsometry*. Biosensors and Bioelectronics 20, 895-902 (2004).

[41] Baeumner, A., Cohen, R., Miksic, V. & Min, J. *RNA biosensor for the rapid detection of viable Escherichia coli in drinking water*. Biosensors and Bioelectronics 18, 405-413 (2003).

[42] Jenkins, S., Heineman, W. & Halsall, H. *Extending the detection limit of solid-phase electrochemical enzyme immunoassay to the attomole level*. Analytical Biochemistry 168, 292-299 (1988).

[43] Skottrup, P. D., Nicolaisen, M. & Justesen, A. F. *Towards on-site pathogen detection using antibody-based sensors*. Biosensors & Bioelectronics 24, 339-348, Doi 10.1016/J.Bios.2008.06.045 (2008).

[44] Leonard, P., Hearty, S., Quinn, J. & O'Kennedy, R. *A generic approach for the detection of whole Listeria monocytogenes cells in contaminated samples using surface plasmon resonance*. Biosensors & Bioelectronics 19, 1331-1335, Doi 10.1016/J.Bios.2003.11.009 (2004).

[45] Feng, P. *Emergence of rapid methods for identifying microbial pathogens in foods*. Journal of AOAC International 79, 809-812 (1996).

[46] Bunka, D. H. J., Platonova, O. & Stockley, P. G. *Development of aptamer therapeutics*. Curr. Opin. Pharmacol. 10, 557-562, 10.1016/j.coph.2010.06.009 (2010).

[47] Suo, Z. Y., Avci, R., Yang, X. H. & Pascual, D. W. *Efficient immobilization and patterning of live bacterial cells*. Langmuir 24, 4161-4167, Doi 10.1021/La7038653 (2008).

[48] Burkert, K. *et al. Automated preparation method for colloidal crystal arrays of monodisperse and binary colloid mixtures by contact printing with a pintool plotter*. Langmuir 23, 3478-3484 (2007).

[49] Massad-Ivanir, N., Shtenberg, G., Zeidman, T. & Segal, E. *Construction and Characterization of Porous SiO2/Hydrogel Hybrids as Optical Biosensors for Rapid Detection of Bacteria*. Advanced Functional Materials 20, 2269-2277, Doi 10.1002/Adfm.201000406 (2010).

[50] LaBaer, J. & Ramachandran, N. *Protein microarrays as tools for functional proteomics*. Current Opinion in Chemical Biology 9, 14-19, Doi 10.1016/J.Cbpa.2004.12.006 (2005).

[51] Xu, Q. C. & Lam, K. S. *Protein and chemical microarrays - Powerful tools for proteomics*.

Journal of Biomedicine and Biotechnology, 257-266, Pii S1110724303209220 (2003).

[52] Wilson, D. S. & Nock, S. *Functional protein microarrays*. Current Opinion in Chemical Biology 6, 81-85 (2002).

[53] Lynch, M. *et al. Functional protein nanoarrays for biomarker profiling*. Proteomics 4, 1695-1702 (2004).

[54] Wilson, D. S. & Nock, S. *Recent developments in protein microarray technology*. Angewandte Chemie-International Edition 42, 494-500 (2003).

[55] Knezevic, V. *et al. Proteomic profiling of the cancer microenvironment by antibody arrays*. Proteomics 1, 1271-1278 (2001).

[56] Niemeyer, C., Mirkin, CA. Nanobiotechnology: Concepts, Applications and Perspectives (Gebundene Ausgabe). 1 edn, (Wiley-VCH, 2004).

[57] Saviranta, P. *et al. Evaluating sandwich immunoassays in microarray format in terms of the ambient analyte regime*. Clin Chem 50, 1907-1920, Doi 10.1373/Clinchem.2004.037929 (2004).

[58] Tu, S., Uknalis, J., Yamashoji, S., Gehring, A. & Irwin, P. *Luminescent methods to detect viable and total Escherichia coli O157 : H7 in ground beef*. Journal of Rapid Methods and Automation in Microbiology 13, 57-70 (2005).

[59] Lee, K. B., Kim, E. Y., Mirkin, C. A. & Wolinsky, S. M. *The use of nanoarrays for highly sensitive and selective detection of human immunodeficiency virus type 1 in plasma*. Nano Letters 4, 1869-1872, Doi 10.1021/Nl049002y (2004).

[60] Deshpande, S. S. Enzyme Immunoassays: From Concept to Product Development. (Springer, 1996).

[61] Lee, K. B., Park, S. J., Mirkin, C. A., Smith, J. C. & Mrksich, M. *Protein nanoarrays generated by dip-pen nanolithography*. Science 295, 1702-1705 (2002).

[62] Fang, Y., Frutos, A. G. & Lahiri, J. *Membrane protein microarrays*. Journal of the American Chemical Society 124, 2394-2395, Doi 10.1021/Ja017346+ (2002).

[63] MacBeath, G. & Schreiber, S. L. *Printing proteins as microarrays for high-throughput function determination*. Science 289, 1760-1763 (2000).

[64] Zhu, H. *et al. Global analysis of protein activities using proteome chips*. Science 293, 2101-2105 (2001).

[65] Albin, D. M., Gehring, A. G., Reed, S. A. & Tu, S. I. *Apparent Thixotropic Properties of Saline/Glycerol Drops with Biotinylated Antibodies on Streptavidin-Coated Glass Slides:*

Implications for Bacterial Capture on Antibody Microarrays. Sensors 9, 995-1011, Doi 10.3390/S90200995 (2009).

[66] Pallandre, A., De Meersman, B., Blondeau, F., Nysten, B. & Jonas, A. M. *Tuning the orientation of an antigen by adsorption onto nanostriped templates*. Journal of the American Chemical Society 127, 4320-4325, Doi 10.1021/Ja043656r (2005).

[67] Bruckbauer, A. *et al. An addressable antibody nanoarray produced on a nanostructured surface*. Journal of the American Chemical Society 126, 6508-6509 (2004).

[68] Wallraff, G. M. & Hinsberg, W. D. *Lithographic imaging techniques for the formation of nanoscopic features*. Chemical Reviews 99, 1801-1821 (1999).

[69] Perl, A., Reinhoudt, D. N. & Huskens, J. *Microcontact Printing: Limitations and Achievements*. Advanced Materials 21, 2257-2268, Doi 10.1002/Adma.200801864 (2009).

[70] Bain, C. D. *et al. Formation of Monolayer Films by the Spontaneous Assembly of Organic Thiols from Solution onto Gold*. Journal of the American Chemical Society 111, 321-335 (1989).

[71] Schmid, H. & Michel, B. *Siloxane polymers for high-resolution, high-accuracy soft lithography*. Macromolecules 33, 3042-3049 (2000).

[72] Torres, C. Alternative Lithography: Unleashing the Potentials of Nanotechnology. 1 edn, (Springer, 2003).

[73] Favre, E. *Swelling of crosslinked polydimethylsiloxane networks by pure solvents: Influence of temperature*. European Polymer Journal 32, 1183-1188 (1996).

[74] Sharp, K. G., Blackman, G. S., Glassmaker, N. J., Jagota, A. & Hui, C. Y. *Effect of stamp deformation on the quality of microcontact printing: Theory and experiment*. Langmuir 20, 6430-6438, Doi 10.1021/La036332+ (2004).

[75] Lau, K. H. A., Bang, J., Kim, D. H. & Knoll, W. *Self-assembly of Protein Nanoarrays on Block Copolymer Templates*. Advanced Functional Materials 18, 3148-3157, Doi 10.1002/Adfm.200800487 (2008).

[76] Brewster, J. D., Gehring, A. G., Mazenko, R. S., VanHouten, L. J. & Crawford, C. J. *Immunoelectrochemical assays for bacteria: Use of epifluorescence microscopy and rapid-scan electrochemical techniques in development of an assay for Salmonella*. Analytical Chemistry 68, 4153-4159 (1996).

[77] Norde, W. *Adsorption of Proteins at Solid-Liquid Interfaces*. Cells and Materials 5, 97-112 (1995).

[78] Welzel, P. B. *Investigation of adsorption-induced structural changes of proteins at solid/liquid interfaces by differential scanning calorimetry*. Thermochimica Acta 382, 175-188 (2002).

[79] Clarke, M. L., Wang, J. & Chen, Z. *Conformational changes of fibrinogen after adsorption*. Journal of Physical Chemistry B 109, 22027-22035, Doi 10.1021/Jp054456k (2005).

[80] Steiner, G., Tunc, S., Maitz, M. & Salzer, R. *Conformational changes during protein adsorption. FT-IR spectroscopic imaging of adsorbed fibrinogen layers*. Analytical Chemistry 79, 1311-1316, Doi 10.1021/Ac061341j (2007).

[81] Kim, J. & Somorjai, G. A. *Molecular packing of lysozyme, fibrinogen, and bovine serum albumin on hydrophilic and hydrophobic surfaces studied by infrared-visible sum frequency generation and fluorescence microscopy.* Journal of the American Chemical Society 125, 3150-3158, Doi 10.1021/Ja028987n (2003).

[82] Mermut, O. *et al. In situ adsorption studies of a 14-amino acid leucine-lysine peptide onto hydrophobic polystyrene and hydrophilic silica surfaces using quartz crystal microbalance, atomic force microscopy, and sum frequency generation vibrational spectroscopy*. Journal of the American Chemical Society 128, 3598-3607, Doi 10.1021/Ja056031h (2006).

[83] Li, Q., Lau, K. H. A., Sinner, E. K., Kim, D. H. & Knoll, W. *The Effect of Fluid Flow on Selective Protein Adsorption on Polystyrene-block-Poly(methyl methacrylate) Copolymers*. Langmuir 25, 12144-12150, Doi 10.1021/La901658w (2009).

[84] Rosi, N. L. & Mirkin, C. A. *Nanostructures in biodiagnostics*. Chemical Reviews 105, 1547-1562, Doi 10.1021/Cr030067f (2005).

[85] Rozhok, S. *et al. Methods for fabricating microarrays of motile bacteria*. Small 1, 445-451 (2005).

[86] Chován, T. & Guttman, A. *Microfabricated devices in biotechnology and biochemical processing*. TRENDS in Biotechnology 20, 116-122 (2002).

[87] Wolf, C. & Li, Q. *Tunable Two-Dimensional Array Patterning of Antibody Annuli through Microsphere Templating*. Langmuir 26, 12068-12074, Doi 10.1021/La101212y (2010).

[88] Colpo, P., Ruiz, A., Ceriotti, L. & Rossi, F. *Surface Functionalization for Protein and Cell Patterning*. Adv Biochem Eng Biot 117, 109-130, Doi 10.1007/10_2009_2 (2010).

[89] Arya, S., Solanki, P., Datta, M. & Malhotra, B. *Recent advances in self-assembled monolayers based biomolecular electronic devices*. Biosensors and Bioelectronics 24, 2810-2817 (2009).

[90] Byrne, R. & Diamond, D. *Chemo/bio-sensor networks*. Nat Mater 5, 421-424, Doi 10.1038/Nmat1661 (2006).

[91] Medintz, I. *Universal tools for biomolecular attachment to surfaces*. Nat Mater 5, 842-842, Doi 10.1038/Nmat1776 (2006).

[92] Ginger, D. S., Zhang, H. & Mirkin, C. A. *The evolution of dip-pen nanolithography.* Angewandte Chemie-International Edition 43, 30-45, Doi 10.1002/Anie.200300608 (2004).

[93] Piner, R. D., Zhu, J., Xu, F., Hong, S. H. & Mirkin, C. A. *"Dip-pen" nanolithography.* Science 283, 661-663 (1999).

[94] Kim, K., Ke, C., Moldovan, N. & Espinosa, H. *Massively parallel multi-tip nanoscale writer with fluidic capabilities - fountain pen nanolithography (FPN)*. 235-238 (2003).

[95] Johannes, M., Clark, R. & Cole, D. *Joining Dip-Pen Nanolithography and Microcontact Printing Into a Nanolithographic Process: From Engineering Design to Parallel Fabrication*. (2004).

[96] Wilson, D. L. *et al. Surface organization and nanopatterning of collagen by dip-pen nanolithography.* P Natl Acad Sci USA 98, 13660-13664 (2001).

[97] Nyamjav, D., Rozhok, S. & Holz, R. C. *Immobilization of motile bacterial cells via dip-pen nanolithography.* Nanotechnology 21, 235105, 10.1088/0957-4484/21/23/235105 (2010).

[98] Wang, D. B. *et al. Thermochernical Nanolithography of Multifunctional a Nanotemplates for Assembling Nano-objects*. Advanced Functional Materials 19, 3696-3702, Doi 10.1002/Adfm.200901057 (2009).

[99] Xu, H. *et al. Orientation of a monoclonal antibody adsorbed at the solid/solution interface: A combined study using atomic force microscopy and neutron reflectivity*. Langmuir 22, 6313- 6320, 10.1021/la0532454 (2006).

[100] Wang, X. Q., Wang, Y. N., Xu, H., Shan, H. H. & Lub, J. R. *Dynamic adsorption of monoclonal antibody layers on hydrophilic silica surface: A combined study by spectroscopic ellipsometry and AFM*. J. Colloid Interface Sci. 323, 18-25, 10.1016/j.jcis.2008.04.024 (2008).

[101] Reiss, C. R., Taylor, J. S. & Robert, C. *Surface water treatment using nanofiltration - pilot testing results and design considerations*. Desalination 125, 97-112 (1999).

[102] Van der Bruggen, B. & Vandecasteele, C. *Removal of pollutants from surface water and groundwater by nanofiltration: overview of possible applications in the drinking water industry.* Environ Pollut 122, 435-445, Pii S0269-7491(02)00308-1 (2003).

[103] Jacangelo, J. G., Trussell, R. R. & Watson, M. *Role of membrane technology in drinking water treatment in the United States*. Desalination 113, 119-127 (1997).

[104] Yahya, M. T., Cluff, C. B. & Gerba, C. P. *VIRUS REMOVAL BY SLOW SAND FILTRATION AND NANOFILTRATION*. Water Science and Technology 27, 445-448 (1993).

[105] Hahn, M. W. *Broad diversity of viable bacteria in 'sterile' (0.2 mu m) filtered water*. Res Microbiol 155, 688-691, Doi 10.1016/J.Resmic.2004.05.003 (2004).

[106] Kuo, C. W., Shiu, J. Y., Wei, K. H. & Chen, P. *Monolithic integration of well-ordered nanoporous structures in the microfluidic channels for bioseparation*. J. Chromatogr. A 1162, 175-179, 10.1016/j.chroma.2007.06.037 (2007).

[107] Bernardoni, F., Kouba, M. & Fadeev, A. Y. *Effect of curvature on the packing and ordering of organosilane monolayers supported on solids*. Chemistry of Materials 20, 382-387, Doi 10.1021/Cm070842y (2008).

[108] Jonas, U., del Campo, A., Kruger, C., Glasser, G. & Boos, D. *Colloidal assemblies on patterned silane layers*. P Natl Acad Sci USA 99, 5034-5039, Doi 10.1073/Pnas.082634799 (2002).

[109] Wikipedia, keyword “Silanes”, http://en.wikipedia.org/wiki/Silanes, retrieved October 2010

[110] Jonas, U., Krüger, C. *The Effect of Polar, Nonpolar, and Electrostatic Interactions and Wetting Behavior on the Particle Assembly at Patterned Surfaces* Journal of Supramolecular Chemistry 2, 255-270 (2002).

[111] Kessel, C. & Granick, S. *Formation and characterization of a highly ordered and well-anchored alkylsilane monolayer on mica by self-assembly*. Langmuir 7, 532-538 (1991).

[112] Everett, D. H. Basic Principles of Colloid Science. 1st edn, (Royal Society of Chemistry, 1988).

[113] Xia, Y. N., Gates, B., Yin, Y. D. & Lu, Y. *Monodispersed colloidal spheres: Old materials with new applications*. Advanced Materials 12, 693-713 (2000).

[114] Perrin, J. *Brownian motion and molecular reality*. Ann. Chim. Phys. 18, 5-114 (1909).

[115] Gorishnyy, T., Maldovan, M., Ullal, C. & Thomas, E. *Sound ideas*. Phys World 18, 24-29 (2005).

[116] Cheng, W., Wang, J. J., Jonas, U., Fytas, G. & Stefanou, N. *Observation and tuning of hypersonic bandgaps in colloidal crystals*. Nat Mater 5, 830-836, Doi 10.1038/Nmat1727 (2006).

[117] Galisteo-Lopez, J. F., Garcia-Santamaria, F., Juarez, B. H., Lopez, C. & Palacios-Lidon, E.

Materials aspects of opals as photonic crystals. Icton 2004: 6th International Conference on Transparent Optical Networks, Proceedings, Vol 2, 139-144, 347 (2004).

[118] Arsenault, A. *et al. Towards the synthetic all-optical computer: science fiction or reality?* Journal of Materials Chemistry 14, 781-794 (2004).

[119] Li, C. & Qi, L. M. *Colloidal-Crystal-Assisted Patterning of Crystalline Materials*. Advanced Materials 22, 1494-1497, Doi 10.1002/Adma.200903044 (2010).

[120] Stein, A., Li, F. & Denny, N. *Morphological Control in Colloidal Crystal Templating of Inverse Opals, Hierarchical Structures, and Shaped Particles*. Chem. Mater 20, 649-666 (2008).

[121] Aizenberg, J. *Crystallization in patterns: a bio-inspired approach*. Advanced Materials 16, 1295-1302 (2004).

[122] Meldrum, F. & Ludwigs, S. *Template-directed control of crystal morphologies*. Macromolecular bioscience 7, 152-162 (2007).

[123] Mayoral, R. *et al. 3D Long-range ordering in ein SiO2 submicrometer-sphere sintered superstructure*. Advanced Materials 9, 257-260 (1997).

[124] Wijnhoven, J. & Vos, W. *Preparation of photonic crystals made of air spheres in titania*. Science 281, 802 (1998).

[125] Velev, O., Jede, T., Lobo, R. & Lenhoff, A. *Porous silica via colloidal crystallization*. Nature 389, 447-448 (1997).

[126] Trau, M., Saville, D. & Aksay, I. *Assembly of colloidal crystals at electrode interfaces*. Langmuir 13, 6375-6381 (1997).

[127] Deegan, R. D. *et al. Capillary flow as the cause of ring stains from dried liquid drops*. Nature 389, 827-829 (1997).

[128] Cong, H. & Cao, W. X. *Colloidal crystallization induced by capillary force*. Langmuir 19, 8177-8181, Doi 10.1021/La344480 (2003).

[129] Dimitrov, A. & Nagayama, K. *Continuous convective assembling of fine particles into two-dimensional arrays on solid surfaces*. Langmuir 12, 1303-1311 (1996).

[130] Zhang, J. H., Luo, X. Y., Yan, X. J. & Zhu, G. D. *Fabrication of high-quality colloidal crystal films by vertical deposition method integrated with a piezoelectric actuator.* Thin Solid Films 518, 5204-5208, Doi 10.1016/J.Tsf.2010.04.117 (2010).

[131] Image taken by Dr. Markus Retsch.

[132] Ogi, T., Modesto-Lopez, L. B., Iskandar, F. & Okuyama, K. *Fabrication of a large area*

monolayer of silica particles on a sapphire substrate by a spin coating method. Colloids and Surfaces a-Physicochemical and Engineering Aspects 297, 71-78, Doi 10.1016/J.Colsurfa.2006.10.027 (2007).

[133] Hulteen, J. C. & Vanduyne, R. P. *Nanosphere Lithography - a Materials General Fabrication Process for Periodic Particle Array Surfaces*. Journal of Vacuum Science & Technology a-Vacuum Surfaces and Films 13, 1553-1558 (1995).

[134] Denkov, N. D. *et al. Mechanism of Formation of 2-Dimensional Crystals from Latex-Particles on Substrates*. Langmuir 8, 3183-3190 (1992).

[135] Denkov, N. D. *et al. 2-DIMENSIONAL CRYSTALLIZATION*. Nature 361, 26-26 (1993).

[136] Li, Q., Retsch, M., Wang, J., Knoll, W., Jonas, U. *Porous Networks Through Colloidal Templates*. Topics in Current Chemistry (2008).

[137] Teh, L. K., Tan, N. K., Wong, C. C. & Li, S. *Growth imperfections in three-dimensional colloidal self-assembly.* Appl Phys a-Mater 81, 1399-1404, Doi 10.1007/S00339-004-3095-Y (2005).

[138] Park, S. H. & Xia, Y. N. *Macroporous membranes with highly ordered and three-dimensionally interconnected spherical pores*. Advanced Materials 10, 1045-+ (1998).

[139] Hatton, B., Mishchenko, L., Davis, S., Sandhage, K. H. & Aizenberg, J. *Assembly of large-area, highly ordered, crack-free inverse opal films*. P Natl Acad Sci USA 107, 10354-10359, Doi 10.1073/Pnas.1000954107 (2010).

[140] Holland, B. T., Blanford, C. F. & Stein, A. *Synthesis of macroporous minerals with highly ordered three-dimensional arrays of spheroidal voids*. Science 281, 538-540 (1998).

[141] Zhao, X. S. *et al. Templating methods for preparation of porous structures*. Journal of Materials Chemistry 16, 637-648, Doi 10.1039/B513060c (2006).

[142] Johnson, S. A., Ollivier, P. J. & Mallouk, T. E. *Ordered mesoporous polymers of tunable pore size from colloidal silica templates*. Science 283, 963-965 (1999).

[143] Yan, H. W., Blanford, C. F., Smyrl, W. H. & Stein, A. *Preparation and structure of 3D ordered macroporous alloys by PMMA colloidal crystal templating*. Chem Commun, 1477-1478 (2000).

[144] King, J. S., Heineman, D., Graugnard, E. & Summers, C. J. *Atomic layer deposition in porous structures: 3D photonic crystals*. Appl Surf Sci 244, 511-516, Doi 10.1016/J.Apsusc.2004.10.110 (2005).

[145] Blanco, A. *et al. Large-scale synthesis of a silicon photonic crystal with a complete three-*

dimensional bandgap near 1.5 micrometres. Nature 405, 437-440 (2000).

[146] Choi, S. W., Xie, J. W. & Xia, Y. N. *Chitosan-Based Inverse Opals: Three-Dimensional Scaffolds with Uniform Pore Structures for Cell Culture*. Advanced Materials 21, 2997-+, Doi 10.1002/Adma.200803504 (2009).

[147] Lee, Y. J., Pruzinsky, S. A. & Braun, P. V. *Glucose-sensitive inverse opal hydrogels: Analysis of optical diffraction response*. Langmuir 20, 3096-3106, Doi 10.1021/La035555x (2004).

[148] Guan, G. Q. *et al. Preferential CO oxidation over catalysts with well-defined inverse opal structure in microchannels*. Int J Hydrogen Energ 33, 797-801, Doi 10.1016/J.Ijhydene.2007.10.054 (2008).

[149] Velev, O. D. & Lenhoff, A. M. *Colloidal crystals as templates for porous materials*. Curr Opin Colloid In 5, 56-63 (2000).

[150] Xia, Y. N., Gates, B., Yin, Y. D. & Lu, Y. *Monodispersed colloidal spheres: Old materials with new applications*. Advanced Materials 12, 693-713 (2000).

[151] Miguez, H. *et al. Control of the photonic crystal properties of fcc-packed submicrometer SiO2 spheres by sintering*. Advanced Materials 10, 480-+ (1998).

[152] Miguez, H. *et al. Mechanical stability enhancement by pore size and connectivity control in colloidal crystals by layer-by-layer growth of oxide*. Chem Commun, 2736-2737, 10.1039/b208805n (2002).

[153] Oberbauer, B. Theodor Escherich – Leben und Werk. (Futuramed Verlag., 1992).

[154] Schlegel, H. G. Allgemeine Mikrobiologie. 8. Auflage edn, (Thieme, 2006).

[155] Darnton, N., Turner, L., Rojevsky, S. & Berg, H. *On torque and tumbling in swimming Escherichia coli*. Journal of bacteriology 189, 1756-1764 (2007).

[156] Bentley, R. & Meganathan, R. *Biosynthesis of vitamin K (menaquinone) in bacteria*. Microbiology and Molecular Biology Reviews 46, 241-280 (1982).

[157] Hudault, S., Guignot, J. & Servin, A. *Escherichia coli strains colonising the gastrointestinal tract protect germfree mice againstSalmonella typhimuriuminfection*. Gut 49, 47-55 (2001).

[158] Reid, G., Howard, J. & Gan, B. *Can bacterial interference prevent infection?* Trends in microbiology 9, 424-428 (2001).

[159] Center for Disease Control and Prevention, http://www.cdc.gov/ecoli/, retrieved May 2010.

[160] Vogt, R. & Dippold, L. *Escherichia coli O157: H7 outbreak associated with consumption of ground beef, June-July 2002*. Public Health Reports 120, 174-178 (2005).

[161] Kotewicz, M. L., Mammel, M. K., LeClerc, J. E. & Cebula, T. A. *Optical mapping and 454 s*

equencing of Escherichia coli O157:H7 isolates linked to the US 2006 spinach-associated outbreak. Microbiology-(UK) 154, 3518-3528, 10.1099/mic.0.2008/019026-0 (2008).

[162] Copyright Helmholz Centre for Infection Research/Dr. M. Rohde. Courtesy of the Biology Image Library, http://biologyimagelibrary.com/imageID=42872, Retrieved 2010-05-17.

[163] Cosenza, B. J. & Podgwaite, J. D. *A new species of Proteus isolated from larvae of the gypsy moth Porthetria dispar (L.)*. Antonie Van Leeuwenhoek 32, 187-191 (1966).

[164] Garrity, G., Bell, J. & Lilburn, T. *Taxonomic outline of the prokaryotes. Bergey's manual of systematic bacteriology*. New York, NY: Springer, 118 (2002).

[165] Dworkin, M. & Falkow, S. The Prokaryotes: Proteobacteria: gamma subclass. (Springer Verlag, 2006).

[166] Ofek, I., Doyle, R. & Kolenbrander, P. Bacterial adhesion to cells and tissues. (Chapman & Hall New York, 1994).

[167] Podschun, R. & Ullmann, U. *Klebsiella spp. as nosocomial pathogens: epidemiology, taxonomy, typing methods, and pathogenicity factors*. Clin Microbiol Rev 11, 589-603 (1998).

[168] Bertani, G. *Studies on lysogenesis. I. The mode of phage liberation by lysogenic Escherichia coli*. J Bacteriol 62, 293-300 (1951).

[169] Baldrich, E., Vigues, N., Mas, J. & Munoz, F. X. *Sensing bacteria but treating them well: Determination of optimal incubation and storage conditions*. Analytical Biochemistry 383, 68-75, Doi 10.1016/J.Ab.2008.08.005 (2008).

[170] Kausaite-Minkstimiene, A., Ramanaviciene, A., Kirlyte, J. & Ramanavicius, A. *Comparative Study of Random and Oriented Antibody Immobilization Techniques on the Binding Capacity of Immunosensor.* Analytical Chemistry 82, 6401-6408, Doi 10.1021/Ac100468k (2010).

[171] Guddat, L. W., Herron, J. N. & Edmundson, A. B. *3-Dimensional Structure of a Human-Immunoglobulin with a Hinge Deletion*. P Natl Acad Sci USA 90, 4271-4275 (1993).

[172] Huber, R., Deisenhofer, J., Colman, P. M., Matsushima, M. & Palm, W. *Crystallographic Structure Studies of an Igg Molecule and an Fc Fragment*. Nature 264, 415-420 (1976).

[173] Amzel, L. M. & Poljak, R. J. *3-Dimensional Structure of Immunoglobulins*. Annu Rev Biochem 48, 961-997 (1979).

[174] Lu, B., Smyth, M. & O'Kennedy, R. *Tutorial review. Oriented immobilization of antibodies and its applications in immunoassays and immunosensors*. The Analyst 121, 29-32 (1996).

[175] Qian, W. P. *et al. Orientation of antibodies on a 3-aminopropyltriethoxylsilane-modified*

silicon wafer surface. Journal of Inclusion Phenomena and Macrocyclic Chemistry 35, 419-429 (1999).

[176] Staines, N., Brostoff, J. & James, K. Introducing immunology. (St. Louis, 1985).

[177] Lottspeich, F., Zorbas, H. & Engelhard, M. Bioanalytik. (Spektrum, Akad. Verl., 2006).

[178] Guyton, A. & Hall, J. *Textbook of medical physiology*. London: W. B. Saunders Co (1981).

[179] Cole, S., Campling, B., Atlaw, T., Kozbor, D. & Roder, J. *Human monoclonal antibodies*. Molecular and cellular biochemistry 62, 109-120 (1984).

[180] Kabir, S. *Immunoglobulin purification by affinity chromatography using protein A mimetic ligands prepared by combinatorial chemical synthesis*. Immunological investigations 31, 263-278 (2002).

[181] Wikipedia, keyword ”Antibody“, http://en.wikipedia.org/wiki/Antibody, retrieved October 2010.

[182] Rabilloud, T. *Two-dimensional gel electrophoresis in proteomics: Old, old fashioned, but it still climbs up the mountains*. Proteomics 2, 3-10 (2002).

[183] Ferretti, S., Paynter, S., Russell, D., Sapsford David, J. & Kim, E. *Self-assembled monolayers: a versatile tool for the formulation of bio-surfaces*. TrAC Trends in Analytical Chemistry 19, 530-540 (2000).

[184] Peluso, P. *et al. Optimizing antibody immobilization strategies for the construction of protein microarrays*. Analytical Biochemistry 312, 113-124, Pii S0003-2697(02)00442-6 (2003).

[185] Patel, N. *et al. Immobilization of protein molecules onto homogeneous and mixed carboxylate-terminated self-assembled monolayers*. Langmuir 13, 6485-6490 (1997).

[186] Tang, D. Q., Zhang, D. J., Tang, D. Y. & Ai, H. *Amplification of the antigen-antibody interaction from quartz crystal microbalance immunosensors via back-filling immobilization of nanogold on biorecognition surface*. J. Immunol. Methods 316, 144-152, 10.1016/j.jim.2006.08.012 (2006).

[187] Kortt, A., Oddie, G., Iliades, P., Gruen, L. & Hudson, P. *Nonspecific Amine Immobilization of Ligand Can Be a Potential Source of Error in BIAcore Binding Experiments and May Reduce Binding Affinities* 1*. Analytical Biochemistry 253, 103-111 (1997).

[188] Brogan, K., Wolfe, K., Jones, P. & Schoenfisch, M. *Direct oriented immobilization of F (ab') antibody fragments on gold*. Analytica Chimica Acta 496, 73-80 (2003).

[189] Oh, B. K. *et al. Immunosensor for detection of Legionella pneumophila using surface plasmon resonance*. Biosensors & Bioelectronics 18, 605-611, 10.1016/s0956-

5663(03)00032-0 (2003).

[190] Hope, M. J., Bally, M. B., Webb, G. & Cullis, P. R. *Production of Large Unilamellar Vesicles by a Rapid Extrusion Procedure - Characterization of Size Distribution, Trapped Volume and Ability to Maintain a Membrane-Potential*. Biochim Biophys Acta 812, 55-65 (1985).

[191] Frisken, B. J., Asman, C. & Patty, P. J. *Studies of vesicle extrusion*. Langmuir 16, 928-933 (2000).

[192] Avanti Polar Lipids Inc., http://avantilipids.com/index.php?option=com_content& view= article&id=231&Itemid=207&catnumber=850375, retrieved June 2010.

[193] Zernike, F. *How I Discovered Phase Contrast*. Science 121, 345-349 (1955).

[194] Olympus Microscopy Resource Center, http://www.olympusmicro.com/primer/techniques/ phasecontrast/phase.html, retrieved September 2010.

[195] Wikipedia, keyword ”Phase contrast microscopy“, http://en.wikipedia.org/wiki/Phase_con trast_microscopy, retrieved September 2010.

[196] Wikipedia, keyword ”Fluorescence microscope“, http://en.wikipedia.org/wiki/Fluorescence_ microscope, retrieved September 2010.

[197] Hell, S. & Wichmann, J. *Breaking the diffraction resolution limit by stimulated emission: stimulated-emission-depletion fluorescence microscopy*. Optics Letters 19, 780-782 (1994).

[198] The Official Website of the Nobel Prize, http://nobelprize.org/educational/physics/micros copes/fluorescence/, retrieved September 2010.

[199] Gunkel, M. *et al. Dual color localization microscopy of cellular nanostructures*. Biotechnology Journal 4, 927-938 (2009).

[200] Olympus Microscopy Resource Center, http://www.olympusmicro.com/primer/techniques/ fluorescence/fluorescenceintro.html, retrieved September 2010.

[201] Nikon MicroscopyU, http://www.microscopyu.com/articles/fluorescence/fluorescenceintro. html, retrieved September, 2010.

[202] Nikon MicroscopyU, http://www.microscopyu.com/articles/confocal/index.html, retrieved September, 2010.

[203] König, K. *Multiphoton microscopy in life sciences*. Journal of Microscopy 200, 83-104 (2000).

[204] Matsui, H., Eguchi, M. & Kikuchi, Y. *Use of confocal microscopy to detect Salmonella typhimurium within host cells associated with Spv-mediated intracellular proliferation*. Microbial pathogenesis 29, 53-59 (2000).

[205] Pawley, J. & Masters, B. *Handbook of biological confocal microscopy*. Journal of Biomedical Optics 13, 029902 (2008).

[206] Wikipedia, keyword ”Confocal laser scanning microscopy“, http://en.wikipedia.org/wiki/Confocal_laser_scanning_microscopy, retrieved September 2010.

[207] Jalili, N. & Laxminarayana, K. *A review of atomic force microscopy imaging systems: application to molecular metrology and biological sciences*. Mechatronics 14, 907-945, Doi 10.1016/J.Mechatronics.2004.04.005 (2004).

[208] Veeco NanoScope Training Notebook. Rev. 3.0, http://www.veeco.com/contact/user_manuals.aspx, retrieved May 2010.

[209] Magonov, S. N. & Reneker, D. H. *Characterization of polymer surfaces with atomic force microscopy*. Annu Rev Mater Sci 27, 175-222 (1997).

[210] Wikipedia, keyword ”Scanning electron microscope“, http://en.wikipedia.org/wiki/Scanning_electron_microscope, retrieved June 2010.

[211] University of Nebraska-Lincoln, http://www.unl.edu/CMRAcfem/em.htm, retrieved June 2010.

[212] Vezie, D. L., Thomas, E. L. & Adams, W. W. *LOW-VOLTAGE, HIGH-RESOLUTION SCANNING ELECTRON-MICROSCOPY - A NEW CHARACTERIZATION TECHNIQUE FOR POLYMER MORPHOLOGY*. Polymer 36, 1761-1779 (1995).

[213] Butler, J. H., Joy, D. C., Bradley, G. F. & Krause, S. J. *LOW-VOLTAGE SCANNING ELECTRON-MICROSCOPY OF POLYMERS*. Polymer 36, 1781-1790 (1995).

[214] Tredgold, R. H. *An Introduction to Ultrathin Organic Films - from Langmuir-Blodgett to Self-Assembly - Ulman,A*. Nature 354, 120-120 (1991).

[215] Towbin, H., Staehelin, T. & Gordon, J. *Electrophoretic Transfer of Proteins from Polyacrylamide Gels to Nitrocellulose Sheets - Procedure and Some Applications*. P Natl Acad Sci USA 76, 4350-4354 (1979).

[216] Ligler, F. S. *et al. Remote sensing using an airborne biosensor*. Environ. Sci. Technol. 32, 2461-2466 (1998).

[217] Hermanson, G. *Bioconjugation techniques*. Academic Press 10, 0123705010 (2008).

[218] Khorana, H. G. *THE CHEMISTRY OF CARBODIIMIDES*. Chemical Reviews 53, 145-166 (1953).

[219] Staros, J. V., Wright, R. W. & Swingle, D. M. *Enhancement by N-Hydroxysulfosuccinimide of Water-Soluble Carbodiimide-Mediated Coupling Reactions*. Analytical Biochemistry 156,

220-222 (1986).

[220] Grabarek, Z. & Gergely, J. *Zero-Length Crosslinking Procedure with the Use of Active Esters*. Analytical Biochemistry 185, 131-135 (1990).

[221] Taitt, C. R. *et al. A portable array biosensor for detecting multiple analytes in complex samples*. Microb. Ecol. 47, 175-185, 10.1007/s00248-003-1011-1 (2004).

[222] Green, N. *Avidin*. Advances in protein chemistry 29, 85-133 (1975).

[223] Wolny, P. M., Spatz, J. P. & Richter, R. P. *On the Adsorption Behavior of Biotin-Binding Proteins on Gold and Silica*. Langmuir 26, 1029-1034, Doi 10.1021/La902226b (2010).

[224] Sofia, S. J., Premnath, V. & Merrill, E. W. *Poly(ethylene oxide) grafted to silicon surfaces: Grafting density and protein adsorption*. Macromolecules 31, 5059-5070 (1998).

[225] Szleifer, I. *Protein adsorption on surfaces with grafted polymers: A theoretical approach*. Biophys. J. 72, 595-612 (1997).

[226] Lee, J. H., Kopeckova, P., Zhang, J., Kopecek, J. & Andrade, J. D. *Protein Resistance of Polyethylene Oxide Surfaces*. Abstracts of Papers of the American Chemical Society 196, 50-PMSE (1988).

[227] Jeon, S. I., Lee, J. H., Andrade, J. D. & Degennes, P. G. *Protein surface interactions in the presence of polyenthylene oxide. 1. simplified theory*. J. Colloid Interface Sci. 142, 149-158 (1991).

[228] Jeon, S. I. & Andrade, J. D. *Protein Surface Interactions in the Presence of Polyethylene Oxide .2. Effect of Protein Size*. J. Colloid Interface Sci. 142, 159-166 (1991).

[229] Suo, Z. Y. *et al. Antibody Selection for Immobilizing Living Bacteria*. Analytical Chemistry 81, 7571-7578, Doi 10.1021/Ac9014484 (2009).

[230] Renken, J., Dahint, R., Grunze, M. & Josse, F. *Multifrequency evaluation of different immunosorbents on acoustic plate mode sensors*. Analytical Chemistry 68, 176-182 (1996).

[231] Witten, T. A. *Robust fadeout profile of an evaporation stain*. Epl 86, -, Artn 64002 Doi 10.1209/0295-5075/86/64002 (2009).

[232] Thomson, N. H. *Imaging the substructure of antibodies with tapping-mode AFM in air: the importance of a water layer on mica*. Journal of Microscopy-Oxford 217, 193-199 (2005).

[233] Edelman, G. M. *Antibody Structure and Molecular Immunology*. Science 180, 830-840 (1973).

[234] Merkel, J. S., Michaud, G. A., Salcius, M., Schweitzer, B. & Predki, P. F. *Functional protein microarrays: just how functional are they?* Current Opinion in Biotechnology 16, 447-452,

Doi 10.1016/J.Copbio.2005.06.007 (2005).

[235] Giancotti, F. G. & Ruoslahti, E. *Transduction - Integrin signaling*. Science 285, 1028-1032 (1999).

[236] Hynes, R. O. *Integrins: Bidirectional, allosteric signaling machines*. Cell 110, 673-687 (2002).

[237] Arnaout, M. A., Mahalingam, B. & Xiong, J. P. *Integrin structure, allostery, and bidirectional signaling*. Annu Rev Cell Dev Biol 21, 381-410, 10.1146/annurev.cellbio.21.090704.151217(2005).

[238] Stupack, D. G. & Cheresh, D. A. *Integrins and angiogenesis*. Curr Top Dev Biol 64, 207-238 (2004).

[239] Mrksich, M. *What can surface chemistry do for cell biology?* Current Opinion in Chemical Biology 6, 794-797 (2002).

[240] Kumar, C. C. *et al. Biochemical characterization of the binding of echistatin to integrin alpha(v)beta(3) receptor.* J Pharmacol Exp Ther 283, 843-853 (1997).

[241] Faridi, M. H. *et al. High-throughput screening based identification of small molecule antagonists of integrin CD11b/CD18 ligand binding*. Biochem Bioph Res Co 394, 194-199,Doi 10.1016/J.Bbrc.2010.02.151 (2010).

[242] Lossner, D. *et al. Binding of small mono- and oligomeric integrin ligands to membrane-embedded integrins monitored by surface plasmon-enhanced fluorescence spectroscopy.* Analytical Chemistry 78, 4524-4533, 10.1021/ac052078+ (2006).

[243] Streicher, P. *et al. Integrin reconstituted in GUVs: A biomimetic system to study initial steps of cell spreading*. Bba-Biomembranes 1788, 2291-2300, Doi 10.1016/J.Bbamem.2009.07.025 (2009).

[244] Wang, W., Wu, Q., Pasuelo, M., McMurray, J. S. & Li, C. *Probing for integrin alpha(v)ss(3) binding of RGD peptides using fluorescence polarization*. Bioconjugate Chemistry 16, 729-734, Doi 10.1021/Bc049763s (2005).

[245] Hantgan, R. R. *et al. Integrin alpha IIb beta 3 : ligand interactions are linked to binding-site remodeling*. Protein Science 15, 1893-1906, Doi 10.1110/Ps.052049506 (2006).

[246] Huynh-Do, U. *et al. Surface densities of ephrin-B1 determine EphB1-coupled activation of cell attachment through v 3 and 5 1 integrins*. The EMBO Journal 18, 2165-2173 (1999).

[247] Gehring, A. G. *et al. Antibody microarray detection of Escherichia coli O157 : H7: Quantification, assay limitations, and capture efficiency.* Analytical Chemistry 78, 6601-

6607, Doi 10.1021/Ac0608467 (2006).

[248] Motavas, S., Omrane, B. & Papadopoulos, C. *Large-Area Patterning of Carbon Nanotube Ring Arrays*. Langmuir 25, 4655-4658, Doi 10.1021/La803633w (2009).

[249] Kosiorek, A., Kandulski, W., Glaczynska, H. & Giersig, M. *Fabrication of nanoscale rings, dots, and rods by combining shadow nanosphere lithography and annealed polystyrene nanosphere masks*. Small 1, 439-444 (2005).

[250] Vakarelski, I. U., Chan, D. Y. C., Nonoguchi, T., Shinto, H. & Higashitani, K. *Assembly of Gold Nanoparticles into Microwire Networks Induced by Drying Liquid Bridges*. Physical Review Letters 102, -, Artn 058303, Doi 10.1103/Physrevlett.102.058303 (2009).

[251] Vakarelski, I. U., Kwek, J. W., Tang, X. S., O'Shea, S. J. & Chan, D. Y. C. *Particulate Templates and Ordered Liquid Bridge Networks in Evaporative Lithography*. Langmuir 25, 13311-13314, Doi 10.1021/La9033723 (2009).

[252] Khunsin, W. & Kocher, G. *Quantitative analysis of lattice ordering in thin film opal-based photonic crystals*. Advanced Functional Materials 18, 2471-2479 (2008).

[253] Shriver-Lake, L. C. *et al. Antibody immobilization using heterobifunctional crosslinkers*. Biosensors & Bioelectronics 12, 1101-1106 (1997).

10 Publications

10.1 Published Manuscripts

Wolf, C. & Li, Q. *Tunable Two-Dimensional Array Patterning of Antibody Annuli through Microsphere Templating*. Langmuir 26, 12068-12074, Doi 10.1021/La101212y (2010).

10.2 Submitted Manuscripts

Wolf, C, Dorn, J., Li, Q. & Sinner, E.K. *Structured Antibody Surfaces for Bio-recognition.* Submitted to Advanced Functional Materials in November 2010.

11 Acknowledgements

12 Curriculum Vitae